INTERFACING OF NANOGRAPHENE WITH MOUSE BONE MARROW MESENCHYMAL STEM CELLS AND ITS ALLIED MOLECULAR TOXICITY USING *IN VITRO* AND *IN VIVO* METHODS

A THESIS PRESENTED BY

SYAMA. S

TO

THE SREE CHITRA TIRUNAL INSTITUTE FOR MEDICAL SCIENCES AND TECHNOLOGY, TRIVANDRUM

THIRUVANANTHAPURAM

IN PARTIAL FULLFILLMENT OF THE REQUIREMENTS

FOR THE AWARD OF

DOCTOR OF PHILOSOPHY

2016

CERTIFICATE

I, **Syama. S**, hereby certify that I had personally carried out the work depicted in the thesis entitled '***Interfacing of Nanographene with mouse bone marrow mesenchymal stem cells and its allied molecular toxicity using In vitro and In vivo methods'***. No part of the thesis contains any matter previously published or written by another person, nor any material that has been submitted for the award of any other degree or diploma of any University or Institute of higher learning, except where due acknowledgement has been made in the text.

S. Syama

Place: Trivandrum

Signature

Date: 31.12.2016

Name: SYAMA. S

Registration No. 2012/PHD/09

Dr. P.V. Mohanan

Toxicology Division

This is to certify that ***Ms. Syama. S*** in the Division of Toxicology of this institute has fulfilled the requirements prescribed for the Ph.D degree of the Sree Chitra Tirunal Institute for Medical Sciences and Technology, Trivandrum. The thesis entitled ***'Interfacing of Nanographene with mouse bone marrow mesenchymal stem cells and its allied molecular toxicity using In vitro and In vivo methods'*** was carried out under my direct supervision. No part of the thesis was submitted for the award of any degree or diploma prior to this date.

* Clearance was obtained from the Institutional Ethics Committee/Institutional Animal Ethics/Institutional Committee for Stem Cell Research for carrying out the study.

Signature:

Date: 31.12.2016

Dr. P. V. Mohanan
Scientist & Head, Toxicology Division
Sree Chitra Tirunal Institute for Medical-
Sciences and Technology (Govt. of India),
Biomedical Technology Wing, Poojappura,
Thiruvananthapuram-695 012, Kerala, India.

The thesis entitled

INTERFACING OF NANOGRAPHENE WITH MOUSE BONE MARROW MESENCHYMAL STEM CELLS AND ITS ALLIED MOLECULAR TOXICITY USING *IN VITRO* AND *IN VIVO* METHODS

Submitted by
Syama. S

for the degree of

Doctor of Philosophy
of

SREE CHITRA TIRUNAL INSTITUTE
FOR
MEDICAL SCIENCES AND TECHNOLOGY, TRIVANDRUM
Thiruvananthapuram

Is evaluated and approved by

Dr. P.V. Mohanan
(Research Supervisor)

Examiner

DR. RAMA CHANDRA. S.G

ACKNOWLEDGEMENTS

I would like to express my sincere thanks to our Director Prof. Asha Kishore and Dr. Harikrishna Varma PR, Head, Biomedical Technology Wing, Sree Chitra Tirunal Institute for Medical Sciences and Technology for providing necessary support and facilities for completing my PhD work.

I acknowledge my sincere thanks to the Department of Science and Technology, New Delhi for the Junior Research Fellowship and Indian Council of Medical Research (ICMR, New Delhi) for the Senior Research Fellowship.

I express my sincere thanks to our former Directors Prof. K. Radhakrishnan, Prof. Jagan Mohan Tharakan and former Heads of Biomedical Technology Wing Dr. G S Bhuvaneshwar, Dr. CP. Sharma and Mr. OSNK Nair, former Dean Prof. Suresh Nair, Present Dean Dr. Kalliyana Krishnan, Registrar Dr. George, former Deputy Registrar Dr. Sundar Jaya Singh and present Deputy Registrar Dr. Santhosh kumar for providing the necessary support.

I am very much grateful to my Doctoral Advisory Committee Members, Dr. Harikrishna Varma PR, Dr. A. Maya Nandkumar and Dr. PR. Anil Kumar for their kind advice and valuable suggestions during the course of my PhD work.

My deep sense of gratitude and whole hearted thanks to Prof. Toru Maekawa, Prof. D. Sakthikumar, Dr. Aby C and Dr. Neha Chauhan, Toyo University, Saitama, Japan for supporting material characterization.

I would like to acknowledge CEFIPRA for awarding me the prestigious Raman Charpak Fellowship and I also express my sincere gratitude to Prof. Raphael Schneider, LRGP, University of Lorraine, France for all his support during my stay in France.

I express my deep sense of gratitude and respect to all Departments and Divisions Head, especially Dr. Prabha D Nair (former Associate Dean and HoD, DAB), Dr. TV. Kumari (Associate Dean), Dr. Lissy Krishnan, Dr. Sabareeswaran A, Dr. Rekha, Dr. Umashankar P, Dr. Harikrishnan VS for their valuable support for completing this work.

I would like to acknowledge my sincere gratitude to Mr. Sreekanth (Bioceramics), Mr. Willy Paul, Mr. Renjith Kartha, Mr. Pradeepkumar SS. Keerthi S, Amalu Navas (microbiology), Mrs. Susan Mani and Mr. Prem Mohan M for their timely support.

I would like to sincerely thank Dr. Gayathri Easwer, Dr. Remya NS of Toxicology Division. I owe my sincere thanks to my fellow PhD students at Toxicology Division, Ms. Reshma S Cherian, Mrs. Sruthi S, Ms. Reshma VG, my senior Dr. Sheeja Liza Easo and my Laboratory friends, Mr. Shaji S, Mr. Harikumar G, Mrs. Amritha kumari and MS, Mrs. Sreedevi J for their help in developing my PhD work as memorable and enjoyable.

My heartful thanks to all those who have helped me in completing my PhD work by providing valuable information and support, especially all my fellow PhD students.

My sincere gratitude to my beloved mother, father and my sister, for their sustained prayers, constant support and encouragement throughout my work.

Finally my thanks to Dr. P.V. Mohanan, PhD Supervisor for his support in completing my PhD work.

God Almighty for being with me and blessing me for the fulfillment of this work.

CONTENTS

LIST OF FIGURES

LIST OF TABLES

Abbreviations

ADMET	: Absorption, Distribution, Metabolism, Excretion, Toxicity
AFM	: Atomic Force Microscope
AGE	: Agarose Gel Electrophoresis
ALP	: Alkaline Phosphatase
AO	: Acridine Orange
ATP	: Adenosine Triphosphate
BCIP/NBT	: 5-bromo-4-chloro-3-indolyl-phosphate/ nitro blue tetrazolium
Bcl-2	: B-cell lymphoma 2
BMP	: Bone Morphogenetic Protein
BSA	: Bovine Serum Albumin
CFU-F	: Colony Forming Unit Fibroblasts
CLP	: Classification, Labeling and Packaging
CNT	: Carbon Nanotubes
CO_2	: Carbondioxide
COOH	: Carboxyl
CPCSEA	: Committee for the Purpose of Control and Supervision of Experiments on Animals
cpm	: Counts per minute
CPT	: Camptothecin
CVD	: Chemical Vapor Deposition
CXCR4	: C-X-C chemokine receptor type 4
DAPI	: 4, 6-Diamidino-2-Phenylindole
DCC	: N, N'-dicyclohexylcarbodiimide
DCF	: Dichorofluorescein
DCFH-DA	: Dichlorofluorescien diacetate
DLS	: Differential Light Scattering
DMEM	: Dulbecco's Modified Eagle's Medium
DMSO	: Dimethyl Sulfoxide
DNA	: Deoxyribonucleic acid
DOX	: Doxorubicin
DTNB	: 5-5' Dithio bis(2-nitrobenzoic acid)
DTPA	: Diethylene triamine penta acetic acid

E coli	: *Escherichia coli*
ECVAM	: European Centre for Validation of Alternative Methods
EDC	: 1-ethyl-3-(3-dimethylaminopropyl)-carbodiimide
EDTA	: Ethylene diamine tetra acetic acid
EPR	: Enhanced Permeability and Retention
EtBr	: Ethidium Bromide
ETC	: Electron Transport Chain
EU	: Endotoxin Unit
FACS	: Fluorescent Activated Cell Sorter
FBS	: Fetal Bovine Serum
FDA	: Food and Drug Administration
FET	: Field Effect Transistor
FGF	: Fibroblast Growth Factor
FITC	: Fluorescein Isothyocyanate
FPG sites	: Formamidopyrimidine DNA glycosylase
FRET	: Forster Resonance Energy Transfer
FTIR	: Fourier Transform Infra Red Spectroscopy
G	: Graphene
g	: Gram
g	: Gravitational Force
GM-CSF	: Granulocyte Macrophage- Colony Stimulating Factor
GO	: Graphene Oxide
GPX	: Glutathione Peroxidase
GQDs	: Graphene Quantum Dots
GR	: Glutathione Reductase
GSH	: Reduced Glutathione
GSSG	: Glutathione disulfide
H & E	: Hematoxylin and Eosin
h	: Hours
H_2O_2	: Hydrogen peroxide
H_2SO_4	: Sulfuric acid
HCl	: Hydrochloric acid
HCT	: Hematocrit

HGB	: Hemoglobin
HIF-2α	: Hypoxia Induced Factor-2α
HSCs	: Hematopoietic Stem Cells
i.p.	: Intraperitoneal
i.v.	: Intravenous
IAEC	: Institutional Animal Ethics Committee
ICSCR	: Institutional Committee for Stem Cell Research
IGF	: Insulin like growth factor
IL	: Interleukins
ISO	: International Organization for Standardization
JC-1	: 5,5′,6,6′-Tetrachloro-1,1′,3,3′-tetraethyl-imidacarbocyanine iodide
JNK pathway	: Jun amino-terminal kinases
KDa	: Kilo Dalton
kg	: Kilogram
$KHSO_4$	: Potassium bisulfate
$KMnO_4$	: Potassium Permanganate
KOH	: Potassium hydroxide
LIF	: Leukemia Inhibitory Factor
LPO	: Lipid peroxidation
MAP Kinase	: Mitogen Activated Protein Kinase
MCH	: Mean Corpuscular Hemoglobin
MCHC	: Mean Corpuscular Haemoglobin Concentration
MCV	: Mean Corpuscular Volume
MDA	: Malondialdehyde
µci	: Microcurie
µg	: Microgram
µl	: Microlitre
µm	: Micrometre
µM	: Micromolar
mg	: Milligrams
MIC	: Minimum Inhibitory Concentration
min	: Minutes
MIP	: Macrophage inflammatory protein

ml : Millilitre
mm : Millimetre
mM : Millimolar
MMP : Mitochondrial Membrane Potential
Mn_2O_7 : Manganese heptoxide
MRI : Magnetic Resonance Imaging
MSCs : Mesenchymal Stem Cells
MTT : 3-(4,5-dimethyl thiazol-2-yl)-2,5-diphenyl tetrazolium bromide
MWCNTs : Multi walled carbon nanotubes
MyD88 : Myeloid differentiation primary response gene 88
N : Normal
NADPH : Nicotinamide adenine dinucleotide phosphate reduced
NaOH : Sodium hydroxide
NFkB : Nuclear factor k- Beta
NGO : Nano graphene oxide
NIR : Near Infra red
nm : Nanometer
OH : Hydroxyl
PAGE : Poly Acrylamide Gel Electrophoresis
PBS : Phosphate Buffered Saline
PCL : Poly–ε-Caprolactone
PDGF : Platelet derived growth factor
PDT : Photo dynamic therapy
PEG : Poly Ethylene Glycol
PEI : Polyethyleneimine
pH : potential of hydrogen
PI : Propidium Iodide
PL : Poly Lysine
PLT : Platelets
PPARγ : Peroxisome proliferators activated receptor γ
ppm : Parts per million
PrGO : PEGylated reduced graphene oxide
QDs : Quantum dots

RBC : Red Blood Corpuscle

REACH : Registration, Evaluation, Authorization and Restriction of Chemical

RES : Reticulo Endothelial System

RF : Radio Frequency

RFU : Relative Fluorescent Unit

RGO : Reduced Graphene Oxide

RNA : Ribonucleic acid

ROS : Reactive Oxygen Species

rpm : Rotations per minute

RPMI : Roswell Park Memorial Institute medium

s : Seconds

SAED : Selective Area Electron Diffraction

SD : Standard Deviation

SDS : Sodium Dodecyl Sulfate

SERS : Surface Enhanced Raman scattering

SGOT : Serum Glutamic Oxaloacetic Transaminase

SGPT : Serum Glutamic Pyruvic Transaminase

siRNA : Small Interference Ribo Nucleic Acid

α-SMA : α-Smooth Muscle Actin

$SOCl_2$: Thionyl chloride

SOD : Superoxide Dismutase

SiO_2 : Silicon Oxide

SPION : Super Paramagnetic Iron Oxide Nanoparticles

ssDNA : Single Stranded Deoxy Ribonucleic Acid

SWNT : Single Wall Carbon nanotubes

TBA : Thiobarbituric acid

TCA : Trichloroacetic acid

TE : Tris EDTA

TEM : Transmission Electron Microscopy

TEMED : Tetramethylethylenediamine

TGA : Thermo Gravimetric Analysis

TGF-β : Transforming Growth Factor-β

TiO_2	: Titanium Oxide
TIP-1	: Tension Induced Proteins-1
TLR	: Toll like Receptor
TNB	: Thionitrobenzoic acid
TNF	: Tumor Necrosis Factor
TRAF-6	: TNF receptor associated factor-6
USP	: United States Pharmacopoeia
UV	: Ultra Violet
VCAM	: Vascular Cell Adhesion Molecule
WBC	: White Blood Corpuscle
XPS	: X ray Photoelectron Spectroscopy
XRD	: X Ray Diffraction
ZnO	: Zinc Oxide

SYNOPSIS

Interfacing of Nanographene with mouse bone marrow mesenchymal stem cells and its allied molecular toxicity using *In vitro* and *In vivo* methods

Graphene, a single atom thick two dimensional carbon sheets can replace many of the existing nanoparticles due to their exciting physico-chemical properties. The rapid increase in research and the number of papers published on graphene has further expanded its scope from electronic applications towards biomedical areas. Graphene and graphene derivatives can be used in biomedical field as antibacterial agents, drug or gene delivery, photothermal therapy, imaging, bio-sensing and as a scaffold for cell culture. Although research on the synthesis and application of graphene is increasing rapidly, relatively little information is available on their intrinsic safety/toxicity towards living system and the results are contradictory.

The aim of the present work is to elucidate a comprehensive safety and toxicity profile of nanographene (PEGylated reduced graphene oxide) (PrGO) in *in vitro* and *in vivo* conditions. The main hypothesis is to evaluate the biological interaction of PrGO in mice, its interactions on mesenchymal stem cells and subsequent consequences on cell fate. In order to address the hypothesis, the study is divided into two objectives and each objective is subdivided into two phases,

- Objective 1: Synthesis and characterization of PrGO and its biological interaction with mouse bone marrow mesenchymal stem cells (MSCs)
    - Phase 1: Synthesis and characterization of PrGO
    - Phase 2: Isolation and characterization of MSCs and *in vitro* assays using MSCs

- Objective 2: Acute, sub acute exposure of PrGO to mice and to investigate the molecular toxicity, immunotoxicity, bio-distribution, toxicokinetics and histopathological analysis.
    - Phase 3:Acute toxicity studies, bio-distribution and toxicokinetics
    - Phase 4: Sub acute toxicity, immunotoxicity, molecular toxicity and histopathology

The thesis has been divided into four chapters: the first introductory chapter discusses about the nanoparticles, their physico-chemical properties, applications and the cellular responses on exposure to nanoparticles. The advantage of opting stem cells as *in vitro* model for toxicity screening is also emphasized. The second chapter deals with the literature review on graphene, its physicochemical characteristics, various methods of synthesis and its biomedical applications. A detailed description on 'mesenchymal stem cells' as in *vitro* model system has been thoroughly elaborated. Characterization and differentiation potential of MSCs and the rational for studying the interaction of PrGO nanoparticles with MSCs were discussed in detail.

The third chapter deals with the materials and method which is divided into four sections. The first section describes the synthesis and characterization of PrGO. Graphite is exfoliated in presence of acid and oxidized using potassium permanganate, hydrogen peroxide forming water soluble graphene oxide (GO). GO was chemically modified with O,O′- Bis(2-aminoethyl) polyethylene glycol (PEG) under EDC chemistry. GO-PEG was further reduced using sodium borohydride to form PrGO. The obtained PrGO was characterized by standard techniques. Size and surface morphology was characterized by Atomic Force Microscopy (AFM),

Transmission Electron Microscopy (TEM) and Selective Area Electron Diffraction (SAED). Further characterization on crystal structure and chemical composition was studied using X-ray diffraction (XRD) and X-ray Photo Electron Spectroscopy (XPS). The characteristic graphene spectra (G band and D band) were observed by Raman Spectroscopy. PEG coupling was confirmed by Fourier Transform Infrared Spectroscopy (FTIR) and Thermo Gravimetric Analysis (TGA). Endotoxin content was determined using Endosafe PTS LAL assay.

The second section explains the protocol for isolation and characterization of MSCs. The cells were characterized for the expression of MSCs positive marker (CD 90 and CD 44) and lack of CD 35 (negative haematopoietic stem cell marker) using immunostaining and FACS. The cells were studied for their differentiation potential into adipocytes and osteoblasts under controlled culture condition.

The third section focused on *in vitro* toxicity screening of PrGO with isolated MSCs. Cytotoxicity, cell viability and mitochondrial function upon exposure to different concentration of PrGO were assayed by MTT and Neutral red uptake. PrGO uptake by stem cells was studied under microscopy at different time periods. Oxidative stress resulting in ROS production was evaluated using DCFDA assay. Mitochondrial and lysosomal membrane integrity was determined using JC-1 probe and Acridine orange fluorescent dye respectively. Induction of apoptosis in MSCs under PrGO treatment was performed using Annexin V/ PI staining and analyzed by FACS. Activity of caspase enzyme and DNA fragmentation was investigated using Sensolyte Homogenous Caspase 3/7 AMC Assay kit and apoptotic DNA ladder kit.

The fourth section describes the *in vivo* toxicity studies, in which systemic toxicity, bio-distribution, and toxicokinetics of PrGO in mice were studied. Animals were given 10 mg/kg body weight of PrGO for all the studies. Bio-distribution of PrGO after single intravenous and intraperitoneal administration was studied by Raman mapping. Similarly, toxicokinetics was studied in peripheral blood by Raman mapping after both intravenous and intraperitoneal administration. Blood was collected after 1, 3, 6, 24, 48, 72 h and 7 days to estimate the presence of PrGO in blood. Urine sample was collected for studying the excretion of PrGO. Blood sample was collected for haematological and serum was used for clinical chemistry evaluation. Systemic toxicity and immunotoxicity was studied after repeated exposure to PrGO via intraperitoneal injection. Organs such as brain, liver, kidney and spleen were collected for histopathological analysis. Splenocytes were isolated and proliferation study was carried out using thymidine incorporation assay to determine the immune response. Blood was collected for evaluating hematological and clinical chemistry parameters. Formation of lipid peroxides as a measure of oxidative stress and the activity of various antioxidant enzymes were estimated.

The fourth chapter covers results, which splits into four parts. The first part deals with the synthesis and characterization of PrGO. All characterization was compared with reduced graphene oxide (RGO). TEM images showed clean surface morphology of PrGO with folding and wrinkles. Hexagonal crystal lattice structure was evident from SAED. From AFM, lateral dimension and thickness was found to be ~1 µm and 8-9 nm respectively. XRD analysis showed diffraction peak at 25° indicates random pucking of graphene sheets. Characteristics Raman spectra were

observed for PrGO, with G band at 1575 corresponds to graphite peak and D band at 1330 is due to presence of defects. C1s spectrum showed both the presence of sp^2 and sp^3 carbon atoms in PrGO. PEG coating was confirmed by FTIR having peaks at 2845, 1442 and 1050 cm^{-1} in addition to that observed in RGO. TGA analysis showed 50% weight loss at temperature (350-400°C) due to polymer degradation. Endotoxin content of PrGO was found to be <0.1 EU/ml.

The result of the isolation and characterization of MSCs were mentioned in the second part. The isolated cells formed several colonies with spindle shaped fibroblast morphology. The cells also expressed positive surface markers such as CD 90 and CD44 and lacks negative marker CD 45, a haematopoietic stem cells marker. Isolated MSCs was found to be differentiated into adipocytes and osteoblasts when cultured in differentiation medium.

The third part describes the interaction of PrGO on isolated MSCs. The *in vitro* toxicity assays showed absence of any toxicity when MSCs were exposed to PrGO. PrGO seems to be effectively taken up by the cells and distributed throughout the cytoplasm without entering nucleus. Cytotoxicity showed no changes in cellular mitochondrial activity and cell viability. Neutral red and Acridine orange assays showed no alternations in lysosomal membrane integrity. In contrast, the cells showed concentration and time dependent increase in ROS production. Similarly mitochondrial depolarization occurs only at higher concentration (500 µg/ml). Apoptosis studies based on the relocation of phosphotidyl serine staining with Annexin V and expression of caspase enzymes showed no significant changes.

Absence of DNA fragments observed in DNA ladder assay confirmed that PrGO is not directly or indirectly inducing DNA damage.

The *in vivo* bio-distribution, toxicokinetics and immunotoxicity of PrGO in mice after intravenous and intraperitoneal injection were addressed in the fourth part. Raman mapping showed PrGO distribution in liver, brain, spleen and kidney at 7, 14 and 21 days after administration. Toxicokinetics in blood showed increased presence of PrGO after 3 h of intravenous administration and decreases with time. Excretion of PrGO from urine sample showed very weak PrGO intensity stating decreased excretion through kidney. Observation of bone marrow niche showed normal population of MSCs, fat cells and osteoblasts after isolation and culture. In repeated dose, splenocytes proliferation was found to be increased after initial exposure and becomes normal afterwards. Haematological and clinical chemistry revealed significant differences in few parameters. No lipid peroxidation formation was noticed in liver samples. Increased GSH content during 7 and 14 days occurs as a response to increased ROS production. No changes were observed in other antioxidant enzyme activities except superoxide dismutase (SOD) which decreases as a result of oxidative stress. Histopathological analysis showed vacuolarization and presence of kupffer cells in liver cells. Kidney showed congested glomeruli and extramedullary haematopoiesis evidenced in spleen cells.

In the final section, results are summarized and concluded that PrGO (8-9 nm thickness) fails to induce any deleterious response in MSCs and do not alter the proliferation or growth of MSCs under experimental conditions. Accumulation of larger PrGO aggregates and failure to excrete out of the system raises concerns about

their toxicity due to prolonged persistence. The acute, sub acute exposure of PrGO to mice proved that PrGO slightly affected the integrity of the organs. The molecular toxicity, immunotoxicity, bio-distribution and toxicokinetics indicated a slight alteration and the same were recovered to the normal stage. The histopathological investigation showed few lesions in liver, kidney and spleen cells. Further long term studies will be required to declare the PrGO is validated to be safe nanoparticle for clinical application.

CHAPTER 1: INTRODUCTION

1. INTRODUCTION

1.1. NANOMATERIALS

The significance of nanotechnology has been envisaged long back by Richard Feynman (1959) in his lecture, saying "There is a plenty of room at the bottom". The bulk materials can be scaled down to micro and nano range in order to improve its physico-chemical properties. Nanomaterials have been the subject of interest in the recent era as it offers scientist with ease of manipulation according to the desired tunable properties. Nanomaterials are substances with at least one dimension in the nanoscale (1-100 nm) range. Nanoparticles are generally divided into two main categories: (i) natural and (ii) anthropogenic. Natural nanoparticles include soil colloids, fullerenes, carbon nanotubes, magnetite, clay minerals, metal oxides etc. (Buffle, 2006; Nowack & Bucheli, 2007). Man made engineered nanoparticles is intentionally produced by synthetic routes.

It was already reported that the global market production of nanomaterials attained $2.6 trillion in 2015 (GAO, 2010). In 2011, the worldwide production of nanomaterials was more than 230,000 tons and in 2016 it is expected to reach 350,000 tons. United States of America is the world largest market for nanomaterials production and is regulated by Food and Drug Administration (FDA). Products related to electronics devices, pharmaceutical and chemical products are marketed in America. Europe also contributes much to the increased market production of nanomaterials which is regulated by REACH (Registration, Evaluation, Authorization and Restriction of Chemicals) and CLP (Classification, Labeling and Packaging). Increased demand and availability of funds is expected to enhance the nanomaterial production in the forthcoming years

(Vance *et al*., 2015). Though there is a lot of research going on for the production of novel nanoparticles, very few actually hit the market. A well characterized nanoTiO_2 named Degussa P25 with high photocatalytic activity is commercially available (Ohno *et al*., 2001). Dextran functionalized super paramagnetic iron oxide nanoparticles (SPION) has been approved by United States FDA for clinical application (Kunzmann *et al*., 2011). SPIONs such as Ferucarbotran, ferumoxides (SPION larger than 50nm) and SHU555C, ferumoxtran-10 (SPION smaller than 50nm) are clinically approved as contrast agent for Magnetic Resonance Imaging (MRI).

Several national institutes have initiated work on safety evaluation of nanomaterials. These institutes have been provided with the highly equipped facilities for synthesizing different nanoparticles, for their characterization and for preclinical safety evaluation. Tripathi *et al*., 2013 reported the synthesis of polyethylenimine based nanoparticles as a vector for gene and siRNA delivery. Graphene based nanocomposite was developed (Srivastava *et al*., 2012) for the detection of nitrogen dioxide gas. This nanosensor greatly helps in reducing the polluting gas emitted by industries. Kaushik *et* al., 2008 developed a chitosan dispersed iron oxide nanocomposite for the immobilization of glucose oxidase. This biosensor displayed excellent catalytic activity, high sensitivity and low detection limit for glucose. Similarly, chitosan encapsulated dextran functionalized doxorubicin was developed as a carrier for anticancer drug delivery (Mitra *et al*., 2001). This hydrogel offered extended blood retention time and passive tumor accumulation. The advancement of nanotechnology has greatly awakened the public about the side effects/ hazards of nanomaterials exposed to the environment.

Toxicity of widely used nanoparticles was also studied by several groups. Mohanan *et* al., 2014 investigated the molecular toxicity of dextran functionalized iron oxide nanoparticles after dermal exposure to Wistar rats. Oxidative stress induced toxicity of hydroxyapatite nanoparticles (Syama *et al.,* 2014a) and zinc oxide nanoparticles (Syama *et al.,* 2014b) was well established. It was well known that there are no clear regulatory guidelines available for evaluating the safety of these materials. However there are plenty of applications available with these nanomaterials.

1.2. APPLICATION OF NANOMATERIALS

Recently nanoparticles have been integrated into every aspects of our life in the form of drugs, chemicals, cosmetics and other consumer products. Nanoparticles have wide range of applications especially in optical, electronic and biomedical fields. Nanoparticles are widely used in cosmetics (sunscreen) because of its transparency and improved efficacy. Both titanium oxide (TiO_2) and Zinc oxide (ZnO) nanoparticles have already included in some of the cosmetic preparations. Because of its antibacterial property these nanoparticles are widely used in industries for food packaging, water purification and in textiles. Nanoparticles based sensors were also used for detecting the pesticides and *Salmonella* contamination in food. Copper oxide nanoparticles are used in biomedicine as antimicrobial agent (Magaye *et al*., 2012). Cobalt nanoparticles are used as sensors, catalysts, in energy storage devices and also act as an effective contrast agent when used in combination with other metals like gold, iron, graphite and platinum (Alarifi *et al*., 2013). Gharibshahi & Saion (2012) reported that platinum nanoparticles are explored for their anti-cancerous activity and also as catalysts in fuel cells and in the

exhaust systems of cars, gas and glucose sensors. It was reported by Pietruska *et al*., (2011) that nickel nanoparticles are commonly used in rechargeable batteries, electronics and alloys of nickel nanoparticles are used for hyperthermia treatment. Recently, nanorobots were developed to clear the blocks in the arteries of patient's suffering from artherosclerosis. Antibody-nanoparticle complex specifically binds to the plaque formed during atherosclerosis and it helps the clinician to directly monitor the plaque development.

Nanoparticles are widely used in tissue engineering, drug or gene delivery, cancer therapy, bioimaging, MRI contrast agents, detection of metabolites and pathogens. It can also be used for coating medical devices and urinary catheters. Silver nanoparticles are used to coat the surface of the medical devices to prevent bacterial adhesion and biofilm formation (Knetsch & Koole, 2011). Recently it was noted that nanoparticles can be used to stimulate stem cells for regeneration of damaged vascular tissue (Yang *et al*., 2010). Ceramic, polymers and metal based nanoparticles are coated on the surface of the bone implant that greatly enhance cell adhesion, growth and prevent host rejection.

Luminescent nanoparticles are widely used for optical imaging. Nanoparticles in the form of quantum dots (QDs) are used for bioimaging as they are photochemically stable and possess narrow emission spectrum. Magnetic nanoparticles (iron oxide) are used as an excellent biocompatible MRI contrast agent. Drug carrying iron oxide nanoparticles provides dual advantages of simultaneous detection and treatment. Iron nanoparticles show great potential in electrical and biomedical applications such as

labeling and magnetic separation of biological samples, imaging, site directed drug delivery and hyperthermia therapy of cancer (Apopa *et al*., 2009).

Nanoparticles are a suitable candidate for biosensing application owing to their unique physico- chemical properties and increase signal to noise ratio. Among the metal nanoparticles, gold nanoparticles are widely used for biosensing because of their biocompatibility, optical properties and ease of production (Li *et al*., 2010). Luminescent semiconducting nanocrystals called QDs are also used as biosensors owing to their size dependent narrow emission. Forster resonance energy transfer (FRET) based biosensors can be developed using metallic nanoparticles because of their excellent quenching ability. In the absence of DNA strand, both the fluorescent dye and nanoparticles are close enough resulting in the quenching of fluorescence. Fluorescence of the dye can be regained when the target DNA hybridized with the complementary sequence. Magnetic nanoparticles are also used in biosensors as an alternative to fluorescent labels. Carbon nanotubes and graphene are used in biosensors because of its electronic properties. The electronic properties of carbon nanotubes are used in Field Effect Transistor (FET) biosensors in which the biorecognition events results in changes in conductivity of the nanotubes (Holzinger *et al*., 2014).

Controlled and targeted drug delivery can be achieved with nanoparticles. pH responsive nanoparticles can release drugs specifically to cancer cells because of its acidic pH and thereby avoiding harmful side effects on surrounding normal cells. Similarly, thermosensitive polymers can be used for temperature controlled drug release. Nanoparticles can also be used as an effective carrier for biomolecules such as DNA,

RNA and protein. It can protect these biomolecules from damage and carry them across cell membrane barrier (De *et al*., 2008).

Gold nanoparticles are used for photo thermal therapy to treat cancer (Hwang *et al*., 2014). Gold nanoparticles have advantages of strong absorption, high photostability, efficient heat transfer, and low cytotoxicity. The antibody coated gold nanoparticles are transferred to cancer cells and upon light treatment, these nanoparticles heats up and effectively kill cancer cells. Table 1.1 indicates examples of companies commercializing nanomaterials for bio- and medical applications.

1.3. ADVANTAGES OF NANOMATERIALS

Following are some of the major advantages of nanomaterials:

- Size and surface characteristics can be modulated to obtain desired properties.
- Increased surface area with novel properties.
- Nanoparticles are biologically reactive.
- Access to the body parts where larger particles are more difficult to approach.
- Used for fluorescent labeling of biomolecules.
- Highly sensitive and multimodal imaging.
- As a novel drug carrier
    - Protect drugs from degradation
    - site directed delivery and decreased side effects
    - controlled and sustained release of drugs
    - relatively high drug loading
    - various routes of administration

- To heal genetic diseases by delivering functional gene to replace abnormal genes.
- To detect the presence of proteins, DNA and pathogens.
- Detection of some diseases in their early stage (Gold nanoparticles are used to detect early stages of Alzheimer's disease).

Company	Area of activity	Technology
Advectus Life Sciences Inc.	Drug delivery	Polymeric nanoparticles engineered to carry antitumour drug across the blood-brain barrier
Alnis Biosciences, Inc.	Bio-pharmaceutical	Biodegradable polymeric nanoparticles for drug delivery
BASF	Toothpaste	Hydroxyapatite nanoparticles to improve dental surface
Biophan Technologies, Inc.	MRI shielding	Nanomagnetic/carbon composite materials to shield medical devices from RF fields
EnviroSystems, Inc.	Surface disinfectant	Nanoemulsions
KES Science and Technology, Inc.	AiroCide filters	Nano-TiO_2 to destroy airborne pathogens
NanoBio Corporation	Pharmaceutical	Antimicrobal nano-emulsions
NanoCarrier Co., Ltd	Drug delivery	Micellar nanoparticles for encapsulation of drugs, proteins, DNA
Nanoprobes, Inc.	Gold nanoparticles for biological markers	Gold nanoparticles bio-conjugates for TEM and/or fluorescent microscopy
NanoMed Pharmaceutical, Inc.	Drug delivery	Nanoparticles for drug delivery
Oxonica Ltd	Sunscreens	Doped transparent nanoparticles to effectively absorb harmful UV and convert it into heat
PSiVida Ltd	Tissue engineering, implants, drugs and gene delivery, bio-filtration	Exploiting material properties of nanostructured porous silicone
Smith & Nephew	Acticoat bandages	Nanocrystal silver is highly toxic to pathogens

Table 1.1: Commercially available nanoformulations for medical applications (Adapted from J Nanobiotechnology, 2, 2004)

1.4. TOXICITY OF NANOMATERIALS

Nanotoxicology is an interdisciplinary field enclosing experts from material science, biology and toxicology jointly work to facilitate nanoparticles safety evaluation. The methods followed for nanomaterials toxicity assessment is based on chemical toxicity and there is possibility for lack of correlation between biological responses and nanoparticles properties. Thus more standardized methods have to be developed for nanoparticles toxicity with proper characterization of the material and their interaction with the biological system.

The rapid growth in this field along with the increased production and usage, increases the chance of exposure of these nanomaterials to the ecosystem. Despite the increase in scientific interest and potential application, there is a great concern on the safety and toxicity of nanoparticles. The interaction of nanoparticles with the biological system can induce undesirable side effects. These engineered nanoparticles must be evaluated for potential health hazards before validating its use for human beings.

Nanoparticles are intruders that may either interfere with cellular function or can promote harmful cellular responses when enters into the body. Because of their small size and increased surface to volume ratio, the toxicity of nanoparticles differs from their bulk materials. It can pass through the physiological barrier, intermingle with the cells, evade immune recognition and circulate in blood stream with prolonged persistence in the body. The toxicity of nanoparticles still remains a debate; how they evade immune recognition and their fate remains unclear. Nanoparticles get access to the body through various routes; inhalation (respiratory), ingestion (gastrointestinal), dermal exposure (skin) are

the major routes of entry (Stern & McNeil, 2008). The majority of air borne nanoparticles entry is through lungs. Upon inhalation, nanoparticles are translocated out of the respiratory tract through different pathways. Nanoparticles are translocated via endocytosis of alveolar epithelial cells (Elsaesser & Howard, 2012). Nanoparticles are also translocated to other organs via olfactory bulb which provide direct access to the central nervous system. Systemic uptake of nanoparticles via lymph occurs when they are ingested. From systemic circulation, they can distribute to various organs such as liver, spleen, bone marrow, heart etc. The following figure represents the route of exposure and distribution of nanoparticles (Figure 1.1).

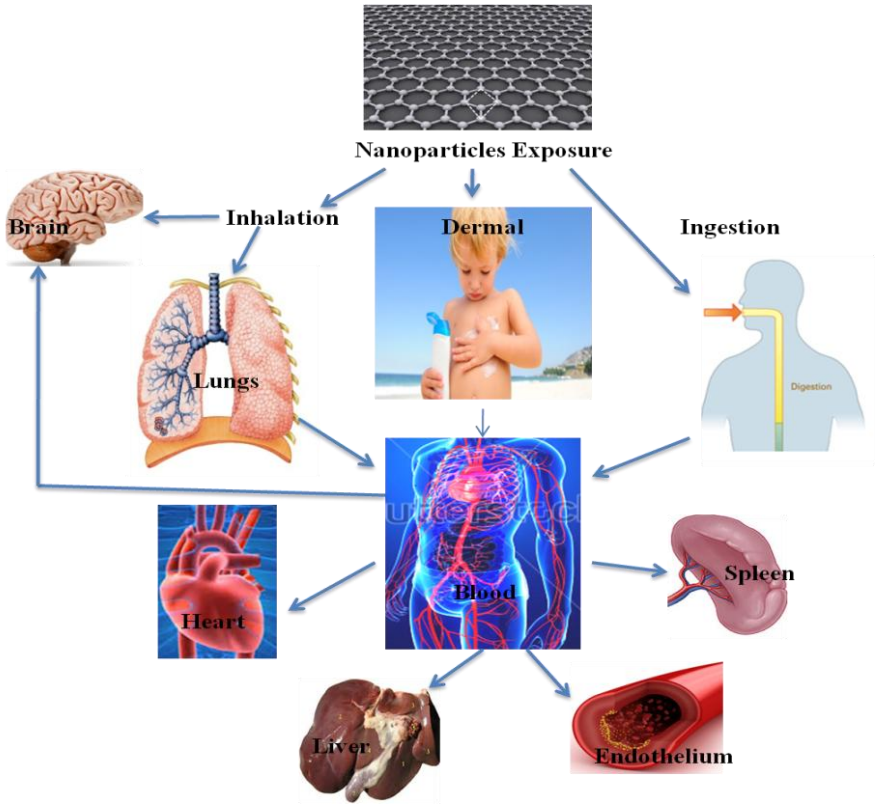

Figure 1.1: Schematic representation of biodistribution of nanomaterials and target organs for toxicity.

Increase in the development of new nanomaterials for drug delivery, consumer products and other application concomitantly increases the exposure to human beings. Intentionally nanoparticles are injected into the human body in the form of nanomedicine or for bioimaging purposes. Unintentional exposure occurs mostly during manufacturing processes. Particle sizes, shape, surface chemistry, crystallinity, state of agglomeration, chemical composition, aggregation are the properties that influence nanoparticles toxicity (Shin *et al*., 2015). In addition, the interaction of nanoparticles with the biological system varies according to the type of cell exposed, dose and duration of exposure. Anxiety rising from the undesirable toxic effects of nanoparticles substantially reduces their potential use. Thus it is vital to evaluate the toxicity/safety of nanoparticles before implementing their use to avoid unintentional health hazard. This will ensure a safe non-hazardous nanomaterial and a risk free safer technology.

1.5. CELLULAR RESPONSES TO NANOMATERIALS

Uptake of nanoparticles correlates with its shape. It was reported (Chellat *et al*., 2005) that the rod shaped nanotubes found less cellular uptake than spherical particles. Uptake is also influenced by particle surface chemistry, size and the type of cell. Nanoparticles can enter into the cell passively and are localized in various organelles such as cytoplasm, mitochondria, nuclear membrane and nucleus. Direct interaction of nanoparticles with the organelle may damage the organelles and leads to cell death. Particle size plays a major role in intracellular distribution of nanoparticles. Nanoparticles with size 2-10 μm are localized in large cytoplasmic vacuoles; small nanoparticles (< 100

nm) are localized in mitochondria. Very small nanoparticles (0.7 nm) can penetrate the cell via ion channel or pores through the cell membrane (Porter *et al*., 2006). Nanoparticle also enter cell via endocytosis or by penetrating through the lipid bilayer (plasma membrane).

Nanoparticles are known to induce reactive oxygen species (ROS) formation in both *in vitro* and *in vivo* conditions. ROS generated inside the cell induce inflammation by recruiting macrophages and release pro-inflammatory cytokines. ROS may either directly formed from the surface of nanoparticles or from the presence of transition metal contaminants. Altered mitochondrial function also promotes ROS formation (Fu *et al*., 2014). The increased ROS formed inside the cells oxidize lipids, proteins, DNA and thereby interferes with the cell signaling. Oxidative stress occurs when there is disequilibrium in redox state of the cell. It is manifested by increased ROS formation that overwhelms the antioxidant defense system of the cell. The ratio of cellular glutathione (GSH) to glutathione disulfide (GSSG) is a measure of oxidative stress.

Ultrafine particles are highly toxic because of their high surface area and reactivity. Human lung epithelial cells and human broncho epithelial cells when exposed to TiO_2 nanoparticles showed increased ROS production (Ekstrand-Hammarström *et al*., 2011). Metal ions can leads to the production of hydroxyl radical via one electron reduction (Ball *et al.*, 2000). Magnetite nanoparticles induce oxidative stress by increased ROS generation, disturb mitochondrial membrane potential (MMP) and are also known to cause DNA lesions (FPG sites) (Karlsson *et al*., 2008). It activates JNK pathway in ROS independent manner and induces DNA damage in a concentration dependent

manner. Nanoparticle mediated ROS formation promote lysosomal membrane destabilization releasing lysosomal content into the cytoplasm or activate caspase 3/7 ending up with apoptosis (Sohaebuddin *et al*., 2010).

AFT-2, a transcription factor increases its expression during early stages of stress signaling indicates cytotoxicity. Mohamed *et al*., (2011) reported that exposure of SiO_2 nanoparticles to A549 cells results in activation of AFT-2 gene. Oxidative stress leads to the release of proinflammatory cytokines. Size and composition are the major factors that contribute to inflammation. It was known that macrophages uptake nanoparticles in larger amount compared to other cells and are more prone to cytolysis by releasing inflammatory mediators which induces systemic response. Similarly, various antioxidants are released from the cells as a response to oxidative stress (Brown *et al*., 2007). Nanoparticles oxidize DNA leading to heritable mutation. Formation of 8-OHdG is a marker for oxidative stress (Zhu *et al*., 2013). Base and sugar lesions, DNA-protein cross links, single and double stranded breaks and formation of abasic sites occurs as a result of oxidative DNA damage.

1.6. BACKGROUND OF THE STUDY

The toxicity, biocompatibility and safety of engineered nanoparticles are of great concern to the scientific community despite their promising potential in many biomedical and other applications. Graphene or its derivatives are one of the new generation materials for biomedical application. The safety and toxicity of graphene or its derivatives is not well established. Because of the lack of *in vitro* and *in vivo* toxicity data, an effort was made to evaluate the toxicity of graphene derivatives at molecular

level using mouse bone marrow mesenchymal stem cells (MSCs) as an *in vitro* and Swiss Albino mice as an *in vivo* model.

1.7. STEM CELLS IN TOXICOLOGY

Stem cells are distinguished into two types: Embryonic stem cells and Adult stem cells. Embryonic stem cells isolated from inner cell mass of blastocysts develop into cells of distinct phenotype. These cells possess indefinite self renewal property. Adult stem cells differentiate into cells of restricted lineages with limited proliferation. Stem cells offer a reliable, consistent and unlimited cell source, closer resemblance to *in vivo* condition. Stem cells differentiate into cells of homogenous population under controlled culture conditions. Stem cells reduce the usage of animals and variability because of differences in donor. It helps us to understand the developmental effects. Stem cell also helps to predict early toxicity screening of drugs. ECVAM (European Centre for Validation of Alternative Methods) committee suggested using mouse embryonic stem cells for studying teratogenic effects of chemicals (Scholz *et al*., 1999). Molecular changes behind the toxicity can be elucidated using stem cell models and it is more suitable model for studying epigenetic toxicants.

Although stem cells seem to be a promising tests system for *in vitro* toxicity studies. There are certain practical limitations associated with the use of stem cells that needs to be addressed. Since stem cells lies in heterogenous population, it is difficult to enrich stem cells from other cells and the genetic stability of stem cells cannot be maintained for a prolonged period.

1.8. WHY STEM CELLS IN TOXICOLOGY?

- Alternative *in vitro* model for predictive toxicity screening.
- Large number of cells will be obtained from single isolation.
- Can be cultured for extended times without loss of basic functionality.
- Reduces the use of animals.
- Helps to investigate the developmental effects (if embryonic stem cells).
- Understanding the mechanism behind toxicity.
- Cells exhibit specific markers and functional properties similar to the adult counterparts.
- Toxic effects on this system results in damage to other parts of the body.
- Basic origin of cells.

1.9. STEM CELLS AND GRAPHENE

MSCs are investigated to be used for repair and regeneration of damaged tissues. Growth and differentiation of MSCs can be manipulated using nanoparticles carrying biomolecules such as growth factors or genes (Cao *et al*., 2012; Corsi *et al*., 2003). Recently graphene has been proposed to be used as a delivery agent for stem cell based therapy. Graphene in the form of quantum dots reported as bioimaging material for *ex vivo* MSCs labeling and stem cell tracking (Talukdar *et al*., 2014). Thus it is indeed imperative to understand their interaction with the stem cells and to determine its toxic dose. Graphene (G) and graphene oxide (GO) act as a perfect platform for stem cells attachment and growth. Both G and GO effectively adsorbs cell adhesion proteins from serum. Oxygenated GO binds serum proteins via electrostatic interactions and

hydrophobic graphene interact with hydrophobic residues in protein with the help of π electrons (Lee *et al*., 2011). Bressan *et* al., (2014) reported that graphene induce osteogenic differentiation and matrix mineralization by adsorbing dexamethasone (glucocorticoid that alter protein expression during bone differentiation) and β- glycerol phosphate (an intracellular alkaline phosphatase enzyme). GO effectively adsorb insulin, forms hydrogen bonds and induces adipogenesis in presence of selected biomolecules (insulin, dexamethasone and indomethacin).

1.10. HYPOTHESIS

The aim of the present study was to synthesize and characterize PEGylated reduced graphene oxide (PrGO) and to evaluate their *in vitro* toxicity using mouse bone marrow mesenchymal stem cells. The *in vivo* toxicity studies including acute, sub acute, biodistribution, toxicokinetics and immunotoxicity were carried out in Swiss Albino mice.

The main objective of the thesis has been divided into two parts:

Objective I:

- Synthesis and characterization of PEGylated reduced graphene oxide (PrGO) and its biological interaction with mouse bone marrow mesenchymal stem cells (MSCs)
    - Phase I: Synthesis and Characterization of PrGO.
    - Phase II: Isolation and characterization of Mouse Bone Marrow Mesenchymal Stem Cells (MSCs) and *in vitro* toxicity assays using MSCs.

Objective II

- Acute, sub acute exposure of PrGO to mice and to investigate the molecular toxicity, immunotoxicity, bio-distributions, toxicokinetics and histopathological analysis.
    - Phase III: Acute toxicity studies, Biodistribution and toxicokinetics
    - Phase IV: Sub acute toxicity, immunotoxicity, molecular toxicity and histopathology

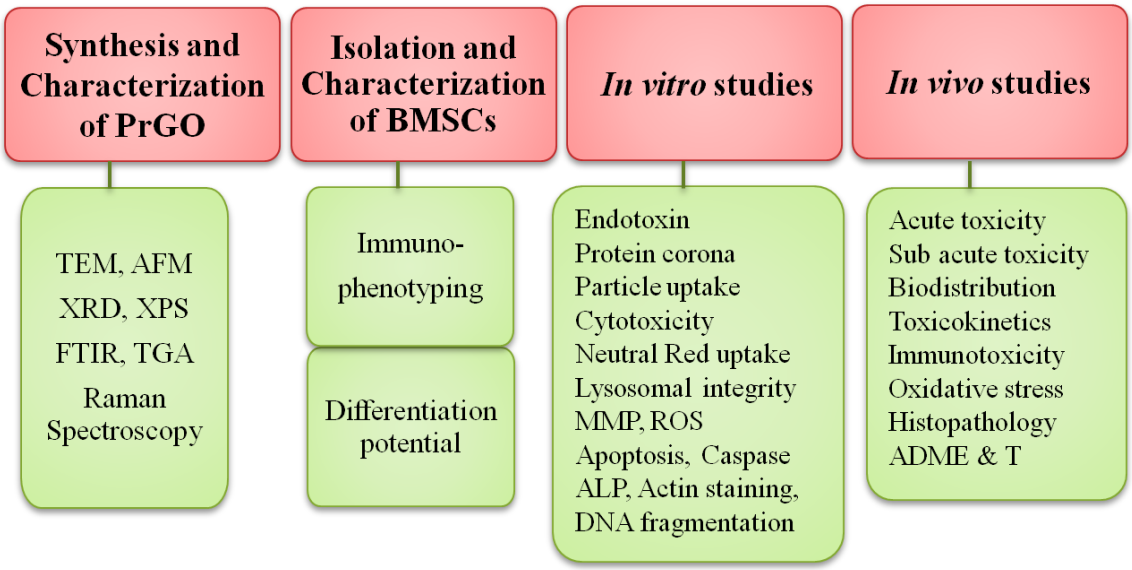

1.11. THESIS OUTLINE

The thesis has been divided into six chapters. The **first chapter** is **Introduction** that describes about the nanoparticles, global status, their applications and advantages over bulk materials. An overview of toxicity mediated by nanoparticles and cellular responses is described. The choice of stem cells as *in vitro* model for toxicity evaluation

is explained. Importance of studying the interaction of stem cells with graphene is highlighted. A well defined hypothesis of the study with specific objectives is also given.

The **second chapter** on **Review of literature** describes in detail on the chemistry of graphene and graphene based materials. Various methods for the synthesis of graphene are explained here. A brief review on biomedical applications of graphene and graphene derived materials is mentioned. Available literature on the toxicity induced by graphene towards mammalian cells is reviewed. Summary of stem cells, their properties and applications is explained in detail.

The **third chapter** describes the **Materials and Methods** and is divided into four sections. The first section deals with the synthesis and characterization of PEGylated reduced graphene oxide (PrGO). The synthesized PrGO was physico-chemically characterized. The second section deals with the establishment of *in vitro* culture model using Mesenchymal stem cells (MSCs) isolated from mouse bone marrow. MSCs are characterized for the expression of surface markers and differentiation potential. The third section deals with the preliminary toxicity evaluation and bio-nano interaction of PrGO with MSCs. Cytotoxicity, oxidative stress, mitochondrial membrane depolarization, lysosomal destabilization, apoptosis, alkaline phosphatase, DNA damage, actin staining were carried out. The fourth section describes the acute and sub-acute toxicity of PrGO. PrGO was administered intravenously and intraperitonealy into mice. Biodistribution and toxicokinetics were studied using Confocal Raman mapping. Absorption, distribution, metabolism and excretion of PrGO were investigated in acute

toxicity. Immunotoxicity, oxidative stress and histopathological examination were carried out in sub-acute toxicity study.

The **fourth chapter** deals with the **results** of all experiments. This chapter is segregated into four sections including synthesize and physico-chemical characterization of PrGO, isolation and characterization of MSCs. It also explains the results of *in vitro* toxicity assessment of PrGO in MSCs. The effect of PrGO on cell viability and function is described. *In vivo* toxicity evaluation emphasize on acute and sub-acute toxicity. Biodistribution and toxicokinetics (ADME & T) is performed after single exposure of PrGO. Immunotoxicity and histopathological analysis were done after multiple exposures to PrGO.

The **fifth chapter** describes the **discussion**. The chapter is divided into four sections. The first section discusses the method followed for PrGO synthesis. The physico-chemical characterization including size, lateral dimension, presence of characteristics graphene peaks, purity of the synthesized PrGO and confirmation of polymer coating is discussed. The second section is on MSCs isolation and characterization. The third section discusses the interaction of PrGO with MSCs and its effect on cellular morphology and function. Results of the preliminary toxicity evaluation of PrGO are discussed in detailed. The fourth section on toxicity evaluation in mice discusses the acute toxic responses induced in animals as a result of nanoparticle exposure and the less explored immunotoxicity. Sub acute toxicity also discusses the effect of PrGO in major organs such as liver, kidney, spleen and brain using histopathology analysis and the effect of PrGO in inducing oxidative stress in mice.

The **sixth chapter** discusses on the **summary and conclusion**. The study concluded that PrGO does not affect the integrity of MSCs. There were no significant decrease in cell viability or cell death was noticed. It also supports the use of stem cells as an alternate *in vitro* model for preliminary toxicity screening. No abnormalities were observed in animals after PrGO administration. However slight changes in clinical chemistry and hematological parameters were seen. Histopathological examination revealed acute hepatic injury and congestion in kidney. Significant changes in antioxidant parameters were observed, the effects were transient and it diminished over time. Future aspects of the study are also given at the end of the chapter.

CHAPTER 2: REVIEW OF LITERATURE

2. REVIEW OF LITERATURE

2.1. GRAPHITE, GRAPHENE OXIDE, REDUCED GRAPHENE OXIDE

Graphite, an allotrope of carbon is a naturally available chemical having numerous defects in its structure. The oxidation of the defect sites can be initiated using different oxidizing agents such as nitric acid, potassium chlorate (Brodie, 1859) and potassium permanganate. Depending on the source of graphite, the oxidant used, the reaction conditions followed the product changes. The primary route for synthesis of GO was developed by Hummers and Offeman by mixing graphite in mixture of potassium permanganate and sulfuric acid (Hummer & Offeman, 1958). The reaction of $KMnO_4$ with conc. H_2SO_4 gives explosive Mn_2O_7 (manganese heptoxide) which oxidizes graphite.

$2\ KMnO_4 + 2\ H_2SO_4 \rightarrow Mn_2O_7 + H_2O + 2\ KHSO_4$ (Koch, 1982)

GO is readily soluble in water (hydrophilic). The oxygen in the epoxide groups of GO forms hydrogen bond interaction with the water molecule (Lerf *et al*., 2006) thereby maintaining the stacked structure of GO. Graphite oxide differs from graphene oxide in its structure but chemically both are similar. Graphite oxide is a highly stacked structure with oxide functionalities whereas graphene oxide has a wide spacing between the layers because of the water intercalation (Buchsteiner *et al*., 2006).

GO contains chemically reactive functional groups like carboxylic acid on the edges and hydroxyl and epoxy groups on the basal plane. These oxygen containing functional groups are used for the modification of GO to make them biocompatible. The carboxylic acid groups are activated by various chemicals like thionyl chloride ($SOCl_2$),

1-ethyl-3-(3-dimethylaminopropyl)-carbodiimide (EDC), N, N'-dicyclohexyl-carbodiimide (DCC) followed by the addition of amines or hydroxyl forming covalent amide or ester bonds. In addition, polymers were also grafted on the carboxylic end of GO making it dispersible in water and solvents. Functionalization of the epoxy groups involves the ring-opening reaction (Dreyer *et al*., 2010) in which the amine groups attacks the α-carbon. Non-covalent functionalization of GO and reduced graphene oxide (RGO) is also possible via π-π stacking, van der Waals interaction.

Chemically reduced graphene looks similar to pristine graphene in terms of electrical, thermal and mechanical properties. Various reducing agents were used for the reduction of GO. The most commonly used one is hydrazine because of its non-reactivity towards water. Reduction of GO results in increased hydrophobicity and loss of functional groups on the surface. The surface area of RGO decreases because of the aggregation or precipitation during reduction and may be because of the incomplete exfoliation. GO is also treated at higher temperature to exfoliate its stacked structure. It extrudes CO_2 gas (McAllister *et al*., 2007) which creates enough pressure to separate the stacked structures. The thermal reduction creates structural defects on the surface of GO which also affects the electronic properties of the materials (Dreyer *et al*., 2010).

Preparation of stable dispersions of graphene remains a problem unsolved because of its hydrophobic nature. This is achieved by sonicating graphene suspension for several hours and also by the use of surfactants. Details of the effect of different solvents, surfactants and the importance of sonication to get a stable aqueous dispersion of GO was well thoroughly investigated (Khan *et al*., 2015). In their study, GO was dispersed in

solvents such as water, DMSO, Pyridine, ethylene glycol and are sonicated for 400 h along with the addition of sodium cholate. The treated GO samples are stable and remained as homogenous dispersion even after three weeks without any aggregation. Zhang & Zhang, (2011) demonstrated the synthesis of aqueous dispersion of single layer GO using simple magnetic stirring and heating. Nano sized GO were obtained by ultrasonication of GO which results in fragmentation from defect regions followed by the elimination of oxygen functional groups at hot spots (Gonçalves *et al*., 2014).

2.2. GRAPHENE

Graphene tagged as the 'strongest material' is a single layer of one atom thick carbon sheets that forms a honey comb lattice structure (Sekiguchi *et al*., 2004). Research based on graphene keeps on increasing rapidly from the time of its invention by Andre Geim and Konstantin Novoselov for which both of them were awarded with Nobel Prize in 2010. High electrical conductivity, mechanical strength, thermal stability and large surface area are the distinct properties of graphene that makes them suitable for wide applications. Graphene has found applications in electronic devices, sensors, composite materials and catalysts. Biomedical application of graphene is a flourishing area still in its infant stage.

The discovery of graphene seems to establish a breakthrough in current global market because there is lot of multinational research going on with these 2D material and several private companies are investing big bucks for large scale synthesis. Very few graphene based product has hit the market that includes flexible smart phone touch screens, Zap & Go (smartphone and tablet charger) that are made entirely with graphene

supercapacitors. Graphene based light bulb with low energy emission, low production cost and longer lifetime was produced by Graphene Lighting PLC. In addition, graphene has been incorporated in many devices like tennis racket, hockey stick, cycle helmet, bicycle rims to increase their toughness and flexibility.

In medical field, graphene is used as a drug carrier, biosensors, imaging, photothermal therapy and tissue engineering. The planar structure with large surface area gives graphene the maximum capacity to load drugs and biomolecules.

2.3. SYNTHESIS OF GRAPHENE

Despite the tremendous increase in the number of literature on graphene synthesis, the industrial large scale production of graphene is hard to achieve because of the various methods adopted based on the application. Graphene is obtained from GO, by removing oxygen containing functional groups via simple chemical or thermal reduction. Basically graphene synthesis is categorized into two types: top down and bottom up approach. Top down approach uses chemical ablation, electrochemical oxidation or plasma treatment to cut down graphene into small pieces. Bottom up method involves building up larger graphene sheets from simple carbon precursors. Mechanical exfoliation of graphene from pyrolitic graphite using Scotch tape was developed by Andre K. Geim and Konstantin S. Novoselov (Novoselov *et al.,* 2004). The advantage of this method is that it maintains the structural integrity of the graphene sheets but this method has disadvantage of uncontrollable thickness, size and cannot be extrapolated for large scale synthesis.

Chemical exfoliation of graphite remains simple, efficient and cost effective method for producing GO. In this method, hydrophilic graphene oxide (GO) was synthesized from graphite powders by chemical oxidation (Hummer & Offeman, 1958). GO is exfoliated in water using mechanical force (sonication). The exfoliation of graphite increases the interplanar space by the intercalating oxygen moieties in the sheets, thereby weakening the interactions between the carbon planes (Marcano *et al*., 2010). The structure of GO can be explained by Lerf–Klinowski model (Loh *et al*., 2010) as a hexagonal carbon lattice with hydroxyl and epoxyl group on the plane and the carboxyl and carbonyl group on the edges. The covalent C-O bond disrupts sp^2 conjugation of lattice making GO an insulator (Konios *et al*., 2014). The electronic and mechanical properties of GO is modified by controlling the rate of oxidation. GO may achieve different confirmations in aqueous solution (folding, bending, scrolling and planar structures), the presence of both hydrophilic and hydrophobic domains promotes bending, the most stable conformation form.

Graphene can also obtain from GO using thermal annealing or chemical reducing agents. This chemically derived graphene sheets are also called reduced graphene oxide (RGO). The chemically reduced graphene sheet undergoes incomplete reduction leaving behind few oxygen containing functional groups. Hydrazine based reduction increases the presence of sp^2 domains on the graphene sheets. Other reducing agents like sodium borohydride (Shin *et al*., 2009), hydroquinone (Wang *et al*., 2008), gaseous hydrogen (Wu *et al*., 2009), strong alkaline solutions (Fan *et al*., 2008) are also employed for the reduction of GO. The disadvantages of using chemical for reduction process are the

presence of impurities in the final product which is sometimes difficult to remove. Chemical reduction of GO is most favorable because of the high yield for large scale applications.

Electrochemical reduction of GO was developed to avoid the use of harmful reductants such as hydrazine. In this method, GO films were deposited on the surface of various substrates, then the electrodes were placed on the opposite end of the film and voltammetry was run (Zhou *et al*., 2009). The exact mechanism of reduction remains unknown, though it was suggested that the hydrogen ions present in the buffer is responsible for the reduction. The main drawback of the electrochemical reduction is scalability. The deposited RGO on the electrode surface hinders further reduction.

Chemical Vapor Deposition (CVD) is one of the most feasible and inexpensive method for synthesizing single or multi layer graphene sheets. Here, graphene sheets were grown on the surface of transition metals such as Ni, Cu, Pd that act as catalysts (Kumar & Lee, 2013). From the metal surface, the graphene sheets must be transferred to insulating materials to fabricate electronic devices. This was achieved by either chemical or thermal etching of graphene sheets from the substrate. Graphene can also be synthesized from longitudinal unzipping of multi walled carbon nanotubes (MWCNTs).

Fan *et al*., (2008) reported that GO was deoxygenated to graphene under alkaline conditions. The method involved the addition of NaOH or KOH to exfoliated GO solution at high temperature. This method is a green route synthesis because NaOH is nontoxic. Graphite oxidizes in presence of strong acids to form GO. The principle behind this method is the reversible deoxygenation of GO in presence of alkaline agents. The

reaction occurs faster at increased pH. In addition, the incomplete removal of oxygen groups under this condition (high pH) makes the negatively charged graphene sheets repulsive and prevents agglomeration.

2.4. BIOMEDICAL APPLICATIONS OF GRAPHENE

Biomedical application of graphene is a new fascinating area that is beyond imagination. The overwhelming properties of GO are amphiphilicity, surface functionality, fluorescence quenching ability and Surface Enhanced Raman scattering property (SERS). Graphene has hydrophobicity, large surface area, ripples and grain boundaries on defective sites which are important factors while considering for biomedical use. First ever use of GO as a nanocarrier for drug delivery has been reported by Sun *et al*., (2008) that paved the way to explore further use of graphene in biomedical field. Presently graphene and GO has been known to be used as a carrier for drug delivery, gene therapy, bioimaging, biosensors, antibacterial composites and scaffold for cell culture in tissue regeneration.

2.4.1. DRUG DELIVERY

GO with its oxygen containing groups (COOH and OH) has been reported as an effective carrier for drug or gene delivery. Despite the presence of functional groups, the high surface area and basal planar structure with sp^2 domain afford them high loading capacity, high solubility and biocompatibility. Multimodal GO with multiple function is produced by conjugating polymers, proteins and biomolecules via simple physisorption or chemical conjugation. GO act as an efficient nanocarrier for delivering water insoluble anticancer drugs. Water insoluble anticancer drug SN38 was successfully loaded onto

amine terminated PEG grafted GO and targeted against cancer cells (Liu *et al*., 2008). Selective killing of cancer cells were achieved by (Sun *et al*., 2008) loading doxorubicin (DOX) onto antibody conjugated PEGylated NGO sheets (Figure 2.1a). Similarly, co-delivery of anticancer drugs such as DOX and Camptothecin (CPT) was demonstrated by Zhang *et al*., (2010) using folic acid conjugated GO complexes. Shen *et al.,* (2012) developed GO based pH sensitive anti-inflammatory and thermo responsive drugs for drug delivery.

2.4.2. GENE DELIVERY

Gene therapy is a technique used to successfully treat various genetic disorders. Successful gene therapy is achieved by developing a vector that protects the DNA from endonuclease and possess high transfection efficiency. GO functionalized with positively charged cationic polyethyleneimine (PEI) was transfected with plasmid DNA (Feng *et al*., 2011). The plasmid DNA was condensed in GO, because of electrostatic interaction resulting from positively charged PEI and negatively charged nucleic acid. This not only formed a stable construct but also improved the transfection efficiency of the vector with decreased cytotoxicity. PEI-GO complexes are also utilized for sequential delivery of Bcl-2 targeted siRNA and drug DOX for enhanced therapeutic purposes (Zhang *et* al., 2011). The complex exhibited higher cytotoxicity because of the synergistic effect of drug and siRNA (Figure 2.1b).

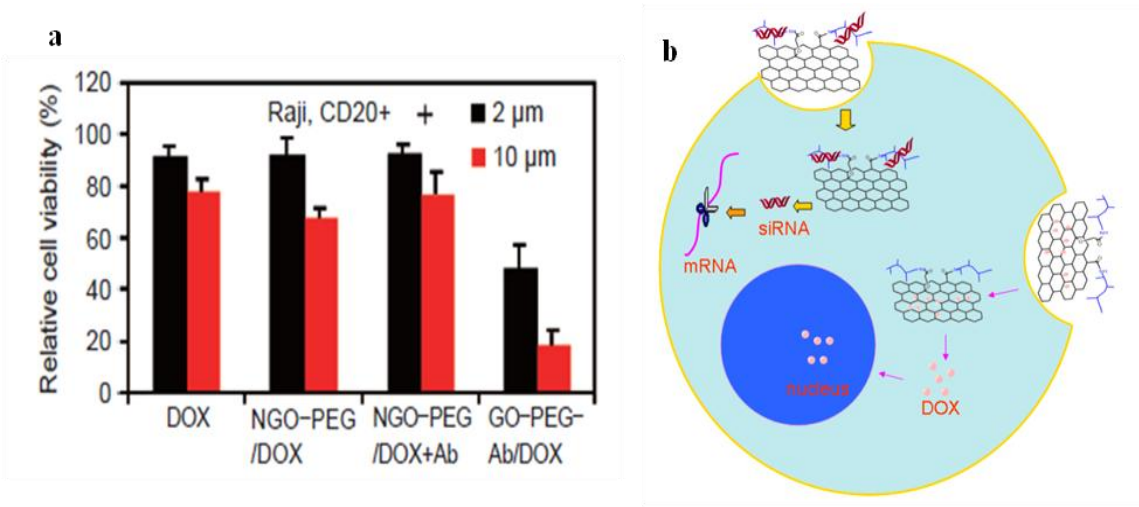

Figure 2.1: Drug delivery and gene delivery. (a) Percentage of cell viability in cancer cells treated with diferent concentration of doxorubicin and PEGylated nanographene oxide (Adapted from Nano Res, 1, 2008); (b) Sequential delivery of siRNA and anticancer drug (Adapted from Small, 7, 2011).

2.4.3. PHOTOTHERMAL THERAPY

GO shows higher absorbance in NIR region, a property that is utilized for photothermal destruction of tumor cells (hyperthermia) (Robinson *et* al., 2011; Yang *et* al., 2013). Yang *et al*., (2010) reported that PEGylated GO showed high tumor uptake efficiency when injected into mouse tumor model. It also exhibited high retention time owing to enhanced permeability and tumor destruction (Figure 2.2a, b). The cell death occurs as a result of oxidative damage, mitochondrial depolarization and caspase activation leads to cytochrome c release resulting in apoptosis and necrosis.

Photodynamic therapy (PDT) is a novel treatment for cancer as it combines photosensitizers mediated targeted killing. Chlorine 6, a photosensitizer has been loaded onto GO via hydrophobic and π-π stacking showed effective killing of cancer cells under irradiation (Huang *et al*., 2008).

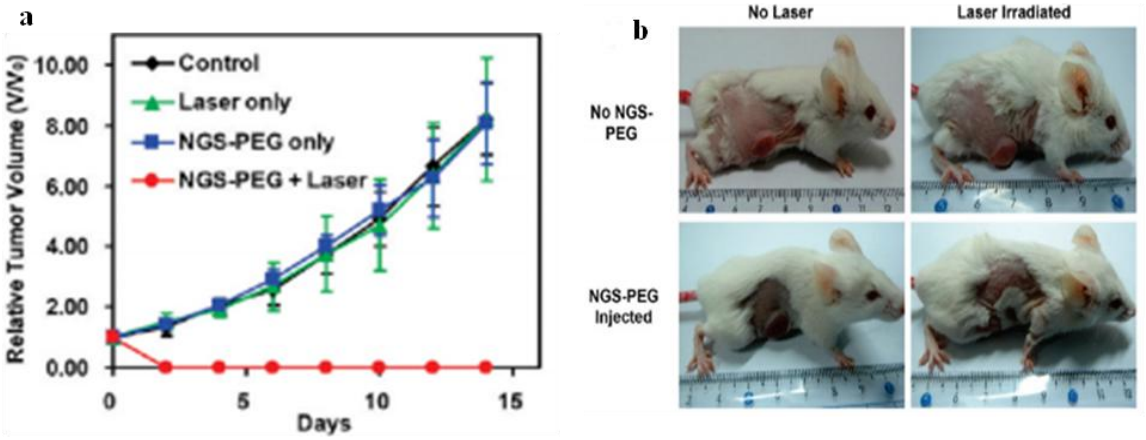

Figure 2.2: Photothermal therapy. (a) Tumor volume after treatment; (b) Photos of tumor in mice after treatment (Adapted from Nano Lett, 10, 2010).

2.4.4. BIOSENSING

Graphene based field effect transistor biosensors has been developed to detect biomolecules like nucleic acids, proteins and growth factors, which monitors changes in electrical signal. Developing graphene based biosensors relies on the fluorescent quenching property of graphene. The detection of nucleic acid was done by tagging GO with fluorescent labeled ssDNA. GO quenches the fluorescence of ssDNA. This ssDNA forms double helical structure when it comes in contact with the target complementary sequence (Figure 2.3a). The formation of double helix displace GO from ssDNA strand resulting in fluorescence recovery. FRET biosensors, FET biosensors, biosensors for DNA detection (Shen *et al*., 2012) were developed with graphene based materials. For example, nitrogen doped graphene FET biosensors for detecting vascular endothelial growth factor, biosensor for catecholamine detection were developed. Lu *et* al., (2009)

developed Chemical Vapor deposition (CVD) graphene FET biosensors for detecting electrical signals from electrogenic cells (cardiomyocytes).

Graphene based biosensor for the detection of pathogens was also developed. Huang *et al*., (2011) demonstrated nanoelectronic biosensor for the detection of *E. coli*. CVD grown graphene film was functionalized with anti *E. coli* antibodies and are passivated using Tween 20. This graphene biosensor detects *E. coli* with high specificty and selectivity (Figure 2.3b). The conductance of the graphene sensor increases with the increase in number of *E. coli* attached on the graphene sheets.

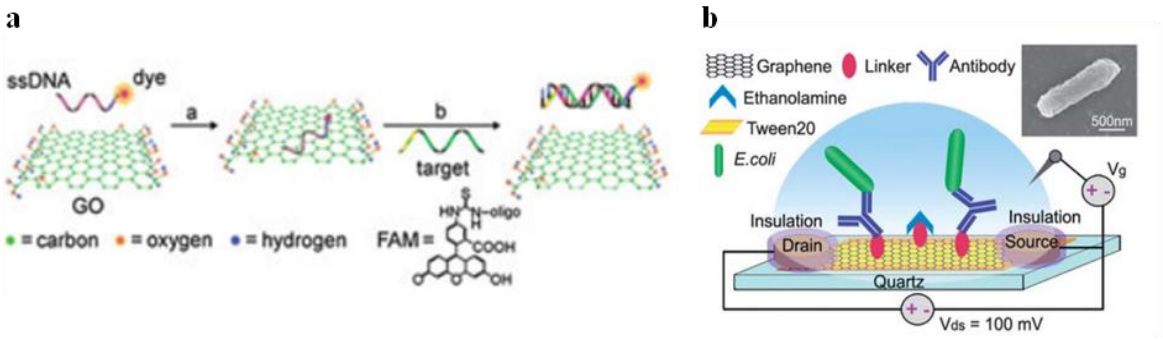

Figure 2.3: Graphene based biosensors. (a) FRET biosensr for nucleic acid detection (Adapted from Angew Chem Int Ed, 2009). (b) Biosensor for the detection of pathogens (Adapted from J Mater Chem, 21, 2011).

2.4.5. BIOIMAGING

Since GO possess strong absorbance and fluorescence property in NIR region, it is used as an imaging tool. The presence of functional groups on the sides of the planar graphene can be conjugated with fluorescent dyes for bioimaging. Jin *et al*., (2013) states that GO in nano form shows photoluminescence properties which arises from the quantum confinement effect utilized for bioimaging purposes. GO with size less than

10nm described as graphene quantum dots (GQDs) is prepared from GO (Figure 2.4a, b, c). GQDs were also prepared from pre oxidized graphene sheets by hydrothermal cutting, oxygen plasma treatment. Compared with conventional fluorescent probes and other QDs, GQDs possess high stability, excellent biocompatibility, good solubility and low cytotoxicity. GQDs also exhibit upconversion fluorescence (excitation at NIR) that reduces interference from autofluorescence (Shen *et al*., 2011).

2.4.6. ANTIBACTERIAL ACTIVITY

Both GO and RGO were known to possess antibacterial activity against wide range of bacteria. It was also found that Gram negative bacteria like *Escherichia coli* was less sensitive to graphene than Gram positive bacteria *Staphylococcus aureus*. The presence of outer membrane on Gram negative bacteria protects them from cellular damage. Graphene exhibit antibacterial activity by directly interacting with the cell membrane. A three step mechanism was explained (Liu *et al*., 2011) for the antibacterial action of graphene: (i) Bacteria attaches to the surface of graphene sheets (ii) membrane damage resulting in intracellular contents leakage and (iii) oxidizes membrane lipids and proteins (Figure 2.5).

RGO nanowalls were found to be more toxic towards bacteria than GO because of the better charge transfer with the bacterial cells and presence of sharp edges of RGO (Akhavan & Ghaderi, 2010). The sharp edges induce membrane perturbation leading to leakage of intracellular contents. Graphene also act as a good electron acceptor and prevent the electron transfer in electron transport chain (ETC) resulting in depletion of Adenosine triphosphate (ATP) and eventually cell death. For Gram negative bacteria,

minimum inhibitory concentration (MIC) was found to be 1 µg/ml whereas for Gram positive bacteria, MIC was found to be 4-8 µg/ml (Krishnamoorthy *et al*., 2012).

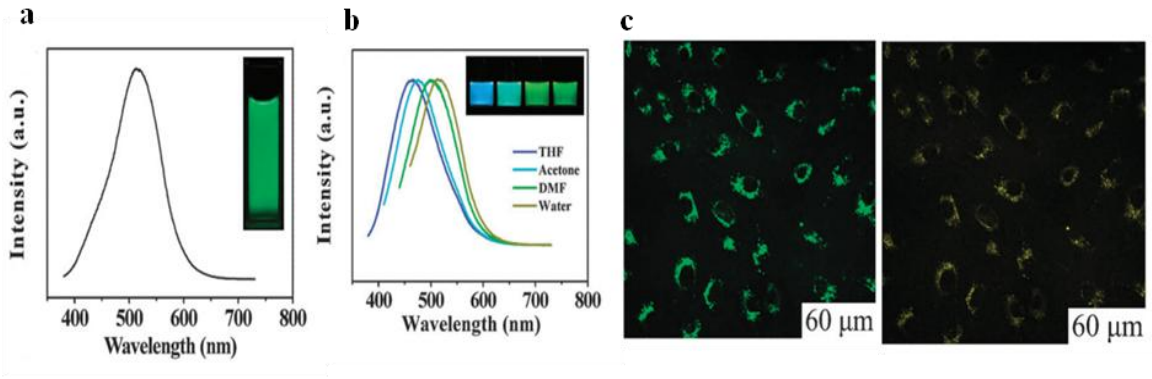

Figure 2.4: Graphene quantum dots for bioimaging. (a) Fluorescence spectra of GQDs excited at 375 nm; (b) Spectra in different solvents; (c) Cellular imaging under different excitation. (Adapted from Chem commun, 47, 2011).

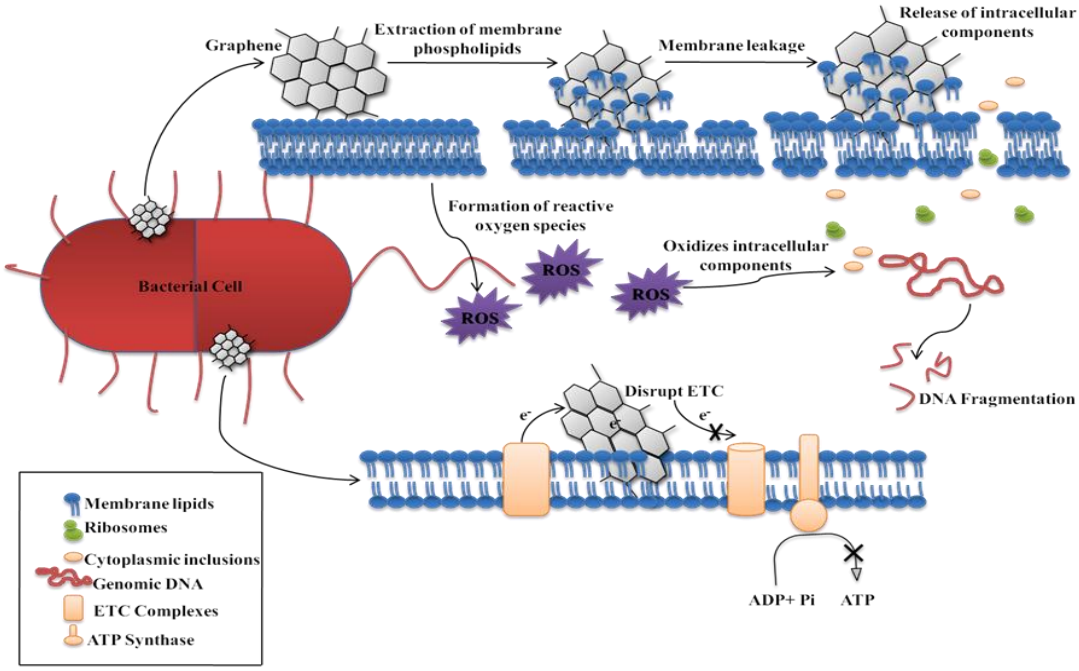

Figure 2.5: Mechanism of bacterial toxicity

2.4.7. TISSUE ENGINEERING

2.4.7.1. SCAFFOLD FOR CELL CULTURE

Successful tissue engineering depends on the substratum that offers cells to attach, grow and must be biocompatible. GO is used as surface coating for implants. Graphene/chitosan film has been observed to induce the proliferation and differentiation of human mesenchymal stem cells. Stem cells are one of the most promising candidates for tissue regeneration because of its differentiation into cells of specific lineage. Recently graphene becomes the spotlight as a reliable scaffold for the attachment and proliferation of stem cells especially mesenchymal stem cells and neuronal cells. Several cell lines were cultured on the surface of graphene coated substratum, for example; osteoblasts (Kalbacova *et al*., 2010), NIH-3T3 cells (Ryoo *et al*., 2010), MCF-7 (Guo *et al*., 2010) and MSCs. MSCs grown on graphene surface attached and form spindle shape with high proliferation and differentiation potential towards osteoblasts lineage (Figure 2.6). GO and graphene exhibit differences in stem cell differentiation because of their different surface chemistry.

Graphene supports osteogenic and suppress adipogenic differentiation (Chung *et al*., 2013) mainly because of different growth factors attached on their surface. Hybrid paper made of RGO and TWEEN was developed by Park *et al*., (2010). This paper is biocompatible and retains antibacterial properties which impede the growth of any bacteria.

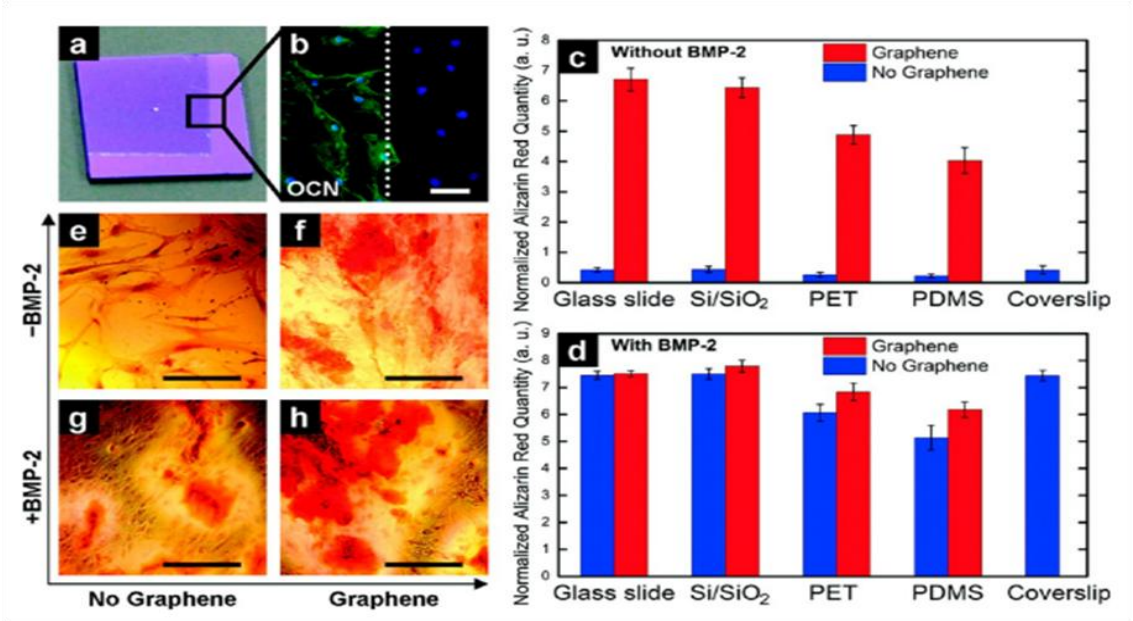

Figure 2.6: Osteogenic differentiation on graphene substratum. (a) graphene coated SiO_2 chip; (b) osteocalcin staining; (c,d) Alizarin red quantification; (e-h) cells grown on polyethylene terephthalate substrate stained with alizarin red. (Adapted from ACS Nano, 2011)

Another important property of graphene is its electrical conductivity. This property enables graphene to modulate neural stem cell activity. The findings suggested that graphene differentiate human neural stem cells into neurons. Neural stem cells are readily and firmly attached on graphene which promote their differentiation into neurons than glial cells (Figure 2.7). Graphene promotes the sprouting of neurites and also increases the number of neurites in mouse hippocampal neural cells (Li *et al*., 2011). The number of neurite and the average length increases in pristine graphene culture compared to tissue culture polystyrene substrate. Various graphene based composites has been developed and tested for their biocompatibility, for example graphene and PCL (poly–ε-caprolactone) (Sayyar *et al*., 2013), graphene and chitosan (Fan *et al*., 2010), graphene

based porous hydrogel scaffolds (Lim *et al*., 2011) and GO-polypropylene carbonate nanofoams (Yang *et al*., 2013a).

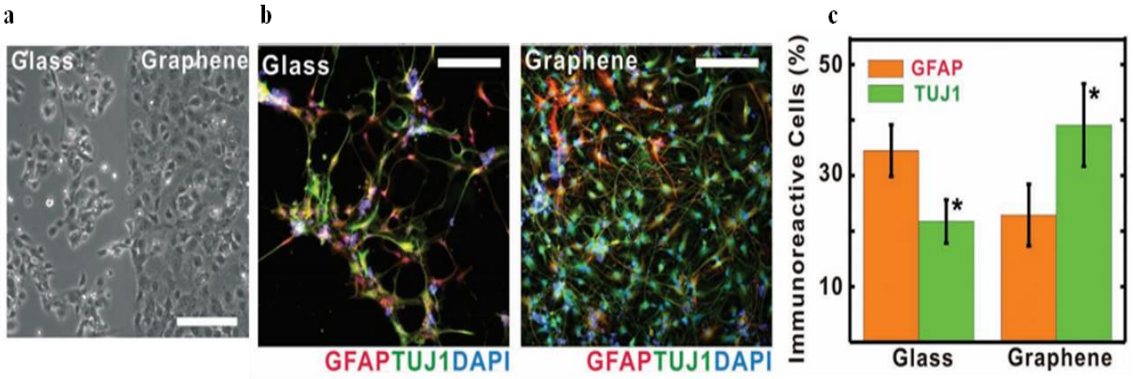

Figure 2.7: Neural stem cells differentiation. (a) Cells grown on glass and graphene; (b) Immunostaining of neuron markers; (c) Quantificaton of expression of neuron markers. (Adapted from Adv Mater, 23, 2011).

2.5. TOXICITY OF GRAPHENE

It is well reported that graphene interacts with the biological system and this complex interaction induces several responses in the cells. Several reports (Li *et al.*, 2012; Sasidharan *et al.*, 2011; Zhou *et al.*, 2012) were available on the toxicity induced by pristine graphene and graphene derivatives towards mammalian cells. The putative hazard arises from the exposure to graphene needs to be addressed before certifying its use for biomedical application. Shape, size, surface chemistry and aggregation status are critical for the bio-nano interaction of graphene derived materials. It was found that physical adsorption of graphene with its sharp edges can penetrate cell membrane causing membrane damage and leakage of cytoplasmic contents. Zhang *et al.*, (2010) supports that planar graphene sheets are less cytotoxic to PC12 cells compared to carbon nanotubes. Smaller GO was found to decrease cell viability and showed increased

hemolytic potential compared to larger GO sheets. The lateral dimension also plays a crucial role in graphene cell interaction. RGO with lateral dimension of 11 nm translocate to the nucleus and induce genotoxicity such as DNA fragmentation and chromosomal aberration (Guo & Mei, 2014). A recent review on safety and biocompatibility of graphene and GO by *in vitro* and *in vivo* methods was published by Syama & Mohanan, (2016).

Physical interaction of graphene with the bacterial cell membrane induces toxicity. The sharp edges of the graphene sheet causes damage on the cell membrane resulting in leakage of intracellular contents. Both GO and RGO induces cytotoxicty, oxidative stress and DNA damage in mammalian cells. GO promotes NADPH oxidase dependent ROS formation coupled with deregulation of antioxidant genes whereas physical stress induced by the presence of RGO results in increased ROS production (Jarosz *et al.,* 2016).

Li *et al*., (2012) reported that pristine graphene provoke cytotoxicity by disrupting mitochondrial membrane potential and activates mitochondria mediated apoptosis. *Bim, Bax* (proapoptotic factors) activation induces mitochondrial permeablization and these factors are released into the cytosol which eventually activates several cascades of caspase enzymes ultimately resulting in cell death. Graphene directly disrupt mitochondrial ETC by acting as an electron acceptor. The disruption of ETC subsequently decreases ATP production leading to cell death by starvation.

RGO elicits innate immune response by activating Toll like receptors-Nuclear Factor kappa beta (TLR-NF-kB). Exposure of macrophages to sub cytotoxic

concentration of graphene (20 µg/ml) activates cell death by MAP Kinase and TGF pathways (Li *et al.*, 2012). Several proinflammatory cytokines (IL-1α, IL-6, IL-10, TNFα and GM-CSF) and chemokines (MCP-1, MIP-1α, MIP-1β) are released upon macrophage activation. Figure 2.8 details the mechanism of toxicity induced by graphene towards mammalian cells.

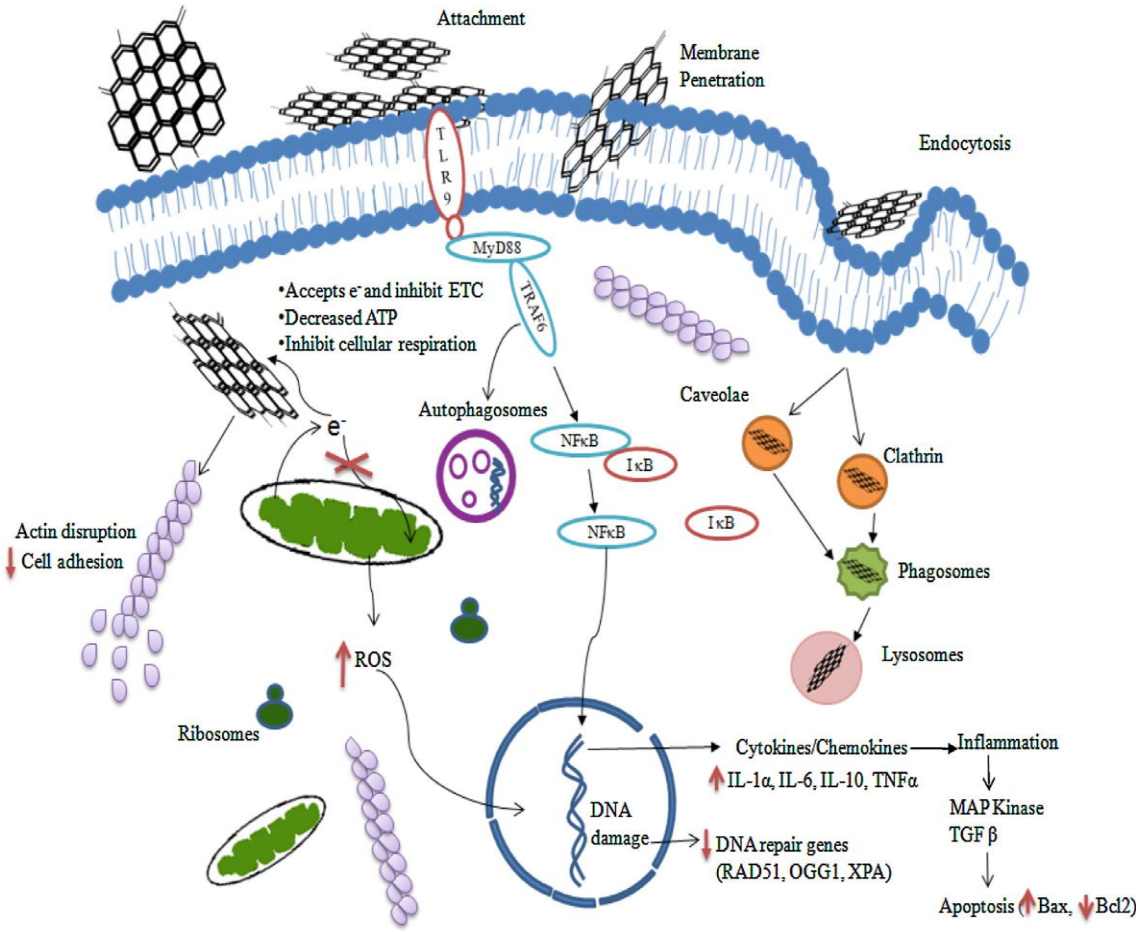

Figure 2.8: Mechanism of toxicity of graphene nanoparticles (Adapted from Int J Biol Macromolec, 86, 2016).

GO is also known to promote autophagy by activating TLR associated pathway (Chen *et al.*, 2012). Upregulation of TLR 4 and TLR 9 activate MyD88, TRAF-6

inducing the formation of autophagosomes. Subsequent activation of NF-kB induces the transcription of several cytokines. Also, the cells treated with GO showed increased expression of Bectin-1 and LC3-II (autophagic marker).

Very few studies reported the genotoxic effects of graphene. Wang *et al*., (2013) reported that GO induce genotoxicity in a dose dependent manner. Graphene effectively interact with genomic DNA and induce mutation such as base transitions and deletions. Exposure to GO increases the expression of DNA repair genes such as *ATM* and *Rad1*.

The above studies focused on the mechanism of toxicity induced by graphene and graphene based materials towards mammalian cells. The interaction of graphene with stem cells is a newly emerged area having great potential in tissue engineering field. The toxicity of graphene or its derivatives is not well established. However, it was reported graphene enhances the proliferation and growth of stem cells. Most of the studies were focused on GO and very few literature were available on the nano-bio interaction of RGO. The *in vivo* biodistribution, toxicokinetics and immunotoxicity of graphene is less explored area. Hence the thesis focused on the interaction of PEGylated reduced graphene oxide (PrGO) with mesenchymal stem cells and also elucidated the toxic profile of PrGO under *in vivo* conditions using Swiss Albino mice.

2.6. MESENCHYMAL STEM CELLS (MSCs)

Mesenchymal stem cells are almost found in all tissues as pericytes. This can be isolated from bone marrow, adipose, muscle, cartilage, bone and tendon. These cells were first isolated from bone marrow stroma, spleen and thymus by Alexander Friedenstein (Friedenstein *et al*., 1976). MSCs can also be isolated from cartilage, periostium, muscle

and tendons, umbilical cord and placenta. Large quantities of cells were obtained from adipose tissue because of its vast existence. Bone marrow is a region in which two distinct lineages of cells (haematopoietic and mesenchymal) co-exist and function together. Bone marrow stem cells are the progenitors of skeletal tissues. Marrow stem cells exhibit transgermal plasticity (ability to differentiate into cells of unrelated origin). Trauma, tumor, necrosis, inflammation will guide MSCs to migrate and differentiate into cells of connective tissue lineage. Bone marrow stromal cells or mesenchymal stem cells are easily separated from the haematopoietic cells in culture by frequent medium change. The stromal cells possess plastic adherence property and are rapidly attach on the culture flasks and appear like fibroblasts (Kundrotas, 2012). The cells form discrete colonies of elongated cells with each colony arising from a single cell called colony forming unit fibroblasts (CFU-F).

Mesenchymal stem cells possess self renewing property and undergo symmetric division. This maintains the stemness and the cells also respond to the environmental cues by differentiating into specific lineage. Upon activation by specific factors, MSCs transdifferentiate into cells of non-mesodermal lineage such as neurons, astrocytes, oligodendrocytes and hepatocytes. In addition to the growth factors and cytokines, Leukemia Inhibitory Factor (LIF), Fibroblast Growth Factor (FGF) and Wnt were studied to maintain stemness. LIF, a pleiotropic cytokine maintain MSCs stemness and activates osteoblasts, repress osteoclast activities (Kolf *et al.,* 2007). It was also found that MSCs also express *oct-4*, *sox-2*, and *rex-1* embryonic stem cell marker. *oct-4* is known to

upregulate HIF-2α (Hypoxia Induced Factor-2α), which is responsible for maintaining the stemness of MSCs under hypoxic condition.

2.7. SURFACE MARKERS OF MSCs

MSCs are great source for tissue engineering purposes because of its ease of isolation from different tissues and it is one of the most thoroughly studied stem cells for regenerative medicine. MSCs were isolated from the other cell population by the expression of their cell surface antigens. MSCs are negative for some of the markers expressed by other cells (CD 11b- immune cell marker, CD45 (Leukocyte common antigen), CD117 - haematopoietic stem cell marker; CD31- endothelial and haematopoietic cells). Positive markers expressed by MSCs are Stro-1 (cells ability to form colonies), CD106 or VCAM (Vascular Cell Adhesion Molecule), CD73 (Ecto-5'-nucleotidase), CD44 (Hyaluronate receptor), CD90 (Thy-1 glycoprotein), CD29 (Very late antigen β) etc. (Kolf *et al*., 2007). They also express α-SMA (α-Smooth Muscle Actin) and 3G5 justifies the perivascular origin.

2.8. DIFFERENTIATION OF MSCs

MSCs readily differentiated into three different cell lineages: chondrocytes, osteoblasts and adipocytes (Figure 2.9). Differentiation is achieved by culturing stem cells under appropriate medium with specific differentiation inducing factors.

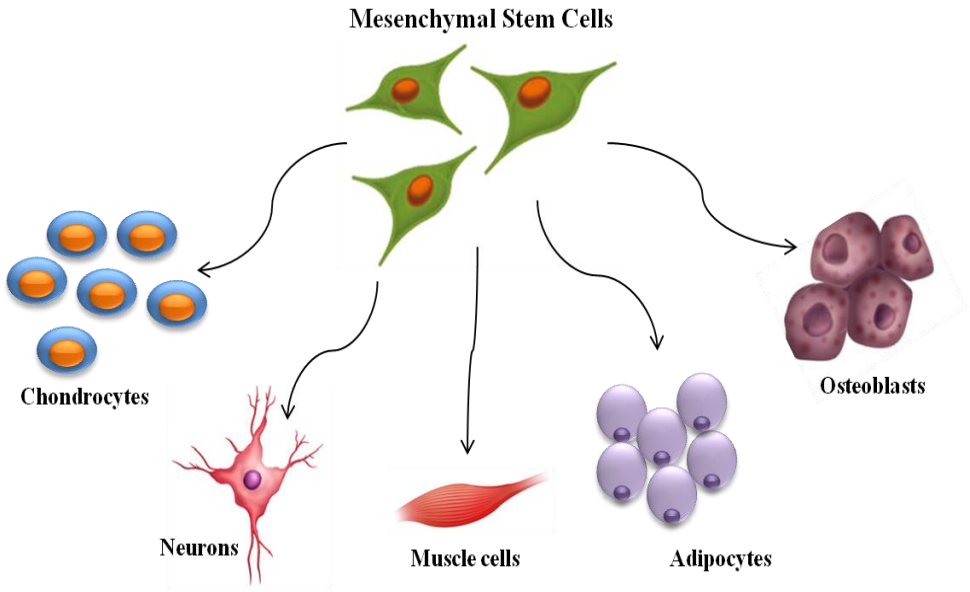

Figure 2.9: Differentiation of MSCs into specific lineages

2.8.1. CHONDROGENESIS

MSCs readily differentiate into chondrocytes and express specific markers like transcription factors (sox 9) and extracellular matrix genes (collagen types II and IX, aggrecan, biglycan, decorin, and cartilage oligomeric matrix protein) (Baksh *et al*., 2004). Transforming Growth Factor (TGF-β) and Bone Morphogenetic Protein (BMP) regulates Mitogen Activated Protein Kinase (MAPK) signaling pathway and activate Smad proteins for chondrogenic differentiation. Wnt plays a critical role in regulating chondrogenesis. Wnt 7a activates TGF-β/BMP signaling pathway whereas Wnt1 inhibits chondrogenesis by upregulating Twist 1, a transcription factor (Reinhold *et al*., 2006).

2.8.2. OSTEOGENESIS

BMP-2 and BMP-6 were known to regulate osteogenesis in specific BMP-2 induces Runx2 acetylation (Jeon *et al*., 2006). Runx2 is a principal osteogenic gene

which is degraded by Smurf proteins during inflammation. Also, tbx -5 a homeobox gene activates *FGF10* osteogenic gene.

2.8.3. ADIPOGENESIS

Peroxisome proliferators activated receptor γ (PPARγ) augments MSCs adipogenesis and inhibits osteogenesis. Stretch mediated mechano stimulation activates Tension Induced Proteins (TIP-1) which is expressed under non stretch condition and activates adipogenesis (Nuttall & Gimble, 2004; Jakkaraju *et al*., 2005). Figure 2.10 illustrates the gene expression and various growth factors responsible for inducing differentiation.

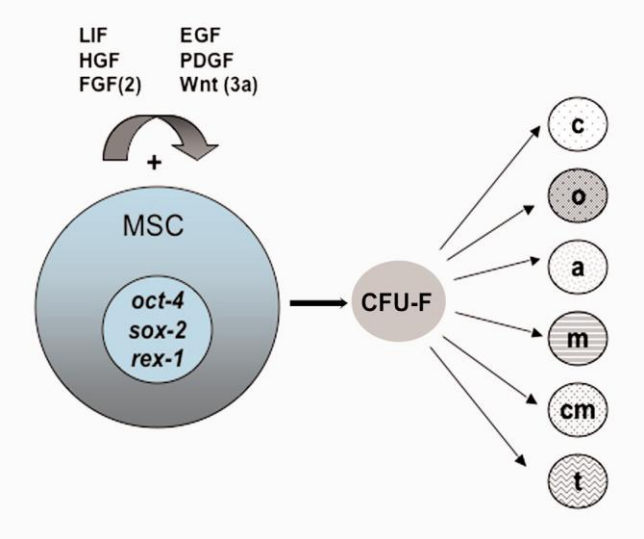

Figure 2.10: Growth factors for MSCs differentiation. (Adapted from Arthritis Res Ther, 9, 2007).

2.9. APPLICATION OF MSCs

MSC has the potential to migrate to the injured site which is regulated by stromal-derived factor-1/CXCR4, hepatocyte growth factor/c-Met complexes and matrix

metalloproteinase (Son *et al*., 2006). MSCs can facilitate fracture healing and remodeling of bone with the help of several growth factors like bone morphogenetic protein (BMP), insulin like growth factor (IGF), platelet derived growth factor (PDGF) and fibroblast growth factor (FGF). Murphy *et al*., (2003) reported that the damaged cartilage was regenerated after MSCs was injected into the injured knee joints. The migration of MSCs towards the injured site helps in treating myocardial infarction, fracture and spinal cord injury (Sohni & Verfaillie, 2013).

The hypothesis of the thesis has two main objectives such as

1. Synthesis and characterization of PEGylated reduced graphene oxide (PrGO) and its biological interaction with Mouse Bone marrow mesenchymal stem cells (BMSCs) and
2. Acute, sub acute exposure of PrGO to mice and to investigate the molecular toxicity, immunotoxicity, bio-distributions, toxicokinetics and histopathological analysis.

   To fulfill the objective of the thesis following methodologies were adapted.

CHAPTER 3: MATERIALS AND METHODS

3. MATERIALS AND METHODS

3.1. CHEMICALS

Ammonium per sulfate, Acrylamide, Ascorbate-2-phosphate, Alizarin red, Bovine serum albumin, Bisacrylamide, Dexamethasone, Dimethyl sulfoxide, 5, 5'-dithiobis- (2-nitrobenzoic acid (DTNB), 1-Ethyl-3-(3-dimethylaminopropyl) carbodiimide (EDC), β-glycerophosphate, Histopaque, Indomethacin, O,O′- Bis(2-aminoethyl) polyethylene glycol (PEG) (Fluka, Mn 1900), Oil Red, Oxidized glutathione (GSSG), Reduced glutathione (GSH), Rhodamine Phalloidin, RPMI-1640, Sodium dodecyl sulfate, SigmaFast BCIP/NBT, Tris base, Thiobarbituric acid and Trypan blue were purchased from Sigma. Concentrated sulfuric acid, ethanol, formaldehyde, graphite, glacial acetic acid, hydrogen peroxide, hydrochloric acid, methanol, sodium borohydride, triethylamine was from Merck, India. Potassium permanganate purchased from Sd Fine Chemicals, Mumbai. Acridine orange, Coomassie Brilliant blue, 4, 6-Diamidino-2-Phenylindole (DAPI), Giemsa stain were purchased from Himedia Laboratories, India. Antibiotic and antimycotic solution (10,000 units/mL of penicillin, 10,000 µg/mL of streptomycin and 25 µg/mL of fungizone® antimycotic) were purchased from Gibco (Grand Island NY, USA). Acridine orange, Apoptosis DNA ladder assay kit, Alexa Flour 488 Annexin V/Dead cell apoptosis kit, 2,7-dichlorodihydrofluorescein diacetate (H_2DCFH-DA), DMEM-High Glucose, Fetal bovine serum (FBS), JC-1 probe, Phosphate buffered saline (Ca^{2+}, Mg^{2+} free; PBS) and 0.25% trypsin EDTA were purchased from Invitrogen, USA. Sensolyte homogenous AMC Caspase-3/7 assay kit (Anaspec, Fremont, CA), Endosafe®-PTS (Charles River, USA). Ethidium bromide, 3-(4, 5-dimethyl thiazol-2-yl)-

2, 5-diphenyltetrazolium bromide (MTT), Neutral red indicator, sodium carbonate and trisodium citrate were from Sisco Research Laboratories (SRL), India. ^{3}H-tritiated thymidine was from American Radiolabelled Chemicals Inc. Rat mAb to CD 90/Thy 1, Rat mAb to CD 44, Rat mAb to CD 45, Rat IgG FITC, Cytopainter were purchased from Abcam. Diethylene triamine penta acetic acid (DTPA), pyrogallol from Central Drug House (CDH) analytical reagents, Delhi. All sterile cell culture plastic wares were purchased from Nunc.

3.2. EQUIPMENTS

UV Visible Spectrophotometer (UV 1601, Shimadzu, Japan, Lamda 25, PerkinElmer, Singapore), Laminar air flow (Mark Air particulars, India), Incubator shaker (New Brunswick Scientific, USA), Biophotometer (Eppendorff, Germany), Steam sterilizer (Nat Steel, India), CO_2 incubator (Sanyo, Japan), Monochromator based multimode microplate reader (BioTeck Instruments, USA), Thermomixer (Eppendorff, Germany), Bio Imaging system (Syngene, UK), Rotor stator homogenizer (Polytron, PT 3100, USA), micro-plate reader (Says Expert plus, Austria), Refrigerated centrifuge (Eppendorf, USA), Fluorescent microscope (Axio Scope A1 Carl Zeiss, Germany), phase contrast microscope (Leica), hematology counter (Animal Blood Counter, India), biochemical analyzer (ERBA, India), FACS Aria III (BD Biosciences). TEM and SAED was done using JEOL JEM 2100 Transmission electron microscope (Japan) under an accelerating voltage of 200 kV. AFM images were recorded with Cypher S Atomic Force Microscope, Asylum Research (United Kingdom). All the images were acquired using a tapping mode under ambient conditions. XRD was analyzed using SmartLab X-ray

diffractometer, RIGAKU (Japan). XPS was carried out using AXIS-His, Kratos, Shimadzu (United Kingdom) at a current of 10 mA and voltage 12 kV using Mg/Al dual anode monochromator. Thermal analysis was carried out with Thermal Analysis Instrument, DTG-60H, Shimadzu (Japan), Raman scattering was done with the help of Lab RAM, HR-800, Horiba Jobin Yvon S.A.S (Japan) with excitation laser wavelength of 633 nm. FTIR was performed using Nicolet iS50, ThermoFisher (United States of America) with ATR module.

3.3. ANIMAL HUSBANDRY AND WELFARE

Swiss Albino mice were procured from the Division of Laboratory Animal Sciences, Biomedical Technology Wing, Sree Chitra Tirunal Institute for Medical Science Technology, Trivandrum. The body weights of the animals were between 17 – 23 g. The animals were maintained in a 12 h light/dark cycle at a constant temperature of 22±3°C and humidity (30-70 %). Commercially available feed and aquaguard filtered water were provided *ad libitum*. Individual animals were identified with picric acid marks on the body. In addition to this, each animal cage was identified with labels having details such as experiment name, number, date, and number of animals. All the animals were acclimatized for a period of 5 days before initiation of the experiment.

3.4. ANIMAL ETHICS

All animals were handled humanely, without making pain or distress and with due care for their welfare. The care and management of the animals will comply with the regulations of the Committee for the Purpose of Control and Supervision of Experimental Animals (CPCSEA), Govt. of India. All the animal experiments were carried out after

getting prior approval from Institutional Animal Ethics Committee (IAEC) and in accordance with approved institutional protocol. The IAEC number for this study is SCT/IAEC-132/December/2014/86.

3.5. INSTITUTIONAL COMMITTEE FOR STEM CELL RESEARCH

Bone marrow mesenchymal stem cells (MSCs) were collected from Swiss Albino mice. All the experiments with MSCs were carried out after getting the approval from Institutional Committee for Stem Cell Research (IC-SCR). The approval number is SCTIMST/ICSCR/No 17/Oct 2014.

3.6. SYNTHESIS OF PEGYLATED REDUCED GRAPHENE OXIDE (PrGO)

3.6.1. SYNTHESIS OF GRAPHENE OXIDE (GO) FROM GRAPHITE

Graphene Oxide (GO) was synthesized from powdered graphite using modified Hummer's method (Hummers & Offeman, 1958). In short, 1g of graphite was mixed with 23 ml of conc. H_2SO_4 in presence of ice. 3 g of $KMnO_4$ was gradually added to the mixture by keeping the reaction temperature below 20°C. The reaction mixture was transferred to a water bath and the temperature was increased to 35 °C. The reaction was kept at this temperature for 30 min with constant stirring. After 30 min, 46 ml of de-ionized water was slowly added and the temperature was increased to 98°C, the reaction was continued for another 15 min. Finally, 140 ml of de-ionized water and 10 ml of H_2O_2 was added to the mixture and the reaction was stopped. The obtained yellow brown precipitate of GO was washed with 5% HCl (centrifuged at 9000 rpm, 5 min) and followed by water to remove acids and sulfate ions.

3.6.2. PEG COUPLING OF GO

For PEG coupling onto GO flakes, 0.5 g of synthesized GO was dispersed in 330 ml of water and the pH of the suspension was changed to basic (pH 8.5) using triethylamine. 600 mg of O,O′- Bis(2-aminoethyl) polyethylene glycol (PEG) was dissolved in 300 ml of de-ionized water and added to the GO dispersion drop wise under magnetic stirring. 0.5 g of EDC was dissolved in 100 ml of de-ionized water and added to the above mixture two times intermittently. The reaction was kept under constant stirring for overnight.

3.6.3. SYNTHESIS OF PEGYLATED REDUCED GRAPHENE OXIDE (PrGO)

The GO-PEG solution was centrifuged at 4000 rpm for 15 min and the supernatant was filtered using filter paper (PALL life science, Grade P1, P1125) and the filtrate was collected. 2 g of sodium borohydride ($NaBH_4$) dispersed in 100 ml of ice cooled water was added drop wise to the above filtrate and the reaction temperature was set at 70°C. The reduction reaction was continued for 2 h and the obtained PrGO was centrifuged (12000 rpm, 15 min) and washed in de-ionized water several times in order to remove any impurities. The flowchart of the synthesis protocol is given in Figure 3.1 and the photographic representation is given in Figure 3.2.

3.6.4. SYNTHESIS OF REDUCED GRAPHENE OXIDE (RGO)

Reduced Graphene oxide (RGO) was synthesized from GO using $NaBH_4$ as reductant. In short, 500 mg of GO was dispersed in 330 ml of de-ionized water. 4 g $NaBH_4$ dissolved in 100 ml of ice cold de-ionized water was added slowly and the reaction mixture was stirred at 80°C for 1 h. The final black precipitate was washed

(centrifuged at 12000 rpm, 15 min) several times using de-ionized water. The synthesized RGO was solely used for characterization purpose and compared with PrGO.

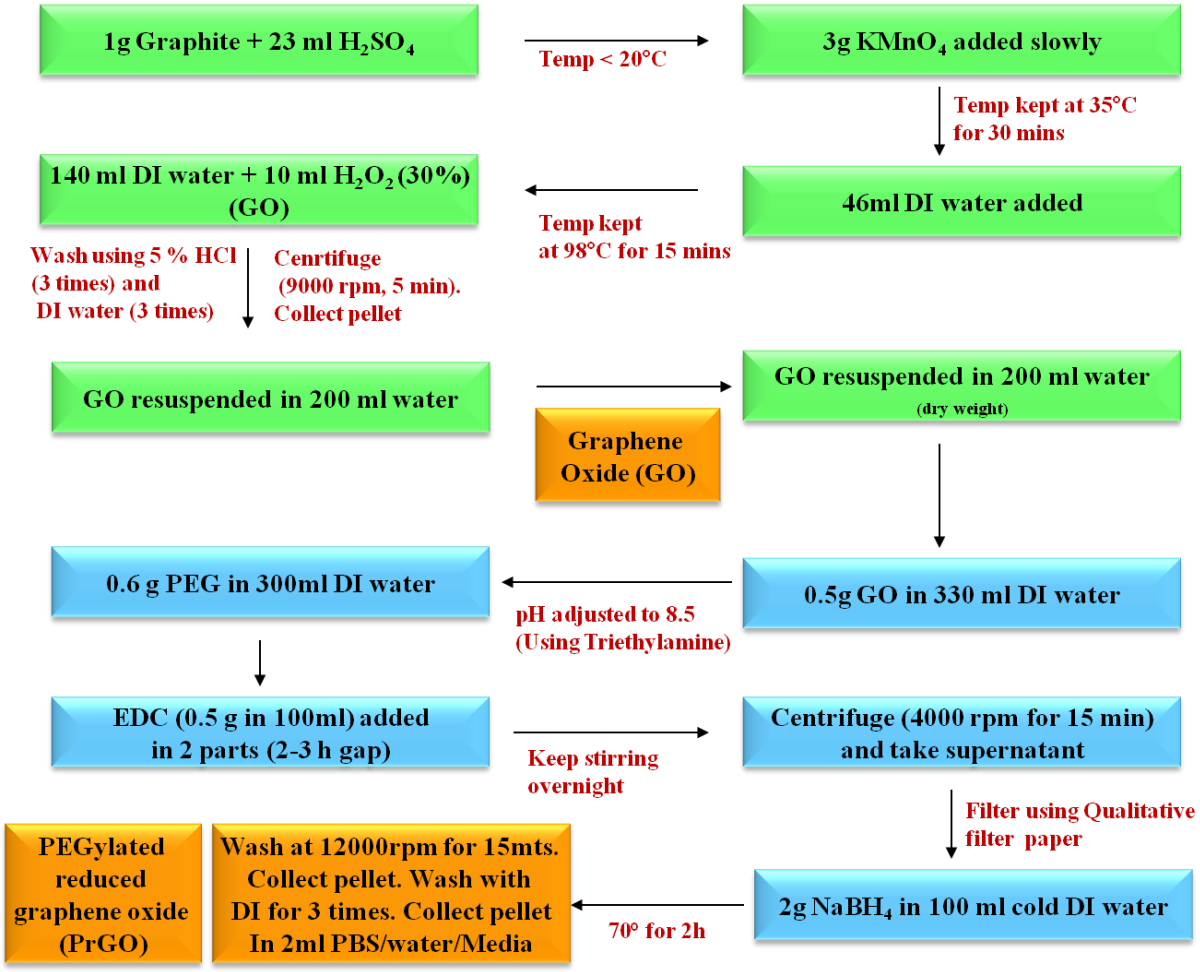

Figure 3.1: Flowchart for PrGO synthesis

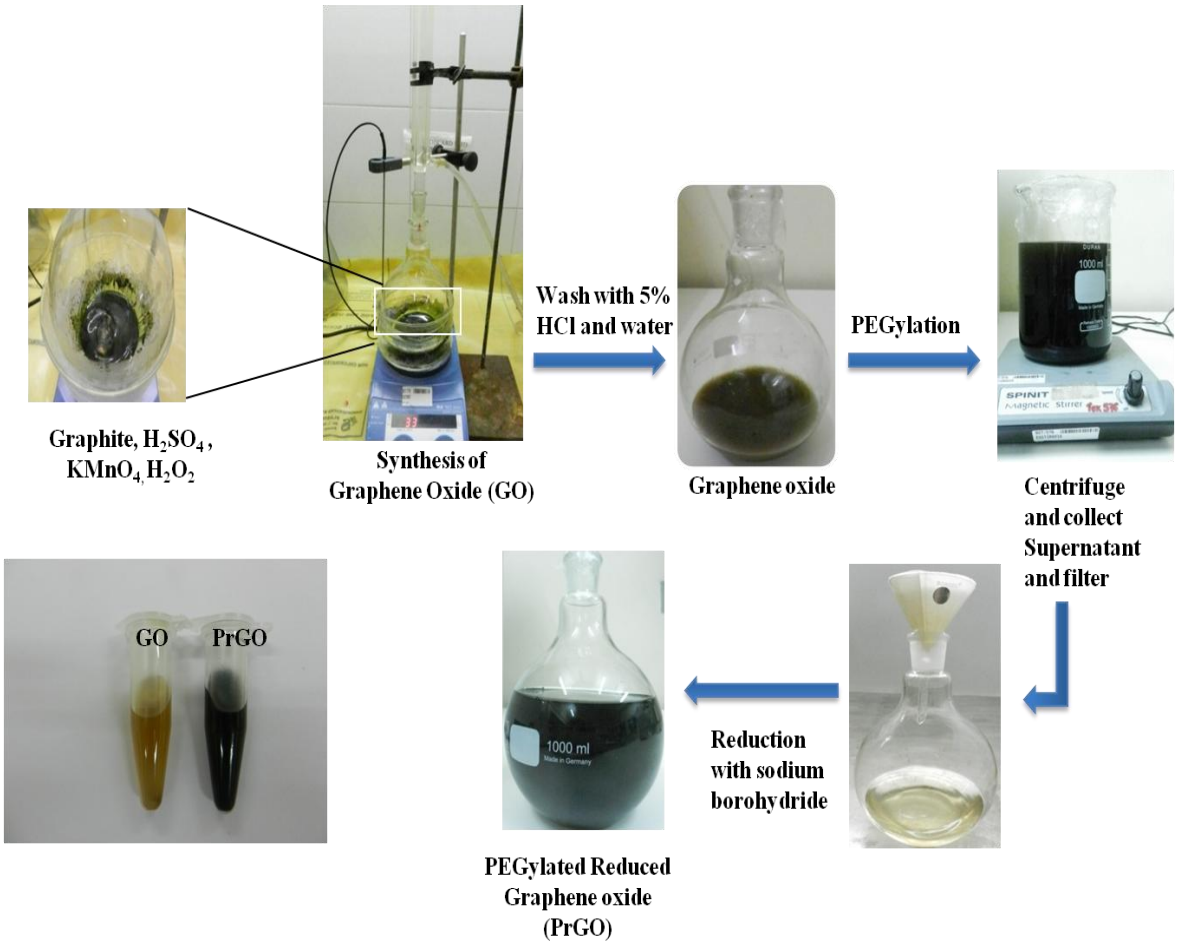

Figure 3.2: Photographic representation of PrGO synthesis

3.7. CHARACTERIZATION

Both PrGO and RGO were characterized by Transmission Electron Microscopy (TEM), Atomic Force Microscopy (AFM), X- ray diffraction (XRD), X-ray photo electron spectroscopy (XPS), SAED (Selective Area Electron Diffraction), FTIR (Fourier Transform Infrared Spectroscopy), TGA (Thermo gravimetric analysis) and Raman Spectroscopy.

3.7.1. TRANSMISSION ELECTRON MICROSCOPY (TEM)

Surface topography of both PrGO and RGO was analyzed using TEM. TEM samples were prepared by drop casting graphene samples dispersed in water on to the TEM 200 mesh Cu micro grid without film and kept for overnight drying. TEM and SAED was done using JEOL JEM 2100 Transmission electron microscope (Japan) under an accelerating voltage of 200 kV.

3.7.2. ATOMIC FORCE MICROSCOPY (AFM)

Height profile and lateral size distribution was examined by AFM. AFM analysis was done by drop casting graphene samples dispersed in water onto the cleaned silicon substrate and kept for drying. AFM images were recorded with Cypher S Atomic Force Microscope, Asylum Research (United Kingdom). All the images were acquired using a tapping mode under ambient conditions.

3.7.3. X-RAY PHOTOELECTRON SPECTROSCOPY (XPS)

XPS analysis was performed to study the elemental composition of the samples. For XPS analysis, samples were prepared on the silicon substrate. The graphene samples were drop casted onto the silicon substrate and dried overnight. XPS was carried out using AXIS-His, Kratos, Shimadzu (United Kingdom) at a current of 10 mA and voltage 12 kV using Mg/Al dual anode monochromator.

3.7.4. FOURIER TRANSFORM INFRARED SPECTROSCOPY (FTIR)

FTIR spectra correlate to the vibrational energy of atoms or group of atoms in graphene samples. FTIR was performed using Nicolet iS50, Thermo Fisher (United

States of America) with ATR module. Powdered graphene samples were used to measure the FTIR on ATR crystal.

3.7.5. RAMAN SPECTROSCOPY

Raman scattering was done with the help of Lab RAM, HR-800, Horiba Jobin Yvon S.A.S (Japan) with excitation laser wavelength of 633 nm.

3.7.6. X-RAY DIFFRACTION (XRD)

XRD was done to determine the crystal characteristics of the graphene samples. XRD peaks were analyzed using Smart Lab X-ray diffractometer, RIGAKU (Japan).

3.7.7. THERMOGRAVIMETRIC ANALYSIS (TGA)

TGA analysis measures the changes in material weight as a function of temperature. For TGA analysis, powdered graphene samples were directly weighed and used. Thermal analysis was carried out with Thermal Analysis Instrument, DTG-60H, Shimadzu (Japan).

3.8. ENDOTOXIN CONTENT

The endotoxin contamination in PrGO and RGO was estimated using FDA approved Endosafe®-PTS (Charles River, USA). This is a rapid test system that utilizes Limulus Amoebocyte Lysate (LAL) test. Supernatant of 100 μg/ml of PrGO and RGO were taken and 25 μl was added to each well of the cartridge. The cartridge was inserted into the portable reader and the reading was taken spectrophotometrically.

3.9. ISOLATION AND CHARACTERIZATION OF MESENCHYMAL STEM CELLS (MSCs)

3.9.1. ISOLATION

Swiss albino mice aged 6-8 weeks old were sacrificed by cervical dislocation and disinfected with 70% ethanol. Femur was dissected and collected in petridishes containing ice cold sterile PBS. The connective tissues in the femurs were removed and the MSCs were isolated as per described protocol in (Remya *et al*., 2014). Briefly, the end of the femur was clipped off to remove epiphysis and the marrow was flushed out using 1 ml syringe and collected in centrifuge tubes containing complete DMEM media (DMEM + 20% FBS). The cells were centrifuged (2500 rpm, 10 min) and the pellets were resuspended in complete DMEM and cultured in T25 flask. The cells were maintained at 37°C in presence of 5% CO_2. Media was changed daily to remove non adherent hematopoietic stem cells for the first week followed by every three to four days. The cells were sub-cultured using 0.25% Trypsin-EDTA once it reaches confluent and maintained until other experiments. Cells after every third passage were used for *in vitro* toxicity evaluation. Figure 3.3 below shows the schematic illustration of the isolation process.

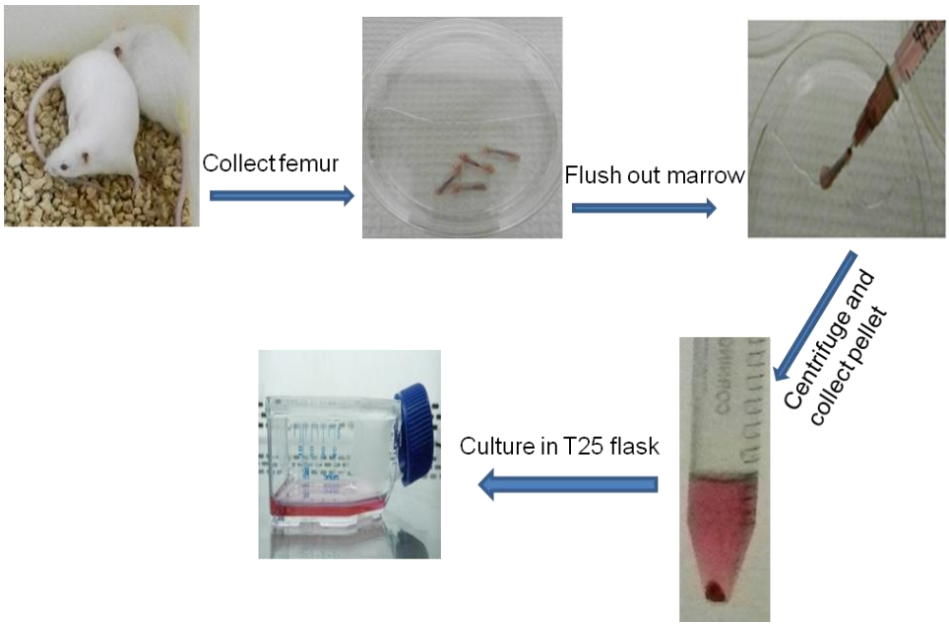

Figure 3.3: Isolation and culture of MSCs from mouse bone marrow

3.9.2. CHARACTERIZATION

The cells were cultured in cover slips for characterization of surface markers. For immunostaining, media was removed and the cells were washed with PBS. The cells were fixed in 4% formaldehyde for 2-3 min and blocked with 1% BSA solution. Excess blocking agent was washed away with PBS and the cells were incubated with MSCs specific positive primary antibodies (CD 90, CD 44) (1:100 dilution in 1% BSA) and negative primary antibody (CD 45) (1:100 dilution in 1% BSA) for 3-4 h, followed by incubation in fluorescent tagged secondary antibodies Rat IgG FITC (1:400 dilution in 1% BSA) for 1 h. Excess antibodies were removed and the cells were counterstained with DAPI (nuclear stain) for 5 min and observed under fluorescent microscope (Syama *et al*., 2014b).

3.9.3. DIFFERENTIATION

One of the important aspects of stem cells is their ability to differentiate into specific cell types when cultured under certain conditions. Cells were cultured in coverslips and incubated with differentiation medium (adipocytes and osteogenic). The differentiation medium was changed every 3-4 days and the cells were cultured for 21 days. For adipogenic differentiation, the cells were cultured in DMEM containing 20% FBS, 50 µg/ml Ascorbate-2-phosphate, 50 µg/ml indomethacin and 10^{-7}M dexamethasone. For osteogenic differentiation, the cells were cultured in DMEM with 20% FBS, 10 mM β-glycero phosphate, 50 µg/ml Ascorbate-2-phosphate, 10^{-7}M dexamethasone. After 21 days of culture, the media was removed and the differentiated cells were fixed with 4% formaldehyde. The differentiated adipocytes were stained with Oil Red and osteoblasts were with Alizarin Red as described below.

3.9.3.1. OIL RED AND ALIZARIN RED STAINING

1. PREPARATION OF OIL RED

Stock: 0.3 % Oil red in isopropanol and kept in dark

Working solution: 3 parts of Oil red (stock) + 2 parts of distilled water

2. PREPARATION OF ALIZARIN RED

2 g of alizarin red was dissolved in 90 ml of distilled water. The pH of the staining solution was adjusted to 4.3 using HCl. The solution was made up to 100 ml, filtered and stored in dark at 4°C.

3. STAINING

Adipocytes were washed to remove media and the cells were fixed in 4% formaldehyde for 5 min. After fixation, the cells were washed with PBS and lipid granules in cells were stained with Oil Red for 15 min at room temperature. Excess dye was removed and the cells were observed under light microscope. Similarly, osteoblasts were fixed in 4% formaldehyde and washed with PBS. The calcium deposits of the osteoblasts were stained with Alizarin red for 15 min and the cells were observed under microscope.

3.9.4. ACTIN STAINING OF ISOLATED MSCs

The isolated cells were cultured in cover slips and the cells were stained for F-actin filaments using Rhodamine Phalloidin as described by Syama *et al*., (2014b). The cells were fixed and permeabilized using 0.1% Triton X-100 for 2 min. The fixative was removed, the cells were washed with PBS and the cells were incubated with Rhodamine Phalloidin (1:100 dilutions) for 15 min, counterstained with DAPI (nuclear stain) for 10 min and observed under fluorescence microscope.

3.10. PROTEIN CORONA

To isolate the hard corona, two different concentration of PrGO (10, 100 µg/ml) was incubated with 10% FBS solution for different time periods (5 min, 30 min and 2 h) at 37°C. After incubation, the nanoparticle suspension with FBS was washed three times in PBS (12,000 rpm for 10 min). Supernatant containing the proteins loosely attached (soft corona) to PrGO was discarded. After the final wash, the hard corona was isolated

by incubating the sample in SDS sample loading buffer and heated at 95ºC for 5 min. The isolated and denatured protein samples were then separated in polyacrylamide gel**.**

3.10.1. PROTOCOL FOR SDS PAGE

Composition of the stacking and separating gels are given in the table 3.1. The ingredients of the separating gel was mixed and poured into the gel casting assembly without any air bubbles. Immediately, water saturated butanol was overlaid to even the surface of the separating gel. The gel was allowed to polymerize and after polymerization, the butanol was removed and the surface of the gel was cleaned with de-ionized water. Stacking gel mix was prepared, poured on top of the separating gel and the comb was placed immediately without trapping any air bubbles. After polymerization, the wells were cleaned and samples were loaded.

Components	**Separating gel (12%)**	**Stacking gel**
Water	3.2 ml	2.975 ml
Tris buffer	2.6 ml; pH (8.8)	pH (6.8)
Acrylamide/Bisacrylamide (30% / 0.8%)	4 ml	0.675 ml
10% SDS	100 µl	50 µl
TEMED	10 µl	10 µl
APS (10%)	100 µl	100 µl

Table 3.1: Composition of Separating and Stacking gel for SDS-PAGE

The gel was run at 60-100 V in Tris-Glycine running buffer for 3-4 h. After completion of the run, the gel was stained overnight in Coomassie Brilliant Blue stain.

The next day, the gel was destained in destaining solution (methanol: acetic acid: water (30:10:60)) and stained protein bands were imaged with Bio imaging system.

3.11. *IN VITRO* EXPERMENTS

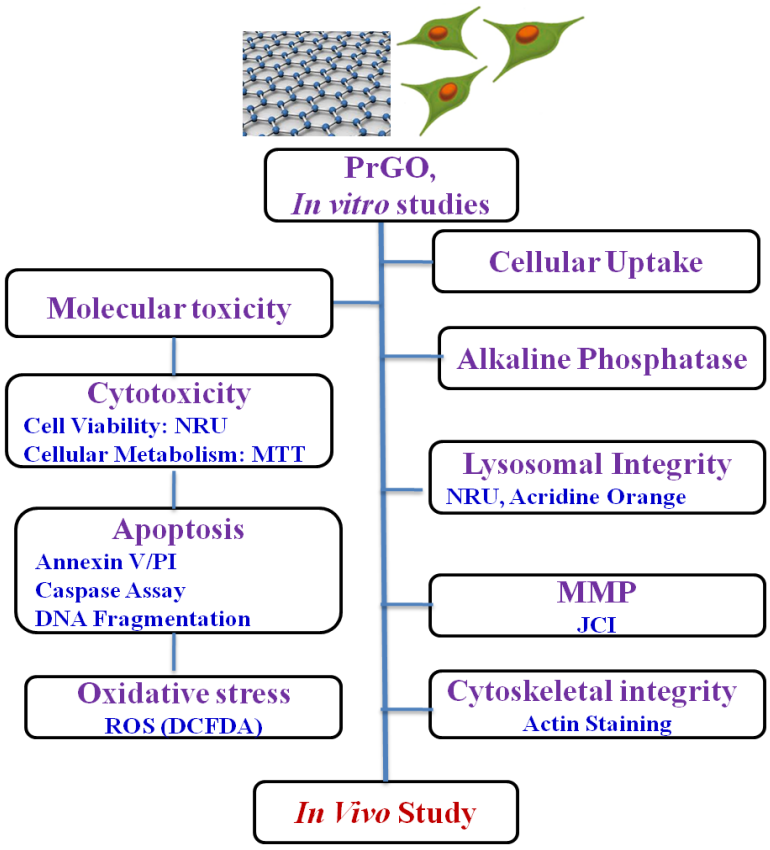

Figure 3.4: Flow chart for *In vitro* studies

3.11.1. CELLULAR UPTAKE OF PrGO

The cellular uptake of PrGO was studied by incubating MSCs with 100 µg/ml of PrGO for different time period (24, 48 and 72 h). After incubation, the cells were washed with sterile PBS and observed under microscope for qualitative uptake analysis. Similarly for TEM analysis, cells were cultured in presence of 20 µg/ml of PrGO for 24 h. Following incubation, the cells were trypsinized, washed with PBS and fixed in 1% glutaraldehyde,

osmium tetraoxide and dehydrated in a graded alcohol series. Sections were collected using microtome for TEM analysis after embedding in epoxy resin. The sections were stained with uranyl acetate, lead citrate and observed under TEM. Cell morphology, PrGO uptake and distribution were examined.

3.11.2. CYTOTOXICITY

3.11.2.1. CELL VIABILITY AND METABOLIC ACTIVITY: MTT ASSAY

Confluent cells were trypsinized and seeded at a density of 20,000 cells/well. The plates were incubated at 37°C for 24 h in 5% CO_2 for cell attachment. The next day, old medium was replaced with fresh medium containing different concentration of PrGO (5, 10, 50 and 100 µg/ml). The cells were exposed for different time period (24, 48 and 72 h). On the day of MTT assay, the medium was discarded and the wells were washed with PBS, 100 µl of (50 µg/well) MTT dye was added and the plates were incubated at 37°C for 4 h in dark. The assay is based on the metabolic reduction of soluble MTT by mitochondrial dehydrogenase to insoluble colored formazan product. The formazan crystals formed by metabolically active cells were then dissolved by adding 200 µl of DMSO and the absorbance was read at 540 nm using an automated microplate reader (ELx 808 IU ultra microplate reader, Bio-Tek Instruments, USA). The percentage of cell viability was calculated using the formula:

$$\% \text{ cell viability} = \frac{\text{Number of viable cells}}{\text{Total number of cells}} X100$$

3.11.2.2. CELL VIABILITY (LYSOSOMAL ACTIVITY): NEUTRAL RED ASSAY

Cells were seeded in 96 well microplate and cultured for 24 h in presence of 5% CO_2 at 37°C. Different concentration of PrGO (10, 25, 50, 100 and 250 µg/ml) was exposed to cells for different time periods (24, 48 and 72 h). After exposure, the cells were incubated with 100 µl of neutral red solution (40 µg/ml) prepared in culture medium for 3 h in dark. This assay is based on the principle that viable cells incorporate neutral red, a weak cationic dye within their lysosomes. Excess neutral red was washed away after incubation and the neutral red stored in lysosomes were extracted with acid/alcohol treatment (1% glacial acetic acid, 50% ethanol and 49% distilled water) for 30 min. The absorbance was read at 540 nm using an automated microplate reader (ELx 808 IU ultra microplate reader, Bio-Tek Instruments, USA). Cells without nanomaterials were treated as control and the results were expressed in percentage of neutral red uptake. The cells were also observed under light microscope and are imaged for qualitative analysis of neutral red uptake.

3.11.3. REACTIVE OXYGEN SPECIES (ROS)

Reactive oxygen species (ROS) production inside the cells was quantified using 2,7-dichlorodihydrofluorescein diacetate (H_2-DCFDA). Upon entry into the cells, the acetate group of H_2DCFDA is removed by the intracellular esterase forming 2',7'-dichlorofluorescin (DCF). In presence of ROS, non-fluorescent DCF formed is converted into a fluorescent product. The increase in fluorescence intensity is proportional to the oxidation of the fluorescent probe. For ROS assay, the cells were seeded at a density of 20,000 cells/well and cultured for 24 h. The cells were incubated with different

concentration of PrGO (10, 25, 50, 100, 250 and 500 µg/ml) for 4 and 24 h. After incubation, the cells were loaded with H_2DCFDA (2.5 µM/well) and incubated for 45 min in dark. The wells were washed with PBS to remove excess H_2DCFDA. The fluorescence was measured using fluorescent microplate reader (Monochromator based multimode microplate reader, BioTeck Instruments, USA) with excitation at 495 nm and emission at 530 nm. The fluorescent images of the cells were taken using Axio Scope A1 fluorescent microscope (Carl Zeiss, Germany).

3.11.4. MITOCHONDRIAL MEMBRANE POTENTIAL (MMP)

Mitochondrial membrane potential (MMP) in cells treated with PrGO was monitored using JC-1 probe. JC-1 is a membrane permeable dye that accumulates within the mitochondria as aggregates and emits red color. Decreased MMP can translocate this probe into cytoplasm where it remains in the monomeric form and emit green fluorescence. Therefore, decrease in red fluorescent is an indicative of depolarization and increase represents hyperpolarization. Cells were exposed to three different concentration of PrGO (10, 100 and 500 µg/ml) for 24 h. 2 µM of JC-1 was added onto the wells and the cells were incubated at 37°C for 30 min. The cells were imaged under Axio Scope A1 fluorescent microscope (Carl Zeiss, Germany).

3.11.5. LYSOSOMAL MEMBRANE INTEGRITY: ACRIDINE ORANGE ASSAY

Cells cultured on 96 microwell titre plate (20,000 cells/well) were exposed to different concentration of PrGO (10, 25, 50, 100, 250 and 500 µg/ml) for 24 h. The cells were incubated with 5 µg/ml of acridine orange (AO) for 15 min after particle exposure. AO is an acidophilic dye that can readily incorporate inside the lysosomes because of its

acidic pH. AO can also bind both DNA and RNA. In lysosomes, AO appears red color and in cytoplasm it emits green. The intensity ratio of red to green is a measure of lysosomal membrane damage. The wells were then washed to remove excess AO and quantitative analysis of AO relocation was done using fluorescent microplate reader (Monochromator based multimode microplate reader, BioTeck Instruments, USA) with excitation at 450 nm and emission at 530 nm (green cytoplasmic AO) and 620 nm (red lysosomal AO). Similarly for qualitative assay, the cells grown on cover slips were exposed to PrGO and incubated with AO for 15minutes. After incubation, the cells were washed with PBS and observed under fluorescent microscopy (Axio Scope A1 fluorescent microscope, Carl Zeiss, Germany).

3.11.6. CELL ADHESION: ACTIN STAINING

The influence of PrGO on the cell adhesion properties of MSCs were studied using Cytopainter staining of F-actin filaments. The cells were seeded onto 4 well plates and exposed to three different concentration of PrGO (10, 100 and 500 µg/ml). After exposure for 24 h, the medium was removed and the cells were washed in PBS. Cells were fixed using 4% paraformaldehyde for 2 min. The cells were washed, permeabilized using 0.1% Triton-X and stained with Cytopainter for 30 min. Excess stain was removed and the cells were counter stained with DAPI for nucleus. The actin stained cells were observed under fluorescence microscope for changes in cytoskeletal structure.

3.11.7. APOPTOSIS ASSAY

3.11.7.1. LIVE DEAD ASSAY: ANNEXIN V/PI

Apoptotic cells were identified by fluorescein isothiocyanate-conjugated (FITC)-annexin V/PI staining (Molecular Probes, Invitrogen). Annexin V binds to the phosphotidyl serine residues exposed on the surface of the cells undergoing apoptosis, whereas propidium iodide stains necrotic cells. Briefly, $1x10^6$ cells were seeded onto the cover slips and exposed to different concentrations of PrGO (10, 100 and 500 µg/ml) for 16 h. After treatment, the cells were washed in PBS, incubated with annexin binding buffer and stained with annexin V/PI as per the manufacturer's instruction. The cells were viewed under fluorescence microscope for the presence of apoptotic or dead cells.

3.11.7.2. CASPASE ASSAY

Caspases are intracellular proteases that are responsible for the formation of apoptotic bodies. Both caspase 3 and 7 are involved in the execution phase of apoptosis (Slee *et al*., 1999). Cells were exposed to different concentration of PrGO (10, 25, 50, 100, 250 and 500 µg/ml) for 24 h. After 24 h of exposure, the cells were examined for the activation of caspase using Sensolyte Homogenous AMC Caspase-3/7 assay kit (Anaspec, Fremont, CA). The protocol was done as per manufacturer's instruction. 50 µl of caspase substrate solution was added and the plates were incubated in shaker for 1 h at 37ºC in dark. The plates were read using fluorescent plate reader with excitation at 344 nm and emission at 442 nm. The results were expressed in relative fluorescent units (RFU).

3.11.7.3. APOPTOTIC DNA LADDER ASSAY

Cells were cultured in six well plates and exposed to two different concentrations of RGO and PrGO (10 and 100 µg/ml) for 24 h. Following exposure, the cells were washed with PBS, trypsinized and pellets were obtained. Apoptotic DNA ladder assay was performed as per manufacturer's instruction. Briefly, 35 µl of TE lysis buffer was added and the cells were resuspended followed by the addition of Enzyme A and Enzyme B. The cells were incubated in both the enzymes under appropriate temperature as mentioned in the kit. Ammonium acetate and 100 µl of absolute alcohol were added and the pellets were resuspended in 70% ice cold ethanol. DNA was allowed to precipitate at -20°C and the tubes were air dried to evaporate excess ethanol. DNA samples were resuspended in suspension buffer and loaded onto agarose gel. The isolated DNA samples were run on 1% Agarose gel under 60 V. After electrophoresis, the DNA bands were stained with ethidium bromide and visualized under Gel Doc imaging system.

3.11.8. ALKALINE PHOSPHATASE ASSAY

Cells were seeded onto six well plates and exposed to PrGO (10 and 100 µg/ml) for 24 h. After 24 h, the cells were cultured both in presence and absence of osteogenic medium. The effect of PrGO on the osteogenic differentiation of MSCs was monitored after two weeks of culture using alkaline phosphatase assay. Medium was changed every four days. After 14 days, the medium was removed and the cells were fixed in 10% neutral buffered saline and washed with washing buffer (0.05% tween 80 in PBS). The cells were then stained with Sigma Fast BCIP/NBT substrate for 10 min under dark and

observed under microscope. Hydrolysis of BCIP by ALP and the simultaneous reduction of NBT results in the formation of deep purple colored product.

3.12. *IN VIVO* EXPERIMENTS

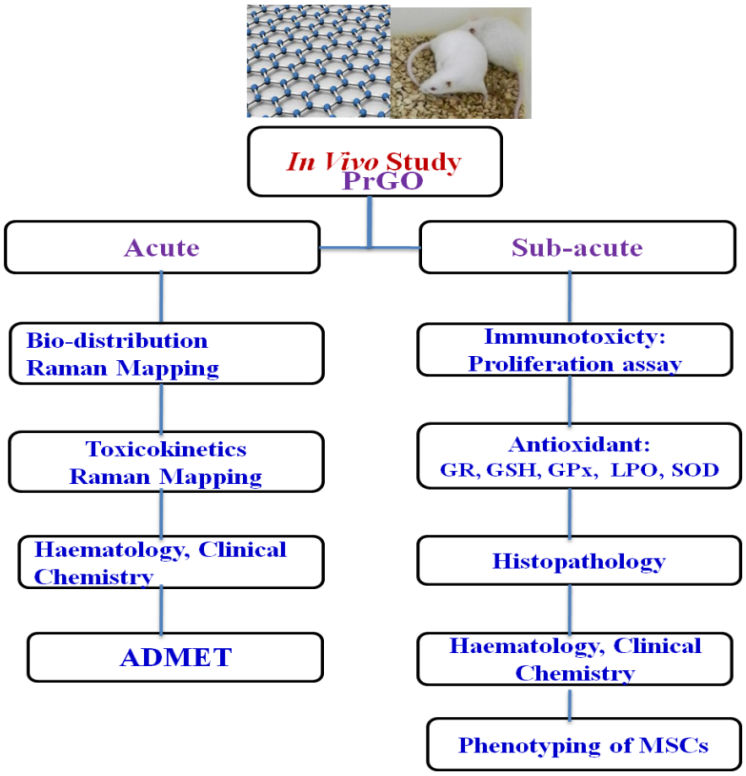

Figure 3.5: Flow chart for *In vivo* studies

3.12.1. ACUTE TOXICITY

Acute toxicity is to determine the adverse effect of animal after single or multiple exposures of a compound within a period of 24 h. The acute toxicity determines the dose-response relationship and lethal dose.

EXPERIMENTAL DESIGN

Group	Dose (PrGO) (mg/kg body weight)	Route of exposure (Single dose)	No. of mice	No. of animals sacrificed (post exposure)				
				0 day	3 days	7 days	14 days	21 days
1	10 mg/kg	Intravenous	15	3	3	3	3	3
2	10mg/kg	Intraperitoneal	15	3	3	3	3	3

Table 3.2: Experimental design of acute toxicity study

Figure 3.6: Photomicrograph of intravenous and intraperitoneal injection in mice

PrGO was prepared at a concentration of 10 mg/kg body weight in water for injection. The volume of injection was 50 ml/kg body weight (ISO 10993-11).

During the experimental period all the animals were observed for clinical symptoms response such as respiratory, motor, convulsion, reflexes, ocular signs, cardiovascular signs, salivation, piloerection, analgesia and gastrointestinal. Body weight and Organ indices were calculated for each group.

3.12.1.1. BIODISTRIBUTION AND TOXICOKINETICS

Absorption, distribution, metabolism and excretion were determined from the acute toxicity study. At the end of the experimental period, the animals were anaesthetized and blood was collected from the orbital sinus for hematological and

clinical chemistry evaluation for metabolism studies. Urine was collected from intravenously administered group for excretion studies. Organs such as liver, kidney, spleen and brain were used for bio-distribution studies.

EXPERIMENTAL DESIGN (same acute experiment)

Group	Dose (PrGO) (mg/kg body weight)	Route of exposure (single exposure)	No. of mice	Name of Organs	No. of animals sacrificed (post exposure)				
					Days				
					0	3	7	14	21
1	10 mg/kg	Intravenous	15	Liver, Kidney, spleen, brain, bone marrow	3	3	3	3	3
2	10 mg/kg	Intraperitoneal	15		3	3	3	3	3

Table 3.3: Experimental design for biodistribution and toxicokinetics studies

3.12.1.1.1. DETECTION OF PrGO IN TISSUES

PrGO was prepared in water for injection for all animal experiments. A total of 30 Swiss albino mice were selected for bio-distribution studies; 15 mice each for intraperitoneal and intravenous administration. The animals were given single dose of PrGO (10 mg/kg body weight) by intraperitoneal and intravenous (tail vein) injection. All the animals were sacrificed by cervical dislocation at 3, 7, 14 and 21 days post exposure. Organs such as liver, spleen, kidney and brain were collected for bio-distribution studies. Tissues were sliced, dehydrated and focused under Raman microscope for mapping.

PROCESSING OF TISSUE SAMPLES FOR RAMAN MAPPING

Tissue sections of organs such as liver, brain, kidney and spleen were collected from mice treated with PrGO (intravenous and intraperitoneal administration). The

collected tissue slices were dehydrated in alcohol as given in table 3.4. The dehydrated tissues were transferred onto slides and observed under Raman microscope.

Percentage (%) of alcohol	**Duration**	**No. of wash**
80% alcohol	30 min each	2
90% alcohol	30 min	1
100% alcohol	15 min each 30 min	2 1

Table 3.4: Alcohol dehydration protocol for Raman mapping

RAMAN MAPPING OF TISSUE SAMPLES

Raman spectral measurements were carried out in a WITec Raman microscope (Witec Inc. Germany, alpha 300R) with a laser beam directed to the sample through a 60× water immersion objective (Nikon, NA=1.0) and a Peltier cooled CCD detector. Samples were excited with a 532 nm frequency doubled Nd: YAG laser and Stokes shifted Raman spectra were collected in the range of 400 to 4000 cm^{-1} with 1 cm^{-1} spectral resolution. Prior to every measurement, a calibration with a silicon standard (Raman peak centered at 520 cm^{-1}) was performed. WITec Project plus (v 2.1) software package was used for data evaluation. The tissue samples in physiological medium (PBS) were investigated with the Spectral Imaging Mode of the Confocal Raman Microscope. A spectrum at every pixel was taken (Scan Range: 7 x 7μm^2, 50 x 50 pixel, 2500 spectra). Using the integrated video camera, a suitable area was focused and scanned with an integration time of 2s. The imaged-data were evaluated utilizing the cluster analysis feature of Witec Project Plus software.

3.12.1.1.2. DETECTION OF PrGO IN URINE

Urine was also collected from the animals exposed to PrGO at the end of 3, 7, 14 and 21 days after exposure. Spectra of urine samples were analyzed in air using confocal Raman microscope (20x objective) with an integration time of 0.2 s.

3.12.1.1.3. DETECTION OF PrGO IN BONE MARROW

Bone marrow was isolated from mice given intraperitoneal administration of PrGO. The bone marrow extract was collected in glass slides and dehydrated in alcohol for Raman mapping.

3.12.1.1.4. DETECTION OF PrGO IN BLOOD

Mice were exposed to 10 mg/kg body weight of PrGO by intravenous and intraperitoneal injection. Blood was collected from each mouse after 1, 3, 6, 24, 48, 72 h and 7 days after injection from tail vein. Blood smear was prepared on microscopic glass slides, air dried and dehydrated with alcohol to remove RBC.

EXPERIMENTAL DESIGN

Group	Dose (PrGO) (mg/kg body weight)	Route of exposure	No. of mice	Blood collection on (Post exposure)						
1	10 mg/kg	Intravenous (single exposure)	3	1 h	3 h	6 h	24 h	48 h	72 h	7 Days
2	10 mg/kg	Intraperitoneal (single exposure)	3	1 h	3 h	6 h	24 h	48 h	72 h	7 Days

Table 3.5: Experimental design for detection of PrGO in blood

SLIDE PROCESSING OF BONE MARROW, BLOOD AND URINE SAMPLE

The slides containing bone marrow, blood and urine sample was processed and dehydrated in alcohol for confocal Raman mapping. The protocol of alcohol dehydration was done as described in table 3.4. Spectra of the samples were analyzed in air using a 20 x objective; with an integration time of 0.2 s.

3.12.1.2. HEMATOLOGY AND CLINICAL CHEMISTRY

Blood was collected from mice for hematological and clinical chemistry analysis. Blood was collected in anticoagulant (3.8% trisodium citrate) containing tubes for hematology. Parameters such as red blood corpuscles (RBC), white blood corpuscles (WBC), hemoglobin concentration (HGB), hematocrit (HCT), mean corpuscular volume (MCV), mean corpuscular hemoglobin content (MCH), mean corpuscular hemoglobin concentration (MCHC) and platelet counts (PLT) were evaluated using hematology counter (Animal counter, India). Whole blood was allowed to clot and centrifuged at 3000 rpm for 10 min; serum was separated and used for clinical chemistry evaluations. Parameters such as Glucose, Urea, Creatinine, Cholesterol, Albumin, Serum Glutamic Oxaloacetic Transaminase (SGOT), Serum Glutamic Pyruvate Transaminase (SGPT) and total protein were estimated using a fully automated biochemical analyzer (ERBA XL 300).

3.12.1.3. BODY WEIGHT AND ORGAN INDEX

Organ index is used as a screening tool for studying treatment related effects. Both body weight and organ indices give general impression about toxicity of the nanoparticles.

3.12.1.4. ABSORPTION, DISTRIBUTION, METABOLISM, EXCRETION AND TOXICITY (ADME & T)

ABSORPTION

10 mg/kg body weight of PrGO was injected into mice via intravenous and intraperitoneal administration. The absorption of PrGO from site of exposure to systemic circulation was studied in blood samples of acute toxicity study using Confocal Raman microscope.

DISTRIBUTION

Distribution of PrGO in various organs after i.p. and i.v. injection was studied by collecting major organs such as liver, brain, kidney, spleen and bone marrow from acute toxicity. The tissue samples were scanned under Confocal Raman microscope.

METABOLISM

The effect of PrGO on metabolic activity of the animals was studied by measuring various clinical chemistry parameters after PrGO exposure (acute toxicity).

EXCRETION

Urine sample was collected from mice administered with PrGO. The samples were dried and dehydrated with alcohol for Raman mapping.

TOXICITY

Toxic effect of PrGO in mice after i.p. and i.v. administration was studied. Changes in organ index, hematology and clinical chemistry parameters were evaluated.

3.12.2. SUB ACUTE TOXICITY

Sub acute toxicity involves repeated exposure of a compound to the animals, over a prolonged period. Sub acute toxicity provides information on the target organs affected by the compound.

EXPERIMENTAL DESIGN

Group	Dose (PrGO)	Route of exposure (3 doses at 1, 3, 5 days)	No. of mice	No. of animals sacrificed (post exposure)				Organs collected*
				0 day	7 days	14 days	21 days	
1	10 mg/kg	Intraperitoneal	20	5	5	5	5	Kidney, Liver, Spleen, Brain

Table 3.6: Experimental design for sub-acute toxicity study

Blood was collected for haematology and clinical chemistry estimation. Organs such as kidney, liver, spleen, brain were collected for histopathology. Spleen was used to determine the immunotoxicity by proliferation assay. Liver was used for the determination of antioxidant parameters such as lipid peroxidation (LPO), total glutathione (GSH), glutathione reductase (GR), Glutathione peroxidase (GPx) and superoxide dismutase (SOD). Bone marrow was used to study the phenotyping of mesenchymal stem cells.

3.12.2.1. BODY WEIGHT

Body weights of the experimental animal were monitored at 7, 14 and 21 days post exposure.

3.12.2.2. HAEMATOLOGY AND CLINICAL CHEMISTRY PARAMETERS

Blood was collected from mice orbital sinus for haematological and clinical chemistry analysis. Blood was collected in anticoagulant (3.8% trisodium citrate) containing tubes for haematological analysis. Parameters such as RBC, WBC, HGB, HCT, MCV, MCH, MCHC, PLT were evaluated in haematology counter (Animal Blood Counter, India). Serum was obtained by centrifugation of clotted blood at 3000 rpm for 10 min for clinical chemistry analysis. Parameters such as Glucose, Urea, Creatinine, Cholesterol, Albumin, Serum Glutamic Oxaloacetic Transaminase (SGOT), Serum Glutamic Pyruvate Transaminase (SGPT) and total protein were estimated using a fully automated biochemical analyzer (ERBA XL 300).

3.12.2.3. GROSS PATHOLOGY

At the end of the experimental period, all animals were euthanized and subjected to a postmortem examination. At necropsy, all organs and tissues were examined for grossly visible lesions.

3.12.2.4. HISTOPATHOLOGICAL ANALYSIS

Organs such as liver, kidney, spleen and brain were dissected from mice exposed to repeated dose of PrGO at various intervals and collected in 10% buffered formalin for histopathological analysis.

SAMPLE PROCESSING

Small pieces of tissue samples were cut, placed into cassettes, dehydrated in isopropanol (twice for 1 h each, cleared in xylene (thrice for 45 min each) and impregnated in paraffin wax (twice for 1 h each).

EMBEDDING

The tissues processed as above were embedded into paraffin blocks. Samples were removed from the cassettes using a pre-warmed pointed forceps. The samples were placed in a mould filled with warm paraffin and orientated in such a way to obtain cross section of the tissue. The mould with the sample was then allowed to cool. After cooling, the paraffin blocks were removed from the mould and stored for sectioning.

CLEANING OF GLASS SLIDES

The glass slides were cleaned thoroughly in cleaning solution before sectioning. Cleaning solution contains 17.5 g NaOH dissolved in 70 ml of MilliQ water under stirring. 105 ml of 96% ethanol was added and mixed well. The glass slides were placed in cleaning solution and rotated on an orbital shaker for 2 h. The slides were then rinsed in excess amount of MilliQ water for 1 min (4 times).

SECTIONING

The paraffin blocks were trimmed at the sides and shaped using a scalpel blade. Opposite edges of the block were maintained parallel. Blocks were sectioned using a rotary microtome (Leica RM 2125 RT). The blocks were trimmed till the tissue surface was completely exposed. The exposed surface of the tissue was cooled with ice cubes and 3-5 µm thick sections were cut. The tissue sections were expanded by keeping the sections in tissue floatation bath (M.C. Dalal & Co., India). Sections were picked onto clean glass slides pre-coated with Meyer's egg albumin.

STAINING

HEMATOXYLIN AND EOSIN (H&E) STAINING

H&E stain is a standard stain used to examine the general morphology and morphological alterations associated with tissue damage. Paraffin sections of the tissue samples were stained with Harris hematoxylin and eosin stain using the following protocol;

Steps	**Duration**
Slides with sections were kept in a 50°C oven	1 h
Immersed in xylene I	10 min
Immersed in xylene II	10 min
Absolute alcohol	5 min
70 % alcohol	5 min
Distilled water	5 min
Harris Hematoxylin	8 min
Tap water	5 min
Acid alcohol	1-2 dips
Tap water	5 min
Scoot’s tap water	4 min
Tap water	5 min
1% Eosin	4 min
70% ethanol	2 dips
Tap water	1 dip

70% alcohol	2 min
Absolute alcohol	5 min
Xylene I	10 min
Xylene II	10 min

Slides were air dried and mounted with cover glasses using DPX mountant

LIGHT MICROSCOPY

Histopathological evaluation of the tissue sections were performed under light microscope (Olympus CX31) and the images were captured using Qcapture Pro^{TM} 6 software.

3.12.2.5. ANTIOXIDANT ASSAYS

10% of liver homogenate (sub acute toxicity study) was prepared in phosphate buffer (pH 7.4) for antioxidant analysis. Enzyme activity of GR, GPx and SOD was estimated using standard protocol. Lipid peroxidation and total GSH level were also determined in mice exposed to repeated dose of PrGO. The antioxidant assays were carried out as per the following protocols.

PREPARATION OF TISSUE HOMOGENATE

Liver samples were collected from mice exposed to PrGO (sub acute toxicity) and processed for antioxidant assays. In brief, 10% of liver homogenate was prepared in phosphate buffer (0.1 M, pH 7.4) using an ice-chilled glass homogenizing vessel in a rotor stator homogenizer at 900 rpm. The samples were centrifuged at 3500 rpm for 10 min. The supernatant was collected and stored in ice (Syama *et al*., 2013). The

measurements were carried out using UV Spectrophotometer (Lamda 25, PerkinElmer, Singapore).

3.12.2.5.1. TOTAL PROTEIN

Total protein content of liver homogenate was determined by Lowry's (Lowry *et al*., 1951) method using bovine albumin serum (BSA) as standard.

3.12.2.5.2. LIPID PEROXIDATION

Lipid peroxides formed in the liver tissue was evaluated by the method described by Ohkawa *et al*., 1979. The principle behind the method is the formation of malondialdehyde (MDA), a lipid peroxide which reacts with thiobarbituric acid (TBA) to form pink colored complex (MDA-TBA). The amount of MDA formed was spectrophotometrically measured at 532 nm and expressed as nmol/mg of protein.

3.12.2.5.3. REDUCED GLUTATHIONE

Total GSH in liver sample was determined by the method of Moron *et al.,* 1979. Ellman's reagent or DTNB (5, 5'-dithiobis- (2-nitrobenzoic acid)), reacts with GSH and form thionitrobenzoic acid (TNB), a chromophore that can be read at 412 nm. The change in absorbance is a linear relation of GSH presence and expressed as nmol/mg protein.

3.12.2.5.4. GLUTATHIONE REDUCTASE

An NADPH dependent enzyme glutathione reductase activity was measured as described by Mize &Langdon, 1962. Intracellular GSSG gets converted to GSH under increased ROS generation. The exhausted GSSG can be retrieved back during NADPH oxidation. Reduction of one μM of GSSG per min is defined as one GR unit. Rate of

NADPH oxidation is accompanied by decrease in absorbance that can be monitored by absorbance reading at 340 nm.

3.12.2.5.5. GLUTATHIONE PEROXIDASE

Glutathione peroxidase use cellular GSH and form GSSG, the activity of which was estimated as described by Rotruck *et al*., 1973. GSH remaining after enzyme catalyzed reaction reacts with DTNB that absorbs maximum wavelength at 412 nm. Activity of GPx was expressed as µg of GSH consumed/min/mg protein.

3.12.2.5.6. SUPEROXIDE DISMUTASE

SOD activity was assessed as described by Marklund & Marklund, 1974. SOD is an enzyme that dismutase superoxide anion radical. Decrease in absorbance at 420 nm correlates with the inhibition of pyrogallol auto oxidation by SOD.

3.12.2.6. MORPHOLOGY OF BONE MARROW MSCs FROM PrGO EXPOSED MICE

Bone marrow was collected from animals exposed to PrGO and MSCs were cultured as described in *in vitro* culture. The cells were observed under microscope for morphological analysis.

3.12.2.7. IMMUNOTOXICITY STUDIES

Immune system can be a target for the toxic effects of drugs, chemicals or xenobiotics. Nanoparticles can either enhance or inhibit the activity of the immune system. 20 mice were given intraperitoneal injection of PrGO (0.2 mg/animal). Animals were given repeated injection on 1, 3 and 5 day and observed carefully until the experimental period. 5 animals each were sacrificed on 7, 14 and 21 days after last

injection. Animal administered with water for injection was treated as control. Spleen was collected and splenocytes proliferation studies were performed.

EXPERIMENTAL DESIGN (FROM SUB ACUTE)

Group	Dose (PrGO)	Route of exposure (3 doses at 1, 3, 5 days)	No. of mice	No. of animals sacrificed (post exposure)				Organs collected
				0 day	7 days	14 days	21 days	
1	10 mg/kg	Intraperitoneal	20	5	5	5	5	Spleen

Table 3.7: Experimental design for splenocyte proliferation study

3.12.2.7.1. SPLENOCYTES PROLIFERATION ASSAY

Mice were sacrificed at the end of experimental period (7, 14 and 21 days post exposure). Spleen were dissected and collected in an ice cold RPMI media. Single cell suspension of splenocytes were obtained using histopaque gradient. In short, the spleens were mashed in nylon mesh and transferred to tubes containing histopaque, followed by centrifugation at 2500 rpm for 40 min. The opaque interface containing spleen cells were separated and washed with PBS. The pellet was resuspended in complete RPMI media (RPMI 1640 + 10% FBS). The cells were counted and ~ 200,000 cells were seeded onto each well of 96 micro well plate. The cells were allowed to grow for 48 h in presence of 5% CO_2 at 37ºC. After 48 h, 0.5 µci of ^{3}H-tritiated thymidine was added and the plates were further incubated for another 24 h. The cells were transferred to micro centrifuge tubes and centrifuged at 10000 g for 15min. The pellet was resuspended in 1 ml of scintillation fluid and the amount of thymidine incorporation was recorded using scintillation counter. The results were obtained in cpm (counts per minute) (Syama *et al*., 2015).

3.13 STATISTICAL ANALYSIS

Results were expressed in mean ± SD and data were analyzed by Student's t-test. In all the cases, $p < 0.05$ was considered statistically significant compared to control.

CHAPTER 4: RESULTS

4. RESULTS

4.1. SYNTHESIS OF PEGYLATED REDUCED GRAPHENE OXIDE (PrGO)

Graphene oxide (GO) was successfully synthesized from graphite using modified Hummer's method. Commercially available graphite was exfoliated and oxidized in acidic medium to form water soluble brown precipitate-GO. The aqueous stability of GO was further increased by conjugating to O,O′- Bis(2-aminoethyl) polyethylene glycol (PEG) under carbodiimide catalyzed reaction forming amide bond. Nanosized GO-PEG was separated from larger sheets of GO using centrifugation and filtration. This engineered nanosized GO-PEG was chemically reduced by sodium borohydride to obtain nanographene (PrGO). GO was chemically reduced by sodium borohydride to obtain reduced graphene oxide (RGO) for characterization (Figure 4.1).

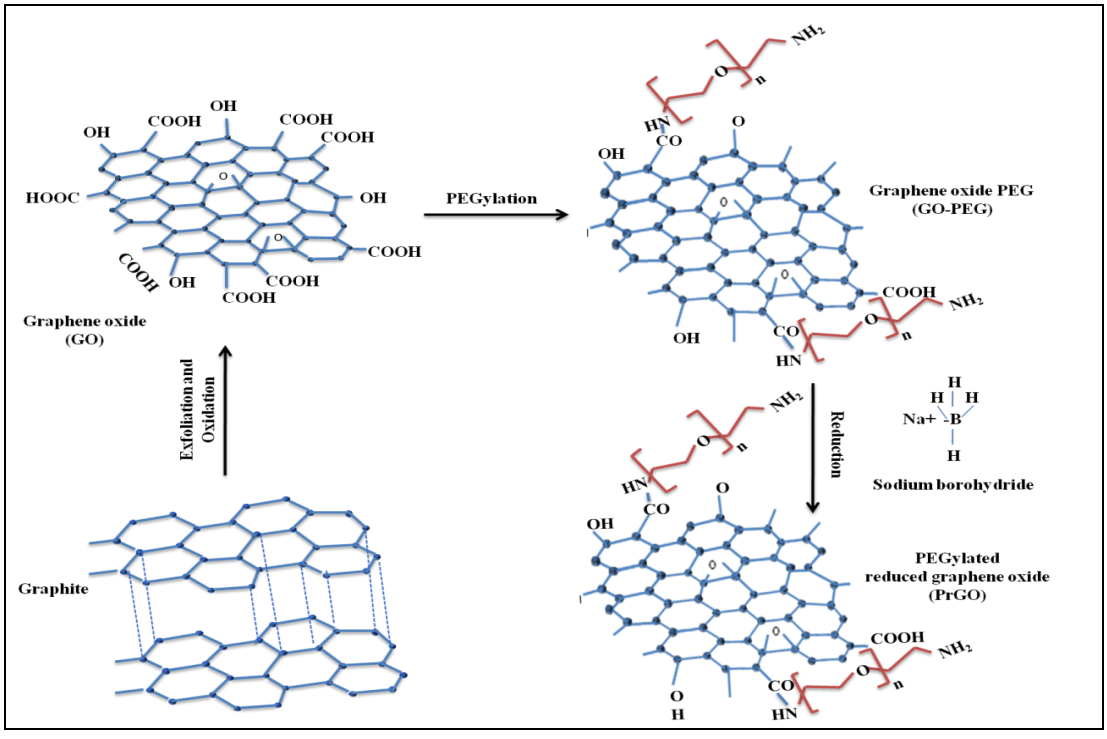

Figure 4.1: Chemical reaction of PrGO synthesis from graphite flakes

4.2. CHARACTERIZATION

The synthesized RGO and PrGO were characterized using following techniques:

4.2.1. TRANSMISSION ELECTRON MICROSCOPY (TEM)

The prepared PrGO was hydrophilic and dispersed well in water. Figure 4.2 shows TEM micrographs of PrGO and RGO. TEM images at low magnification shows very clean surface of graphene sheets with folding and wrinkles. The crystallographic structure of the graphene sheets was characterized by Selective Area Electron Diffraction (SAED). SAED pattern showed that most of the graphene sheets in RGO exhibited a single set of hexagonal diffraction pattern with sharp and clear diffraction spots (inset in Figure 4.2), indicating the high crystallinity of the graphene sheets. In case of PrGO, graphene sheets showed sharp and clear diffraction spot, which confirms their crystallinity. Instead of getting a single set of hexagonal diffraction patterns, multiple spots were observed in PrGO which could be attributed to the multiple layers as observed in TEM image.

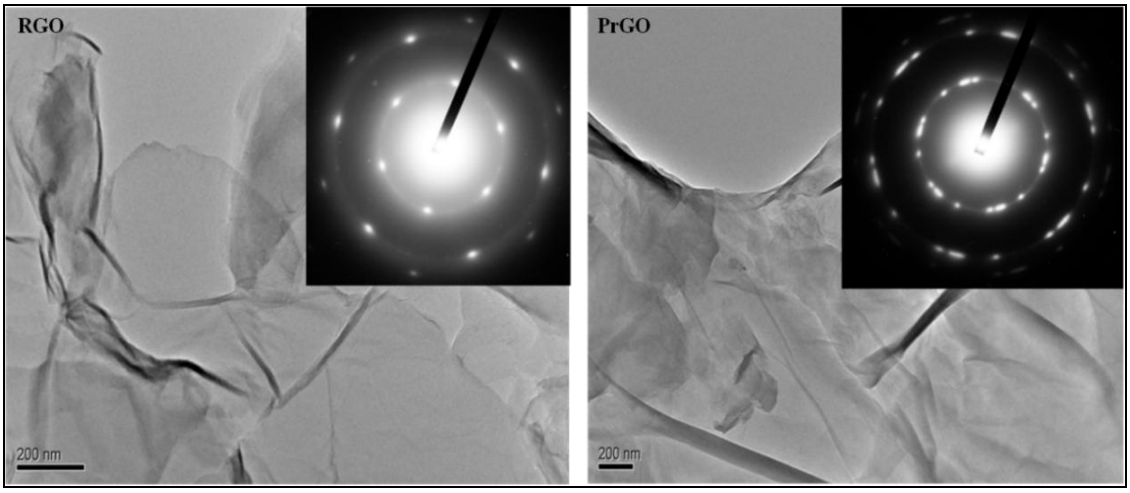

Figure 4.2: TEM micrograph of RGO and PrGO. Inset: SAED pattern of RGO and PrGO. (Scale bar represents 200 nm).

4.2.2. ATOMIC FORCE MICROSCOPY (AFM)

The thickness of the synthesized PrGO and RGO was determined using AFM (Figure 4.3). Based on the sample analysis, the thickness of RGO is around 2-3 nm. No single-layered graphene (less than 1 nm) was identified by the AFM. This could be due to the low constituent of single-layered graphene in the samples as confirmed by the TEM and SAED results. The thickness of PrGO was found to be increased to 8-9 nm, because of the surface modification by PEG. The average lateral dimension was found to be ~ 1µm.

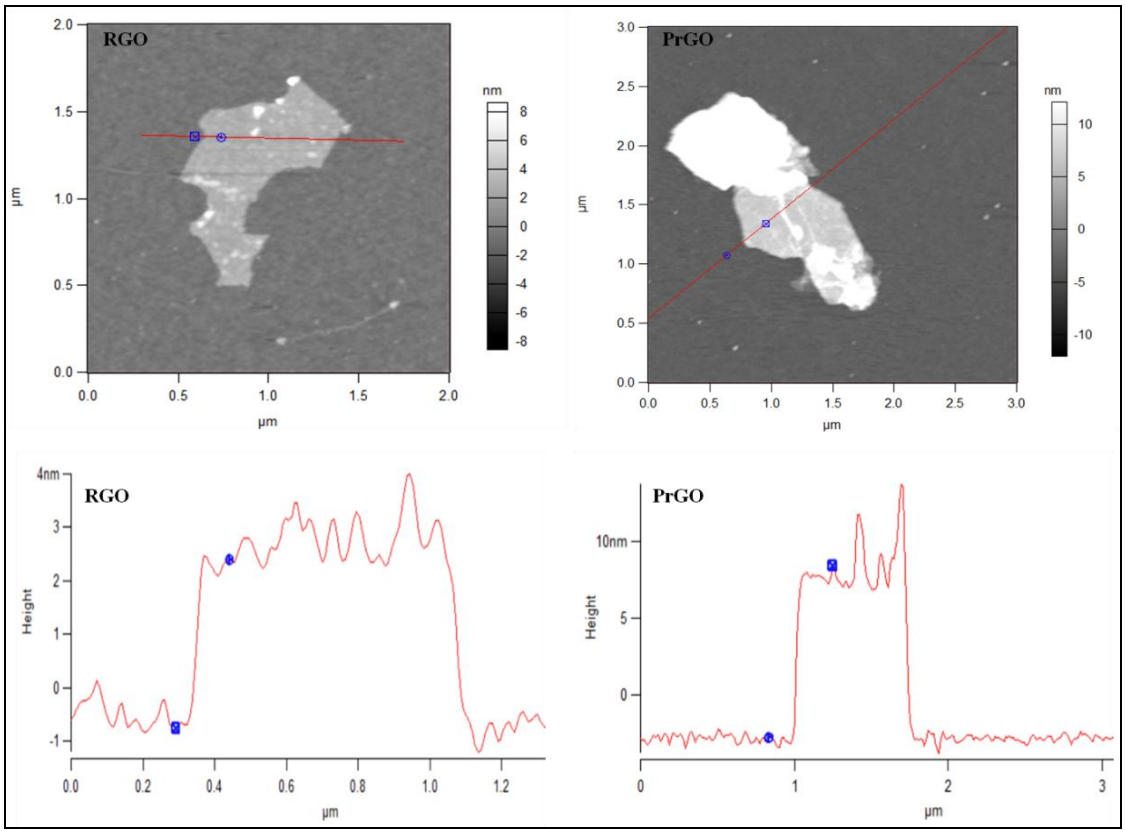

Figure 4.3: AFM image and the corresponding height profile of RGO and PrGO.

4.2.3. X-RAY PHOTOELECTRON SPECTROSCOPY (XPS)

XPS is a sensitive and semi quantitative method to scan the surface of the material to analyze the elemental composition and purity. Binding energy of 1000 eV to 0 eV were scanned to examine the overall composition of elements (Figure 4.4). The synthesized RGO consisted of mainly carbon with some amount of oxygen. The C 1s core level XPS spectrum is shown in Figure 4.4b. Two components in the spectrum at approximately 284.4 and 285.2 keV were identified as the sp^2-bonded carbon atoms (C=C/C-C in aromatic rings) and the sp^3-bonded carbon atoms (C-OH), respectively. These sp^3-bonded carbon atoms were mainly present at the periphery of the graphene sheets and the defective dangling bonds. The intensity of sp^2 carbon atoms was significantly dominant over that of sp^3 carbon atoms in RGO indicating the high quality of the resulting graphene sheets whereas in the case of PrGO, the sp3-bonded carbon peak increased due to the presence of polymer coating.

4.2.4. FOURIER TRANSFORM INFRARED SPECTROSCOPY (FTIR)

The FTIR spectrum of RGO and PrGO is shown in the Figure 4.5. Three additional peaks were observed in PrGO, when compared to RGO. The peaks at 2845, 1442 and 1050 cm^{-1} corresponding to C-H stretching, C-H plane bending and C-O-C stretching confirmed the coating of PEG onto graphene.

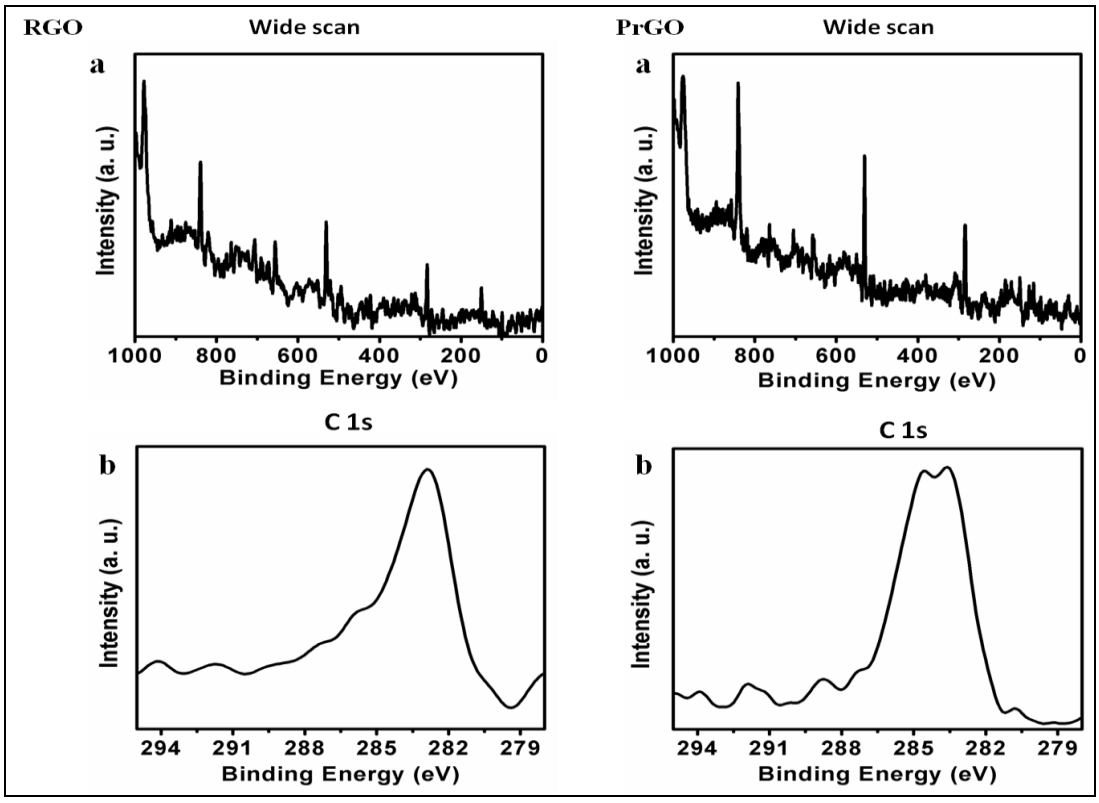

Figure 4.4: XPS analysis of RGO and PrGO. (a) Wide scan XPS spectra (b) C1s XPS spectra

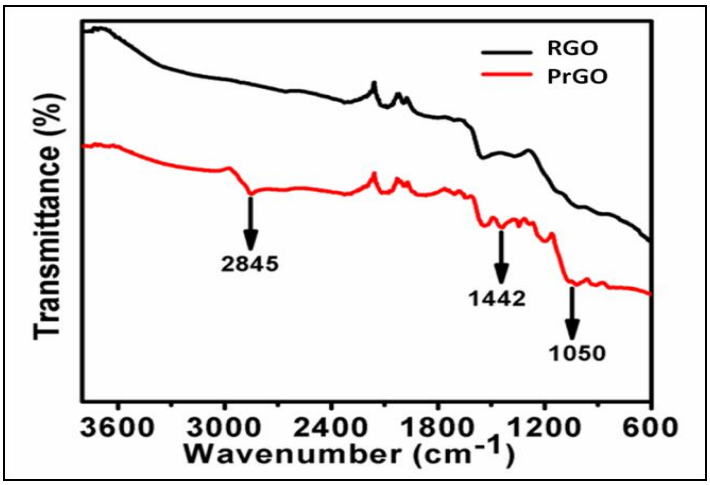

Figure 4.5: FTIR spectra of RGO and PrGO

4.2.5. RAMAN SPECTROSCOPY

Raman spectroscopy is widely used to characterize the structural and electron properties of graphene. Figure 4.6 represents a typical Raman spectrum of the sample. Characteristic peaks are clearly visible at 1330 (D-mode), 1575 (G-mode). D band occurs as a result of disorder structure of graphene while G band is usually assigned to the E_{2g} phonon of C sp^2 atoms. D band is slightly higher than the G band in both the case of RGO and PrGO mainly due to the presence of some defective site and presence of sp^3hybridized carbon.

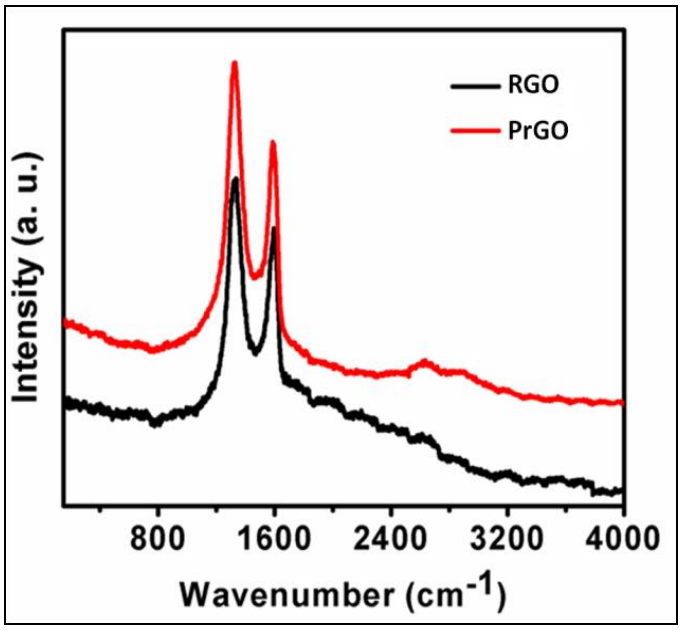

Figure 4.6: Raman spectra of RGO and PrGO

4.2.6. X-RAY DIFFRACTION (XRD)

The powder X-ray diffraction was further used to characterize the bulk structure of the prepared RGO and PrGO (Figure 4.7). The graphite peak is absent in both the spectrum indicating the complete exfoliation. The broad peak around 25° (2θ)

corresponds to *d* spacing of 0.36 nm which is due to restacking of graphene sheets. This peak corresponds to 002 plane of graphite. The removal of oxygen atoms that got into the graphite framework during the intercalation process results in decreased *d* spacing. This confirms the reduction process of graphene oxide to graphene. There is no significant change in the spectral feature of PrGO when compared to RGO indicating that PEG coating does not alter the basic structural feature of RGO.

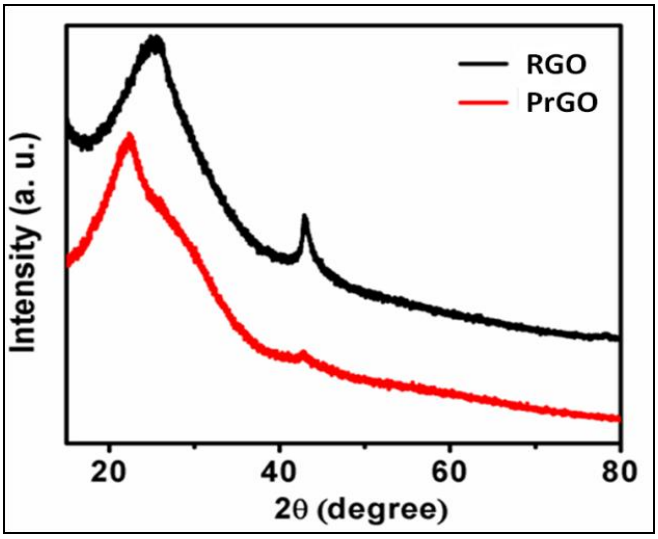

Figure 4.7: XRD pattern of RGO and PrGO

4.2.7. THERMOGRAVIMETRIC ANALYSIS (TGA)

TGA was used to assess the level of reduction of the GO sheets and amount of PEG coating over graphene oxide. Thermograms (Figure 4.8) indicate weight loss as a function of temperature for RGO and PrGO (heating rate of 10°C/min) under a nitrogen atmosphere. The RGO sample showed some weight loss with an onset temperature at slightly greater than 100°C, which was attributed to the elimination of interlamellar water, followed by loss of oxygen from the GO platelets, at slightly higher temperatures.

In PrGO, a significant weight loss around 350-400°C indicates the decomposition of organic material, mainly PEG. From the graph it was estimated that around 50% of total weight of the PrGO was from the PEG.

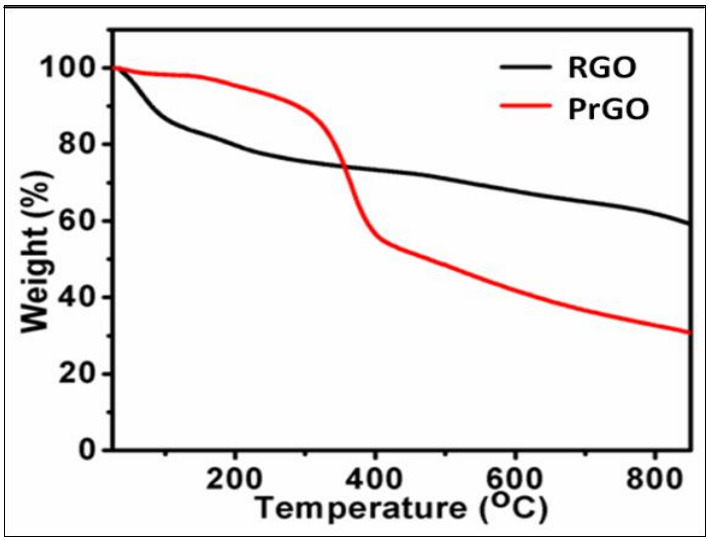

Figure 4.8: TGA curves of RGO and PrGO

4.3. ENDOTOXIN CONTENT

Determination of endotoxin is a mandatory requirement for nanoparticles preparation, to distinguish toxicity mediated by the endotoxin from the nanoparticles. Table 4.1 indicated that the endotoxin content was estimated to <0.1 EU/ml in both RGO and PrGO.

Nanomaterial	**Level of Endotoxin (EU/ml)**
PrGO	<0.1
rGO	<0.1

Table 4.1: The level of endotoxin detected using Endosafe®-PTS

4.4. ISOLATION AND CHARACTERIZATION OF MESENCHYMAL STEM CELLS (MSCs)

MSCs were isolated from mouse bone marrow and cultured on DMEM complete media. The cells readily attached to the culture vessel because of its plastic adherence property. The cells appeared spindle shaped fibroblast morphology and formed discrete colonies (Figure 4.9). Unwanted haematopoietic stem cells were dislodged by frequent medium change. 80% confluent cells were obtained at the end of two weeks. The cells were trypsinized using 0.25% Trypsin-EDTA, sub-cultured and maintained in complete DMEM media. The cells stained for actin filaments using Rhodamine Phalloidin showed that the cells adhered onto the plastic surface of culture plates (Figure 4.10a). The expression of surface markers (Figure 4.10 b, c, d) of MSCs such as positive markers (CD 90 and CD 44) and negative marker (CD 45-haematopoietic stem cell marker) were characterized by immunostaining. Quantitative analysis (FACS) showed around 60-70% of the cells express positive markers, CD 90 and CD 44 (Figure 4.11).

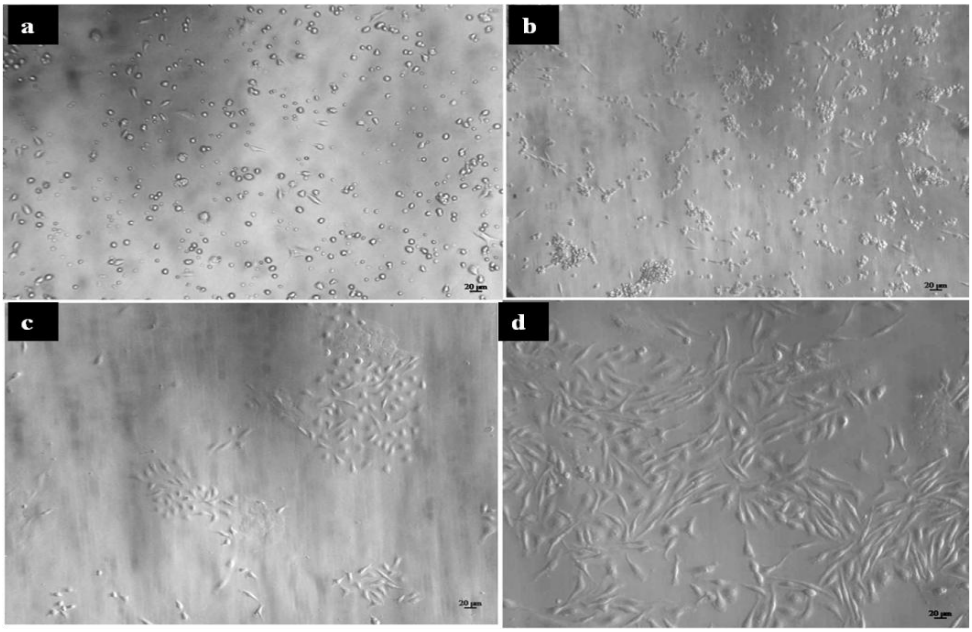

Figure 4.9: Isolation and culture of MSCs from mouse bone marrow. (a) Cells after one day of culture; (b) Cells after 7 days of culture; (c) Cells after 14 days of culture; (d) Cells after 21 days of culture.

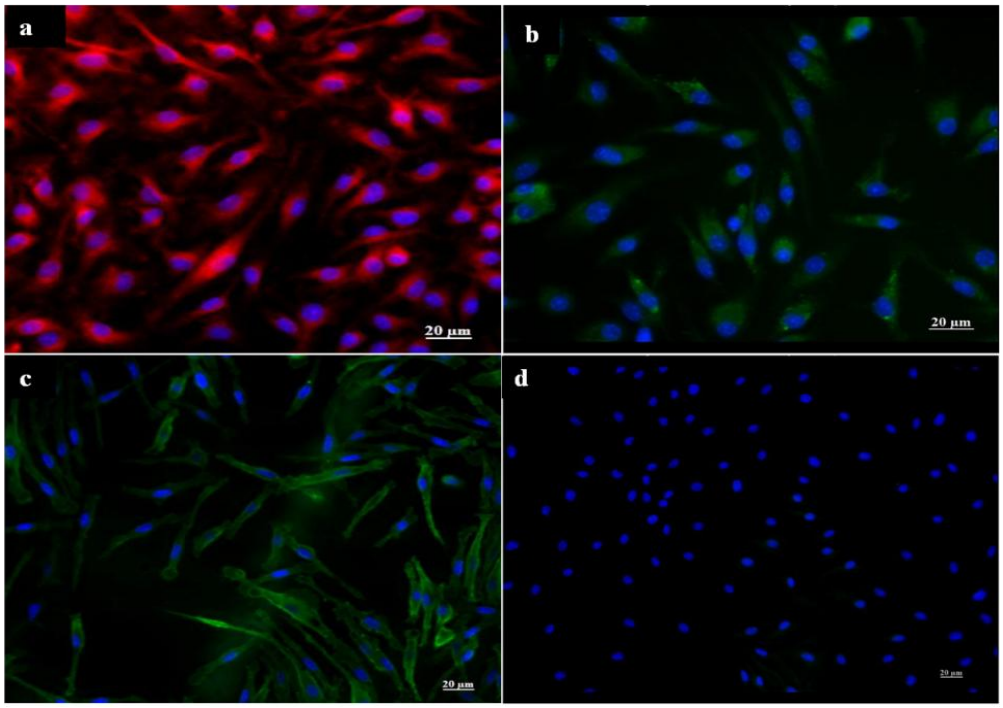

Figure 4.10: Expression of surface markers. (b,c) CD90, CD 44 (positive markers); (d) CD 45 (negative marker). (a) Actin staining of MSCs using Rhodamine Phalloidin. Nucleus counterstained with DAPI. Scale bar represents 20 µm.

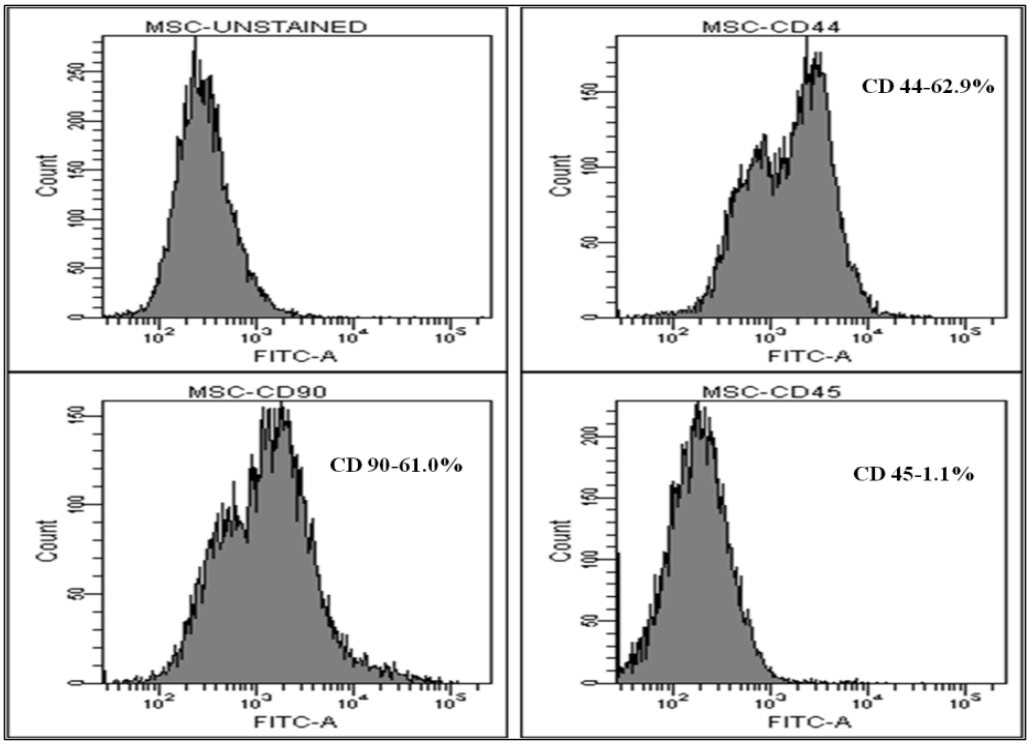

Figure 4.11: FACS analysis of expression of surface markers on isolated MSCs after third passage.

4.4.1. DIFFERENTIATION

The differentiation potential of isolated MSCs was studied by culturing MSCs in adipogenic and osteogenic differentiation medium. At the end of 21 days, MSCs were readily differentiated into adipocytes and osteoblasts. Figure 4.12 and Figure 4.13 shows the adipocytes with lipid granules and extracellular mineralized matrix (calcium deposits) in osteoblasts.

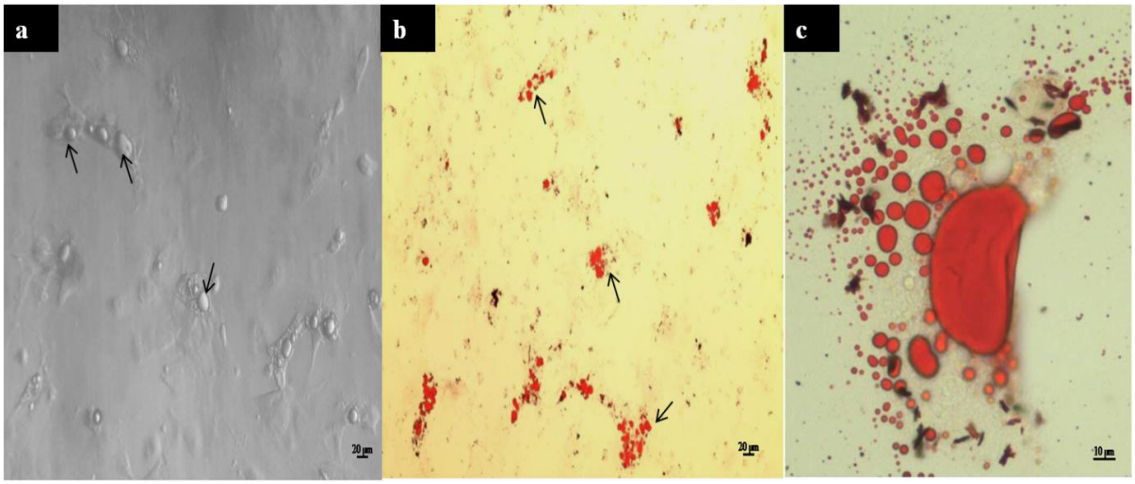

Figure 4.12: Differentiation of MSCs towards adipogenesis. (a) Phase contrast; (b, c) The lipid granules of the adipocytes were stained with Oil Red. Arrows indicates lipid granules.

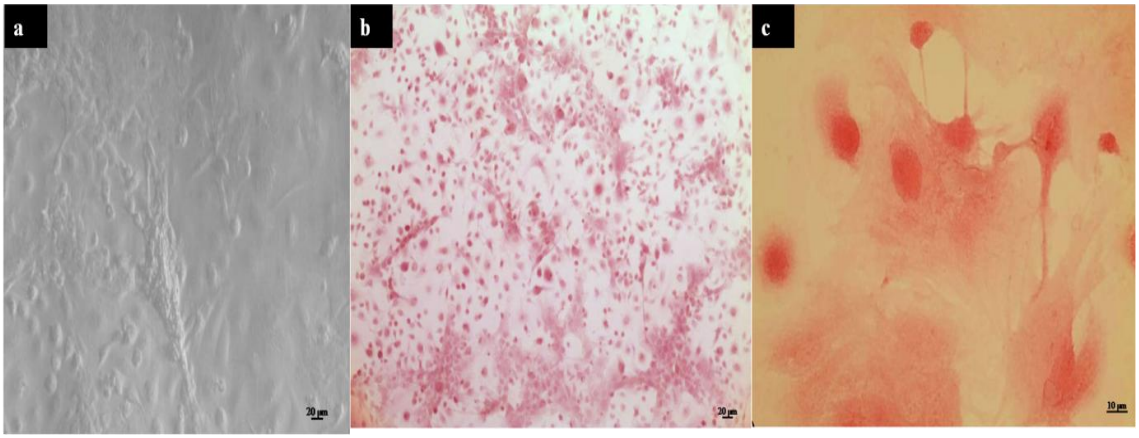

Figure 4.13: Osteogenic differentiation of MSCs. (a) Phase contrast; (b, c) The calcium deposits of osteoblasts were stained with pink with alizarin red

4.5. PROTEIN CORONA

The hard corona proteins were isolated from PrGO after incubation with 10% FBS. Different concentration of PrGO (10 and 100 µg/ml) was incubated with 10% FBS for different time period (5, 30 min and 2 h). The isolated hard corona proteins were separated on SDS –PAGE analysis. The result showed that only BSA strongly adheres to the surface of PrGO (Figure 4.14). All other proteins in FBS were washed away during

centrifugation (soft corona). There were no changes in the intensity of the band observed at different concentration of PrGO and at different time period.

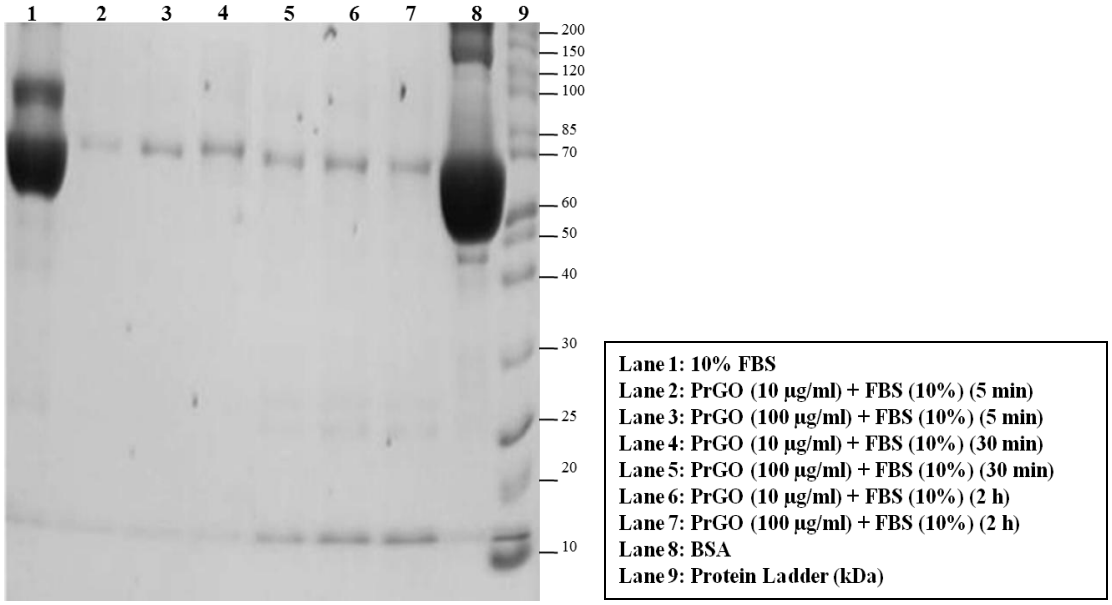

Figure 4.14: SDS-PAGE analysis of hard corona proteins in PrGO after incubation with FBS

4.6. *IN VITRO* EXPERIMENTS

4.6.1. CELLULAR UPTAKE OF PrGO

MSCs were incubated with 100 µg/ml of PrGO at 37°C for 24, 48 and 72 h. There is an effective uptake of PrGO observed in MSCs without showing any morphological distortion. Presence of PrGO was evident throughout the cytoplasm, however no traces of PrGO were observed inside the nucleus (Figure 4.15 a-d). TEM analysis revealed the intracellular distribution of PrGO in cytoplasm and cytoplasmic organelles particularly lysosomes (Figure 4.15e). Despite the entry of PrGO, the cells remain intact without changes in cell membrane integrity.

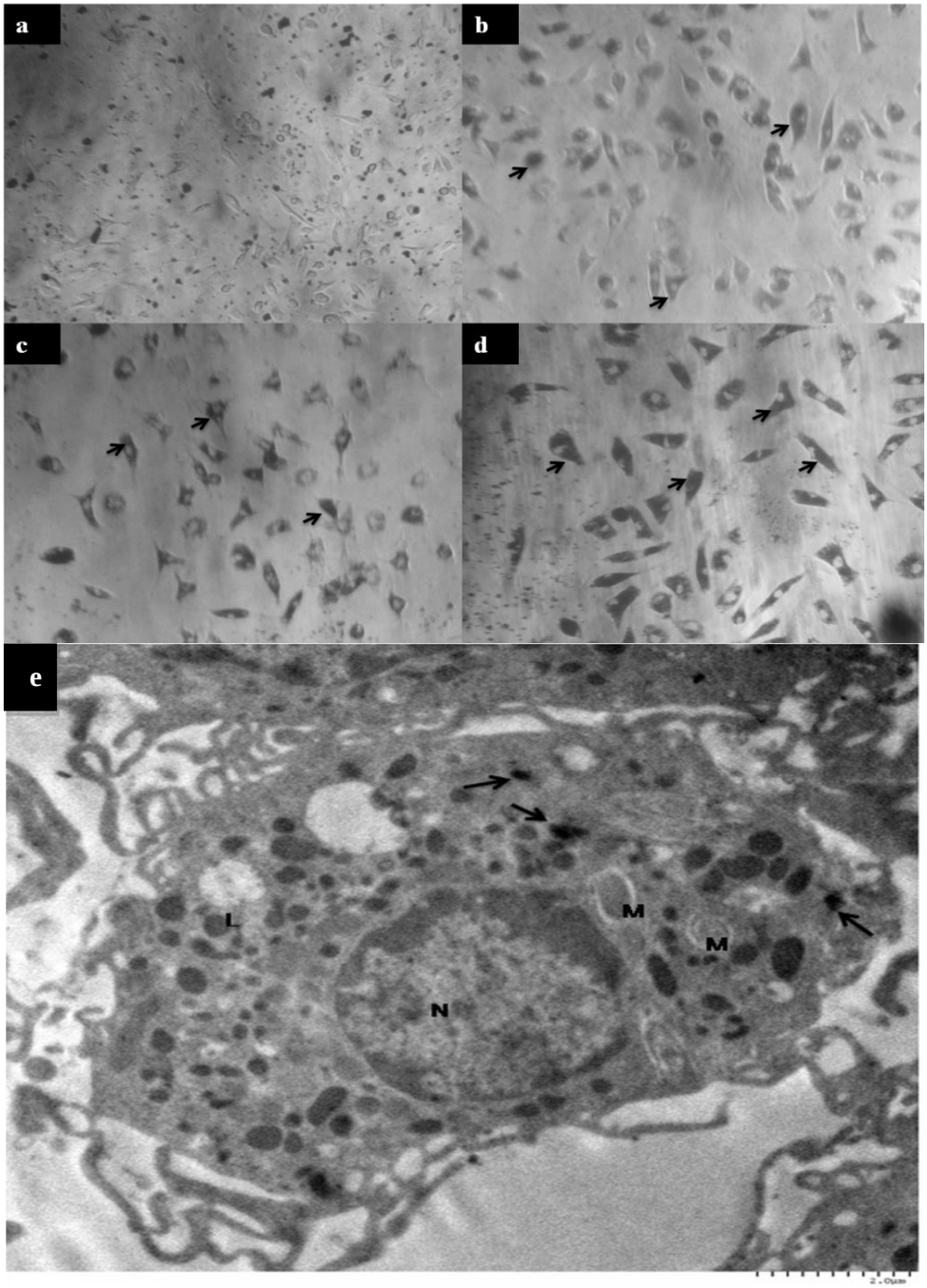

Figure 4.15: Cellular uptake of PrGO. (Phase contrast microscope, 10X). Cells were incubated with 100 µg/ml of PrGO for different time period. (a) Immediately after PrGO exposure, (b) After 24 h of exposure, (c) After 48 h of exposure, (d) After 72 h of exposure. (e) TEM analysis of intracellular distribution of PrGO (N-Nucleus, M-Mitochondria, L- Lysosomes). Arrow indicates presence of PrGO inside the cells.

4.6.2. CYTOTOXICITY

4.6.2.1. CELL VIABILITY AND METABOLIC ACTIVITY (MTT ASSAY)

The cellular viability and metabolic activity of MSCs treated with PrGO was assessed by MTT assay (Figure 4.16). The cell viability or metabolic activity was not affected by the treatment of PrGO at 24, 48 and 72 h. The cells showed excellent viability (100%) when treated with different concentrations (5, 10, 50, 100 µg/ml) of PrGO and an increased metabolic activity observed when compared to control cells. All comparisons were made with untreated (MSCs).

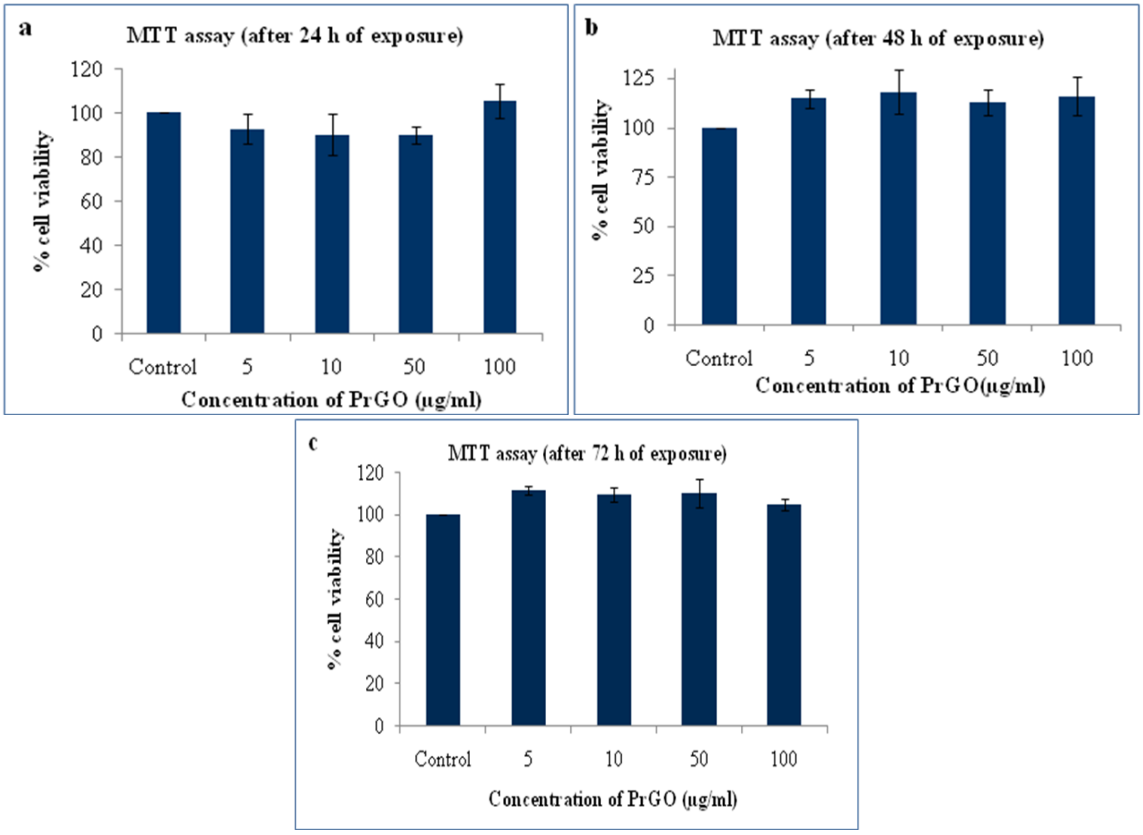

Figure 4.16: Viability and metabolic activity in cells exposed to PrGO. (a) for 24 h; (b) for 48 h; (c) for 72 h.

4.6.2.2. CELL VIABILITY (LYSOSOMAL ACTIVITY): NEUTRAL RED ASSAY

Figure 4.18 shows the viability of cells (lysosomal integrity) exposed to PrGO. MSCs were exposed to different concentration (10, 25, 50, 100, 250 and 500 µg/ml) of PrGO at 24, 48 and 72 h. No significant decrease in cell viability or lysosomal activity was noticed after PrGO treatment at different time periods. The results of the study indicated that an increased neutral red uptake in MSCs treated with high concentration of PrGO when compared to control. An increase in neutral red uptake (one fold) was seen in cells treated with PrGO when compared to control. Neutral red uptake was directly proportional to the concentration and period of exposure as shown in (Figure 4.18). Increased cell viability was observed when cells were treated with higher concentration of PrGO (100% viability even at 250 µg/ml) at 24, 48 and 72 h.

Simultaneously, the cells were observed under microscope and found that no changes in neutral red uptake except at high concentration (500 µg/ml). In 500 µg/ml, because of the increased uptake of PrGO the presence of neutral red was difficult to observe (Figure 4.17).

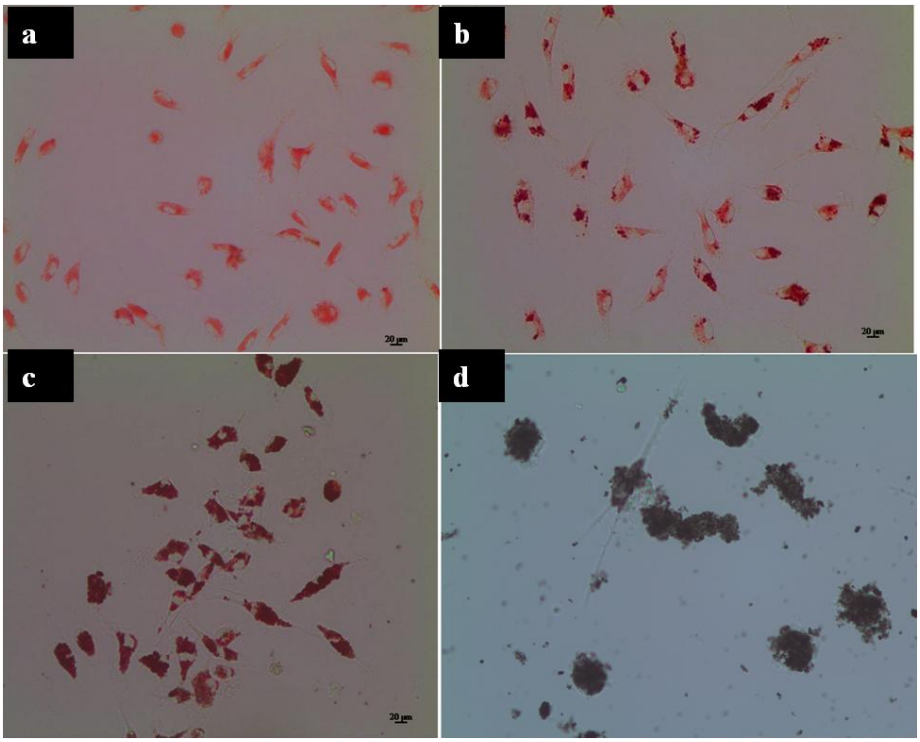

Figure 4.17: Neutral Red uptake assay after 24 h exposure to PrGO (a) Control; (b) 10 µg/ml; (c) 100 µg/ml; (d) 500 µg/ml. Control cells with neutral red in lysosomes. Red colour indicates neutral red, dark black spots indicate PrGO.

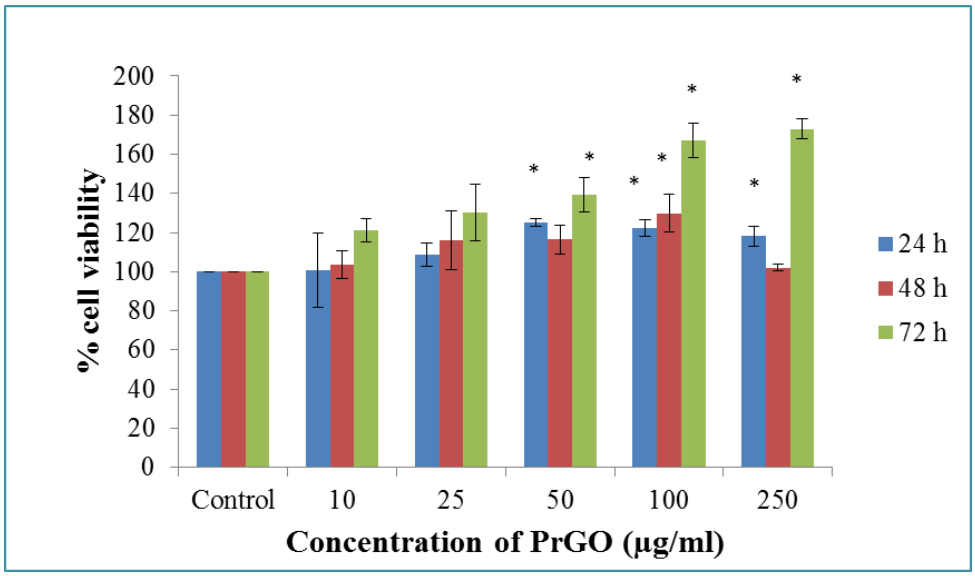

Figure 4.18: Quantitative analysis of cell viability and lysosomal activity using neutral red uptake assay

4.6.3. REACTIVE OXYGEN SPECIES PRODUCTION

The potential of PrGO to induce ROS formation inside the cells was assessed by H_2-DCFDA assay. The results are expressed in relative fluorescence intensity (RFU). There was a concentration and time dependent increase in ROS formation was observed when MSCs were treated with PrGO. Around 2-10 fold increase in fluorescence intensity was observed in cells treated with PrGO whereas the control cells showed DCF fluorescence ~3000-5000 RFU.The cells showed 2, 4, 7 and 10 fold (Figure 4.19) increase in DCF fluorescence when treated with 50, 100, 250 and 500 µg/ml of PrGO. An increased H_2-DCFDA fluorescence was observed in cells treated with high concentration of PrGO (500 µg/ml) under fluorescence microscope (Figure 4.20).

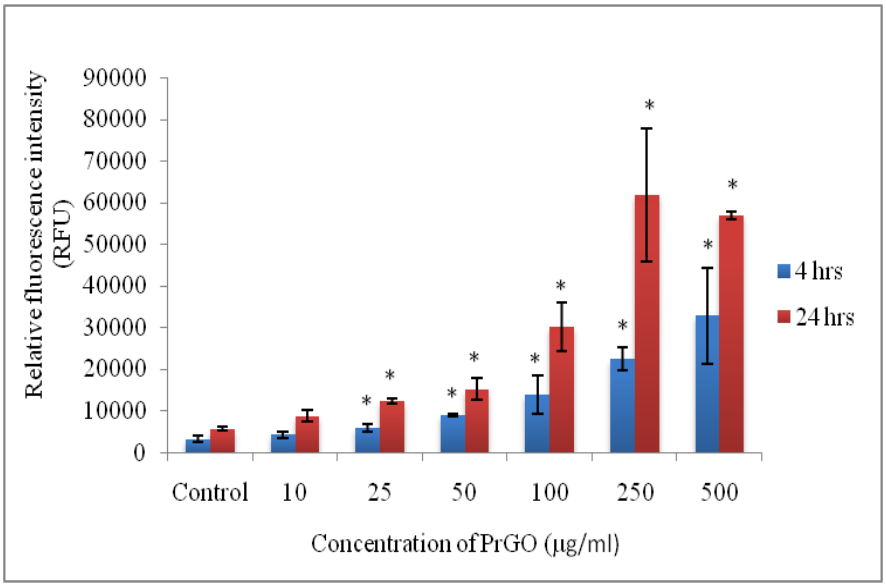

Figure 4.19: ROS production in MSCs when treated with different concentration of PrGO (4 and 24h)

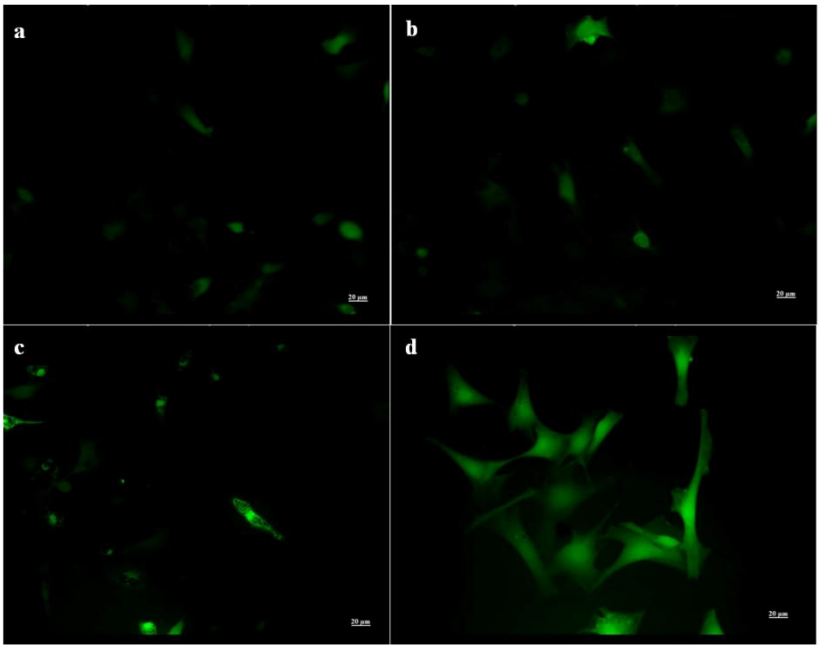

Figure 4.20: Cells stained with DCFDA under fluorescence microscope. (a) Control cells; (b) Cells treated with 10 µg/ml of PrGO; (c) Cells treated with 100 µg/ml of PrGO; (d) Cells treated with 500 µg/ml of PrGO.

4.6.4. MITOCHONDRIAL MEMBRANE POTENTIAL (MMP)

Increased ROS production can leads to mitochondrial membrane depolarization and cell death via apoptosis. Thus the change in mitochondrial membrane potential in cells after 24 h of PrGO (10, 100 and 500 µg/ml) treatment was evaluated. It was observed that no obvious change in MMP was manifested following PrGO exposure, except at high concentration (500 µg/ml). At higher concentration, the green intensity of the probe JC-1 increased and most of the cells lost their spindle shaped morphology and appeared round (Figure 4.21).

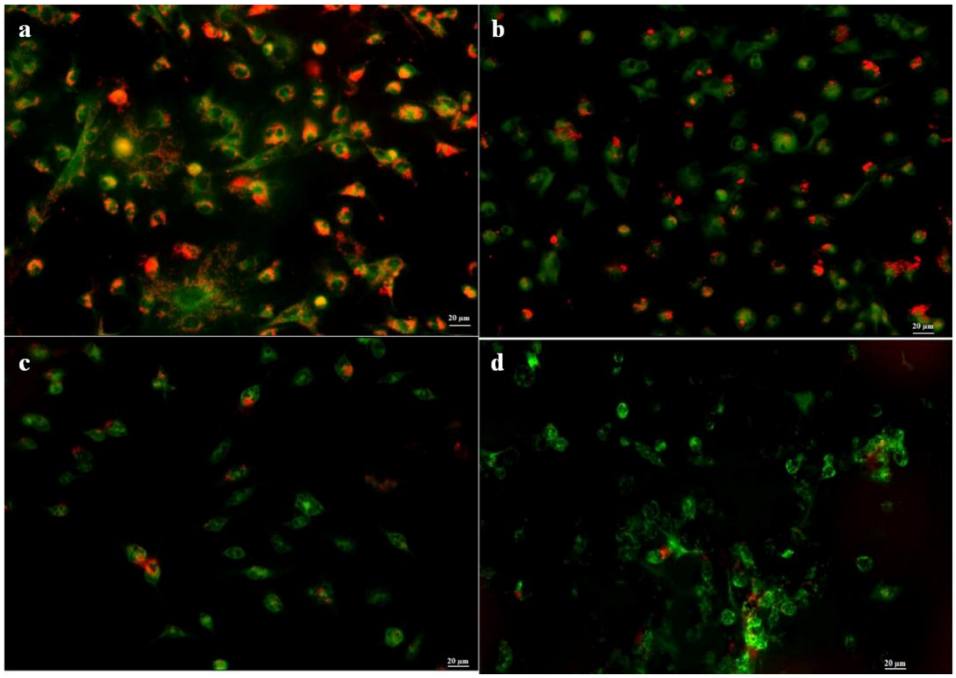

Figure 4.21: Mitochondrial membrane potential in cells after exposure to PrGO for 24 h. Cells were stained with JC-1 probe. (a) Control cells; (b) Cells treated with 10 µg/ml of PrGO; (c) Cells treated with 100 µg/ml of PrGO; (d) Cells treated with 500 µg/ml of PrGO. Scale bar represents 20 µm.

4.6.5. LYSOSOMAL MEMBRANE INTEGRITY (ACRIDINE ORANGE ASSAY)

Increased ROS production can leads to lysosomal membrane destabilization and thus the ability of the nanoparticles to induce lysosome membrane damage was assessed using acridine orange (AO) relocation assay. Qualitative analysis of lysosomal membrane damage was analyzed using fluorescent microscope. The extent of damage was quantified by measuring the fluorescent intensity at 535 nm and 620 nm using fluorescent plate reader. Percentage of AO relocation was calculated by normalizing with untreated control cells. No significant changes in AO relocation was observed in PrGO treated cells when compared to control cell (Figure 4.22). The results suggest that PrGO exposure, does not affect the integrity of lysosomal membrane.

An increased red fluorescence was observed in cells exposed to high concentration of PrGO (100, 500 µg/ml) under fluorescent microscope (Figure 4.23). This clearly states that the lysosomal membrane remains intact after PrGO treatment.

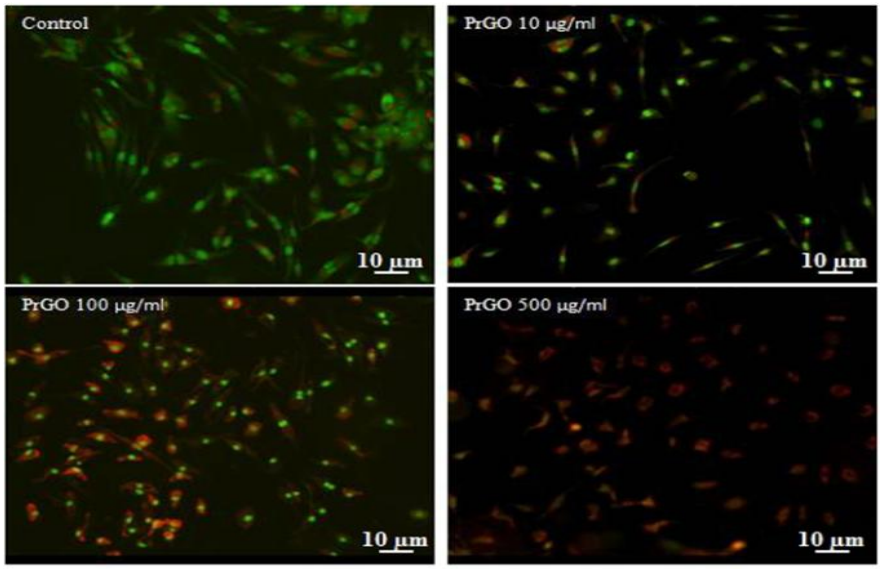

Figure 4.22: Lysosomal membrane integrity after PrGO treatment using acridine orange.

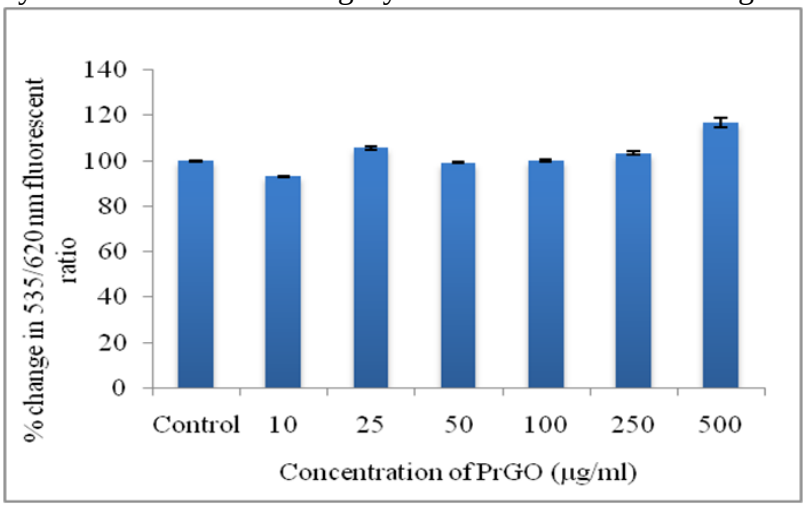

Figure 4.23: Quantification of acridine orange relocation

4.6.6. CELL ADHESION (ACTIN STAINING)

One of the characteristic features of MSCs is their plastic adherence property. Cells were stained for studying integrity of the cytoskeletal protein (actin filaments) using

Rhodamine Phalloidin staining. The actin filaments of the cells were stained red and the nuclei was counterstained using DAPI (blue). No cytoskeletal disruption was evident in cells following PrGO (10, 100, 500 µg/ml) exposure at 24 h. The cytoskeletal proteins of the treated cells remain intact as seen in untreated cells and the cells were firmly attached to the culture plates (Figure 4.24). PrGO internalization was seen in the cells as black spots where the fluorescence is quenched by the presence of PrGO.

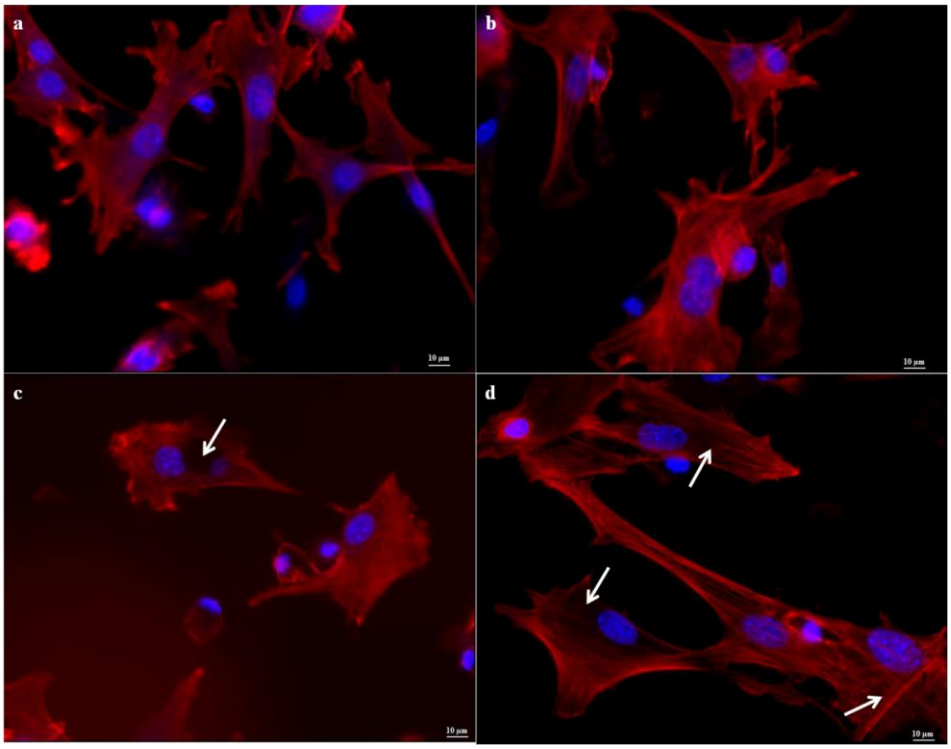

Figure 4.24: Actin staining in cells exposed to PrGO (40X). (a) Control cells; (b) Cells treated with 10 µg/ml of PrGO; (c) Cells treated with 100 µg/ml of PrGO; (d) Cells treated with 500 µg/ml of PrGO. Arrows indicate the presence of PrGO. (Scale bar represents 10 µm)

4.6.7. APOPTOSIS

4.6.7.1. LIVE/DEAD ASSAY: ANNEXIN V/PI

Cells were exposed to different concentration of PrGO (10, 100, 500 µg/ml) and stained using Annexin V/PI for apoptosis assay. From the results, it was observed that no cell death or apoptosis occurred as a result of PrGO exposure. Few early apoptotic cells were observed at high concentration (500 µg/ml) (Figure 4.25). The cells were stained negative for PI indicates absence of necrosis. Quantitative analysis using FACS was unable to perform because of PrGO at high concentration quenches PI.

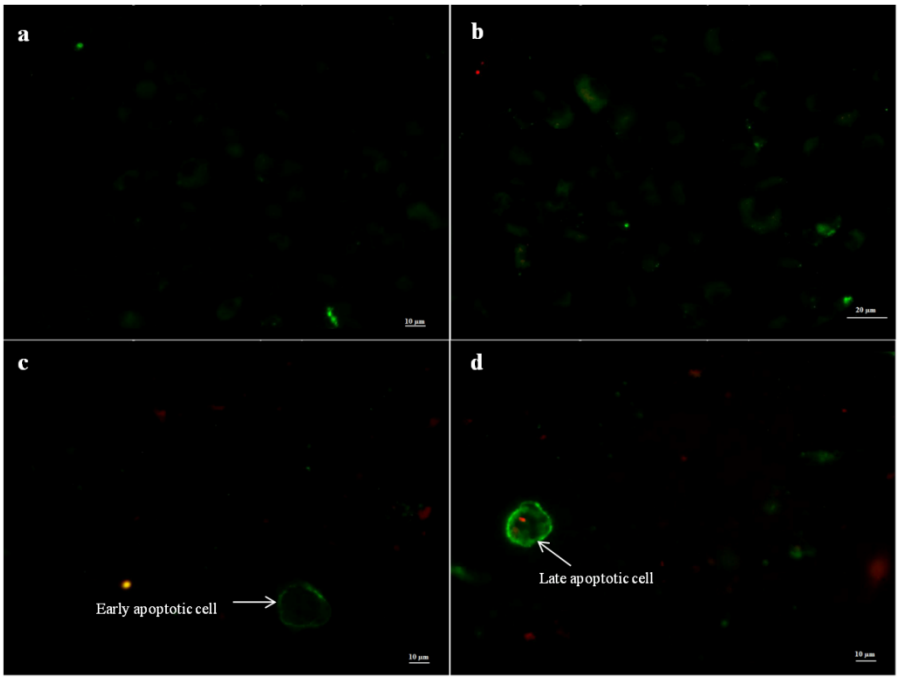

Figure 4.25: Annexin V/PI staining of MSCs after exposure to PrGO (Live/Dead Assay). (a) Control cells; (b) Cells treated with 10 µg/ml of PrGO; (c) Cells treated with 500 µg/ml of PrGO showing early apoptotic cell; (d) Cells treated with 500 µg/ml of PrGO showing late apoptotic cell.

4.6.7.2. CASPASE ASSAY

The increased ROS production, promote caspase activation resulting in cell death via apoptosis. Caspase 3 and caspase 7 are the major caspases involved in the execution phase of apoptosis. The activity of both caspases (caspase 3 and caspase 7) in MSCs exposed to PrGO (10, 25, 50, 100, 250 and 500 µg/ml) was evaluated using Sensolyte Homogenous AMC caspase 3/7 assay kit. No significant caspase activation was observed in cells exposed to different concentration of PrGO compared to control (Figure 4.26). The fluorescence intensity of treated cells (RFU ~63500-74800), which was similar to that of the control (RFU ~73000).

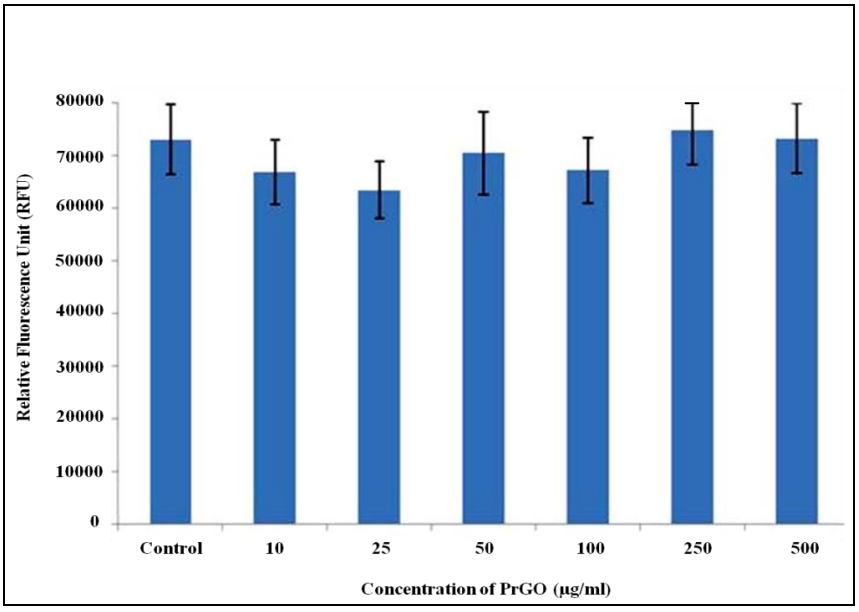

Figure 4.26: Quantification of caspase activity in cells exposed to PrGO

4.6.7.3. APOPTOTIC DNA LADDER ASSAY

The apoptotic effect of PrGO on nuclear DNA was studied using Apoptotic DNA ladder assay kit. DNA was isolated from the cells exposed to PrGO (10, 100 µg/ml) as per the manufacturer's instruction. There was no DNA fragmentation was observed in

cells exposed to PrGO (Figure 4.27). The absence of PrGO in nucleus (from cellular uptake studies) and the absence of DNA fragmentation suggest that PrGO does not affect directly or indirectly the integrity of nuclear DNA.

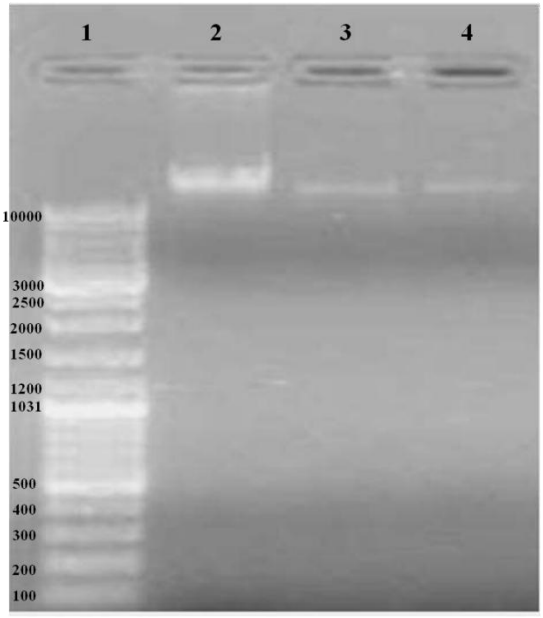

Figure 4.27: DNA fragmentation in cells exposed to PrGO.

4.6.8. ALKALINE PHOSPHATASE (ALP)

The activity of ALP in terms of the functional properties of the cells in MSCs were evaluated after exposure to different concentrations of PrGO (10, 100 µg/ml). After 24 h of PrGO treatment, cells were cultured in presence and absence of osteogenic medium. The ALP activity was analyzed using BCIP/NBT substrate. It was observed that the cells exposed to PrGO develop purple colour following the addition of BCIP/NBT. This indicates that PrGO does not interfere with the ALP activity in MSCs. The intensity of purple colour was more in cells treated with 100 µg/ml of PrGO and cells grown in osteogenic medium (Figure 4.28).

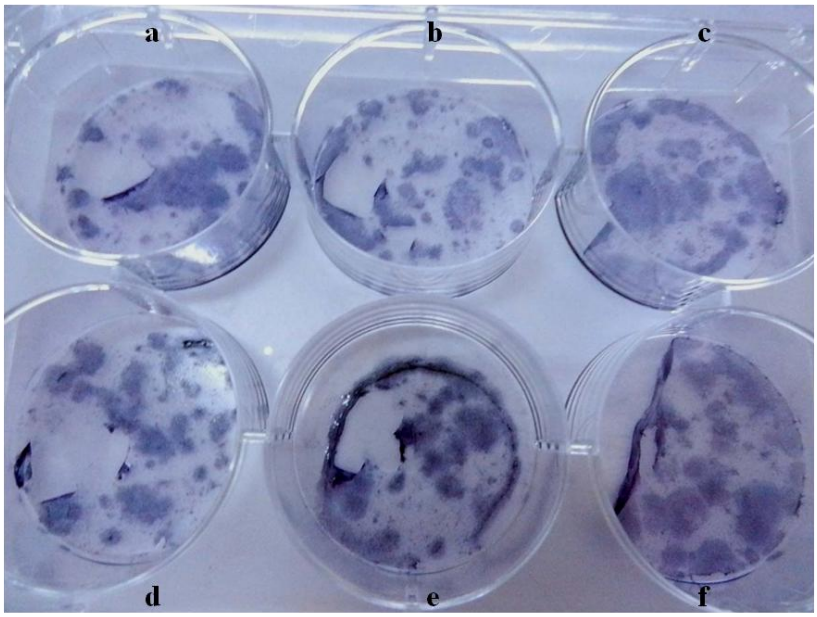

Figure 4.28: ALP activity in MSCs after PrGO exposure. (a) Control cells (DMEM medium); (b) Cells treated with 10 µg/ml of PrGO (DMEM medium); (c) Cells treated with 10 µg/ml of PrGO (osteogenic medium); (d) Cells treated with 100 µg/ml of PrGO (DMEM medium); (e) Cells treated with 100 µg/ml of PrGO (osteogenic medium); (f) Control cells cultured in osteogenic medium.

4.7. *IN VIVO* EXPERIMENTS

4.7.1. ACUTE TOXICITY

Single exposure of PrGO (10 mg/kg body weight) was intraperitoneally and intravenously administered to Swiss Albino mice of body weight between 17-23 g. The animals were kept up to 21 days. None of the animals showed any clinical symptoms such as respiratory, motor, convulsion, reflexes, ocular signs, cardiovascular signs, salivation, piloerection, analgesia and gastrointestinal responses during the experimental period (Table 4.2). There was no adverse toxic symptoms or death observed during the experimental period. Gross observations indicated that no abnormalities seen in any of the major organs.

	Clinical observations									
Volume	0.2 mg/ml Intraperitoneal (Swiss Albino mice)									
Response	1	2	3	4	5	6	7	8	9	10
3 Days	N	N	N	N	N	N	N	N	N	N
7 Days	N	N	N	N	N	N	N	N	N	N
14 Days	N	N	N	N	N	N	N	N	N	N
21 Days	N	N	N	N	N	N	N	N	N	N
Volume	0.2 mg/ml Intravenous (Swiss Albino mice)									
Response	1	2	3	4	5	6	7	8	9	10
3 Days	N	N	N	N	N	N	N	N	N	N
7 Days	N	N	N	N	N	N	N	N	N	N
14 Days	N	N	N	N	N	N	N	N	N	N
21 Days	N	N	N	N	N	N	N	N	N	N

Table 4.2: Clinical response of mice after acute exposure of PrGO
Response: 1. Respiratory, 2. Motor, 3. Convulsion, 4. Reflexes, 5. Ocular signs, 6. Cardiovascular signs, 7. Salivation, 8. Piloerection, 9. Analgesia, 10. Gastrointestinal. N=Normal.

4.7.1.1. BIODISTRIBUTION AND TOXICOKINETICS

4.7.1.1.1. DETECTION OF PrGO IN TISSUES BY RAMAN MAPPING

Liver, spleen, kidney and brain of mice (acute toxicity) were scanned for the presence of PrGO by Confocal Raman microscope. The cluster analysis was performed on the characteristic Raman spectral scan obtained.The color coded Raman image shown in figure 4.29 (a) and (b) corresponds to different tissues, observed at different time intervals. The blue spectrum and region corresponds to the tissue, red spectrum and region corresponding to graphene with the multiplexed signals at 1580 cm^{-1} (G band) and 1340 cm^{-1}(D band) which confirmed the presence of PrGO. The corresponding Raman spectra as a result of cluster analysis of the different tissue samples are similar and a sample spectrum is shown in figure 4.29 (c). Table 4.3 indicates the percentage of PrGO in liver, spleen, kidney and brain.

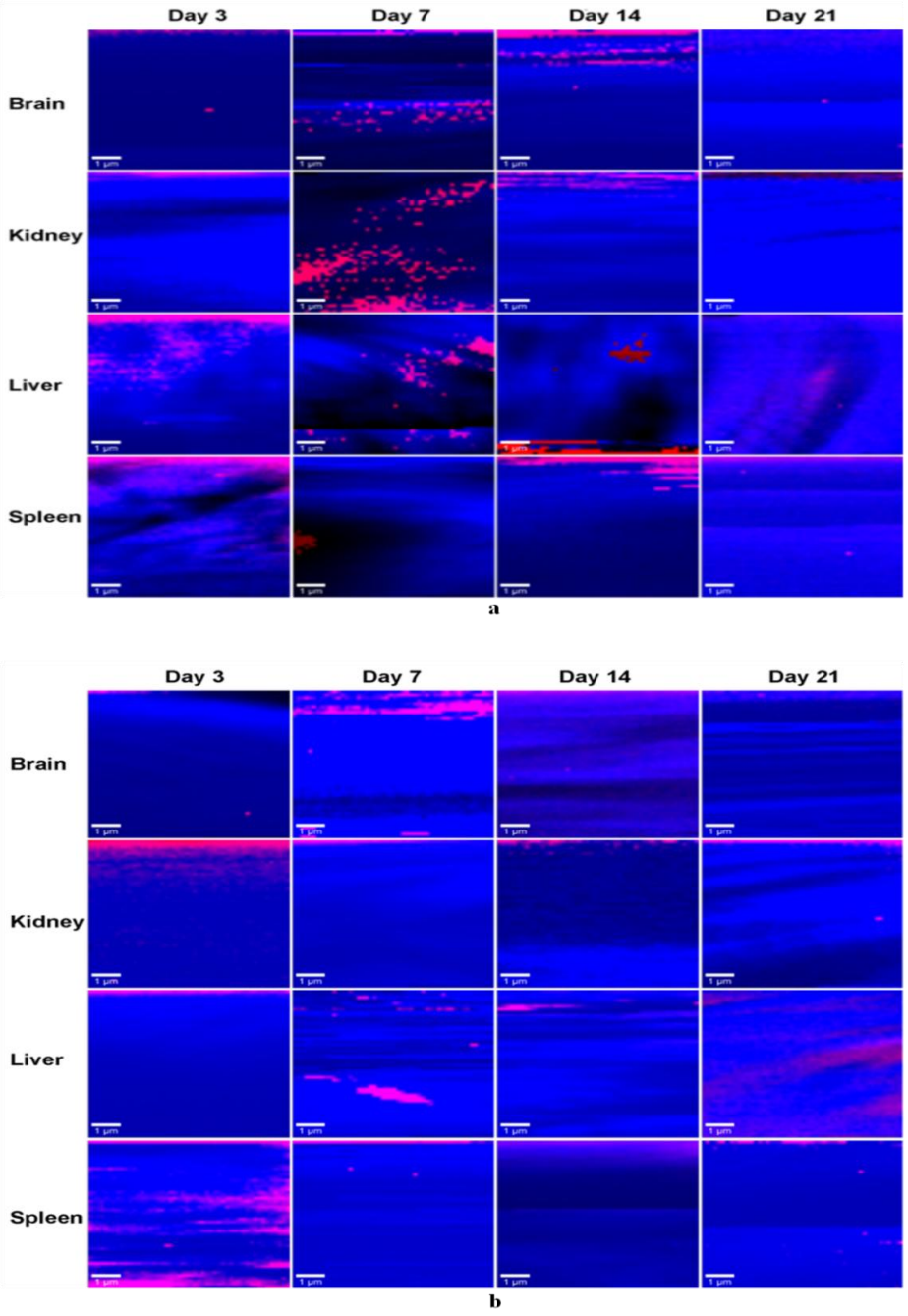

Figure 4.29: Raman mapping of tissue samples after PrGO administration. (a) Color coded Raman cluster map of different tissue samples scanned (area 7 x 7 μm^2) at different timings after intravenous administration of PrGO. Red region being PrGO and blue the tissue; (b) Color coded Raman cluster map of different tissue samples scanned (area 7 x 7 μm^2) at different timings after intraperitoneal administration of PrGO. Red region being PrGO and blue the tissue.

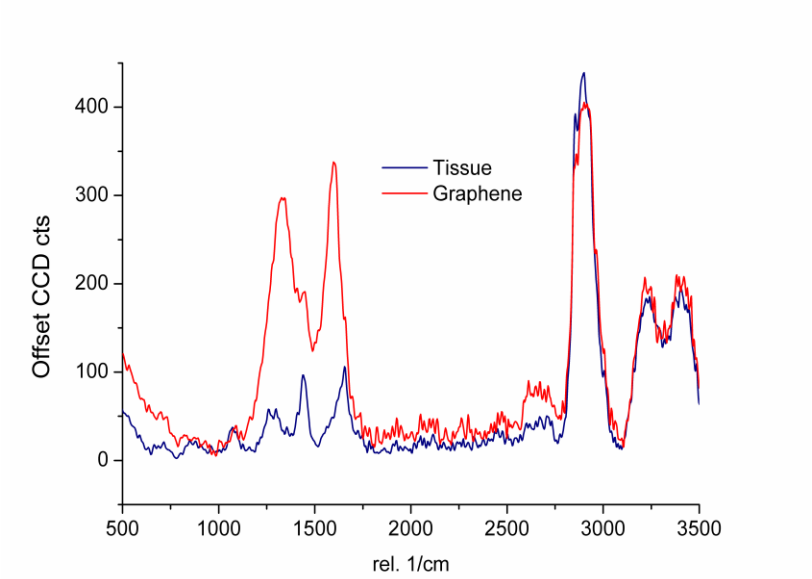

Figure 4.29 (c): The representative demixed Raman spectra as a result of cluster analysis of tissue samples. Red spectrum being PrGO and blue the tissue.

Mode of injection	Organ	Day 3	Day 7	Day 14	Day 21
Intravenous administration	Brain	5.62	12.11	15.24	8.48
	Kidney	5.27	21.95	6.94	6.75
	Liver	20.76	8.99	9.25	17.07
	Spleen	22.06	3.33	9.71	11.16
Intraperitoneal administration	Brain	2.90	15.27	17.42	7.38
	Kidney	2.61	4.77	5.13	5.69
	Liver	5.90	7.86	4.69	31.9
	Spleen	27.92	5.08	7.02	4.45

Table 4.3: Percentage of graphene in each field of observation (7 x 7 μm^2) of Raman chemical map (i.p. and i.v.)

4.7.1.1.2. DETECTION OF PrGO IN BONE MARROW

Presence of PrGO was identified in bone marrow cells by Raman mapping.Intraperitoneally injected PrGO (10 mg/ kg body weight) was efficiently absorbed from the peritoneal cavity to the bone marrow. The intensity of the peaks decreases from day 3 to day 14 reveals the elimination of PrGO (Figure 4.30) from the body.

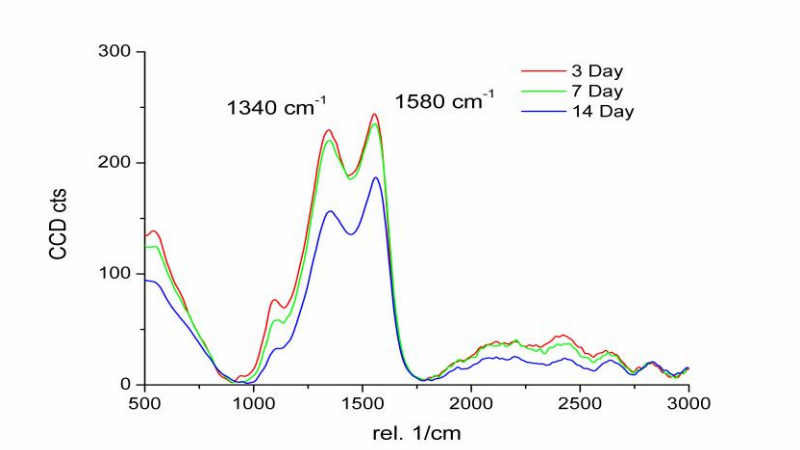

Figure 4.30: Raman mapping of bone marrow for the presence of PrGO

4.7.1.1.3. DETECTION OF PrGO IN URINE

Urine was collected from the PrGO treated animals and analyzed by Raman mapping. The results indicated that very weak PrGO spectra, stating that only a small portion of the injected PrGO excreted via the urine. Presence of PrGO was identified with the multiplexed signals at 1580 cm^{-1} (G band) and 1340 cm^{-1} (D band). The intensity of the spectra gradually decreases from Day 3 to Day 21 (Figure 4.31).

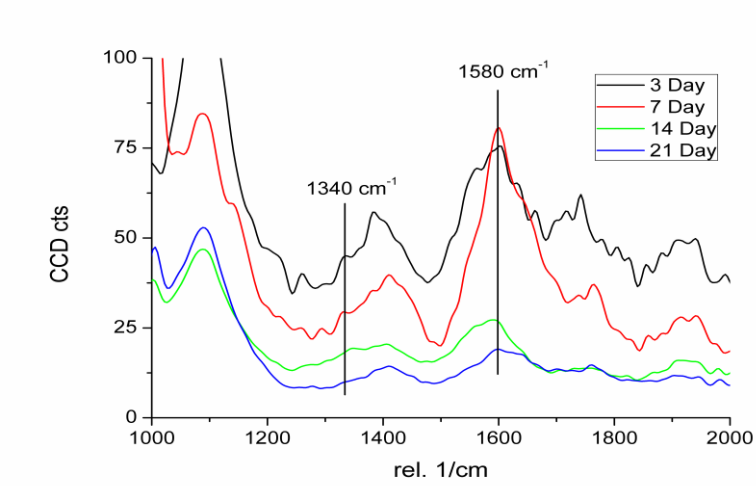

Figure 4.31: Raman mapping of urine sample. Spectra of urine samples were analyzed in air using 20x objective; with an integration time of 0.2 s.

4.7.1.1.4. DETECTION OF PrGO IN BLOOD

The blood sample collected at different time periods after intravenous and intraperitoneal administration of PrGO was subjected to Raman mapping. Maximum release (high intensity spectra) of PrGO in blood was observed at the end of 3 h in both i.v. and i.p. administration (Figure 4.32 a & b). Thereafter a gradual decrease in the spectral intensity was noticed in the following time period.

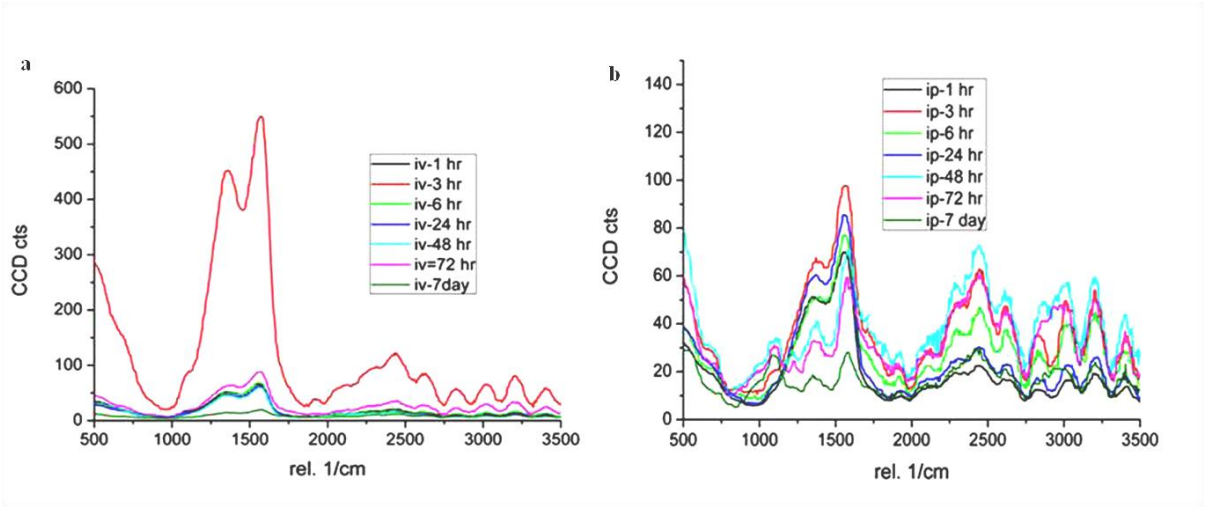

Figure 4.32: Raman mapping of blood sample after PrGO administration. (a) Relative intensities of Raman spectra of blood samples collected at different timings after i.v. administration of PrGO; (b) Relative intensities of Raman spectra of blood samples collected at different timings after i.p. administration of PrGO

4.7.1.2. HAEMATOLOGY AND CLINICAL CHEMISTRY

Analysis of blood sample collected from PrGO treated animals showed significant differences in few parameters. It was observed that the values of RBC (4.38 ± 0.81*), HGB (7.10 ± 1.45*), HCT (20.87 ± 3.00*) were significantly reduced in 7 days compared to control (RBC- 8.93 ± 0.49; HGB-13.53 ± 1.00 and HCT- 42.73 ± 2.00).The RBC, HGB and HCT values were normalized at the end of 14 days of exposure.

Similarly, differences were noticed in few of the clinical chemistry parameters. Parameters such as urea, cholesterol, albumin, total protein, SGOT, SGPT were significantly changed when compared to control except glucose and creatinine. Increased SGOT (210.67 ± 35.80*) and SGPT (153.33 ± 6.11*) activity suggest possible liver injury.

Parameters	Control	3 days	7 days	14 days	21 days
WBC (10^6/mm^3)	5.40 ± 0.20	5.5 ± 0.26	6.90 ± 2.00	5.60 ± 0.26	5.77 ± 0.15
RBC (10^3/mm$^{3)}$	8.93 ± 0.49	8.93 ± 0.06	4.38 ± 0.81*	8.87 ± 0.40	8.83 ± 0.32
HGB (g/dL)	13.53 ± 1.00	12.60 ± 0.66	7.10 ± 1.45*	12.03 ± 0.61	12.13 ± 0.32
HCT (%)	42.73 ± 2.00	43.90 ± 1.54	20.87 ± 3.00*	42.57 ± 1.10	42.80 ± 0.98
MCV (μm^3)	47.47 ± 1.05	47.20 ± 1.54	48.77 ± 0.64	46.53 ± 0.95	46.93 ± 0.95
MCH (pg)	16.87 ± 0.35	17.20 ± 0.30	16.17 ± 0.67	17.27 ± 0.25	17.67 ± 0.15
MCHC (g/dL)	35.67 ± 0.96	36.17 ± 0.64	32.97 ± 1.75	36.07 ± 0.55	36.23 ± 0.25
PLT (10^3/mm^3)	358.33 ± 17.56	357.67 ± 7.51	368.33 ± 33.29	376.67 ± 23.09	370.00± 10.00

Table 4.4: Haematological values of PrGO treated animals (acute toxicity)
All the values were expressed in mean ± SD, n=3.
*****Statistically significant, $p<0.05$

Parameters	Control	3 Days	7 Days	14 Days	21 Days
Glucose (mg/dl)	123.33 ± 11.72	127.33 ± 16.17	167 ± 23.58	120.00 ± 29.82	167.67 ± 129.71
Urea (mg/dl)	38.33 ± 3.51	42.00 ± 2.00	47.67 ± 11.37	40.67 ± 2.31	63.33 ± 3.06*
Creatinine (mg/dl)	0.63 ± 0.21	0.28 ± 0.03	0.27 ± 0.06	0.27 ± 0.06	0.33 ± 0.06
Cholesterol (mg/dl)	114.33 ± 5.13	110.33 ± 3.79*	67.33 ± 9.81	113.33 ± 29.40	81.00 ± 13.86*
Albumin (g/dl)	3.60 ± 0.20	3.43 ± 0.06	3.17 ± 0.58	3.50 ± 0.17	2.93 ± 0.12*
SGOT (IU/I)	68.33 ± 6.51	183.00 ± 1.73*	235.00 ± 25.98*	216.67 ± 21.94*	210.67 ± 35.80*
SGPT (IU/I)	71.00 ± 7.94	79.33 ± 1.15	86.00 ± 2.00	158.67 ± 5.03*	153.33 ± 6.11*
Total Protein (g/dl)	6.70 ± 0.50	6.37 ± 0.06	5.63 ± 1.15	6.40 ± 0.70	4.60 ± 0.17*

Table 4.5: Clinical chemistry values of PrGO treated animals (acute toxicity)
All the values were expressed in mean ± SD, n=3.
*****Statistically significant, $p<0.05$

4.7.1.3. BODY WEIGHT AND ORGAN INDICES

There was no change in body weight (Figure 4.33) were noticed in mice injected with PrGO by intravenous and intraperitoneal administration. When PrGO was exposed intravenously, organ indices showed significant differences in organ weights such as liver, brain and kidney. Similarly, when PrGO was exposed intraperitoneally, the organ indices (liver, brain, kidney and spleen) were significantly changed when compared to control. Feed intake of all the animals was normal during the experimental period.

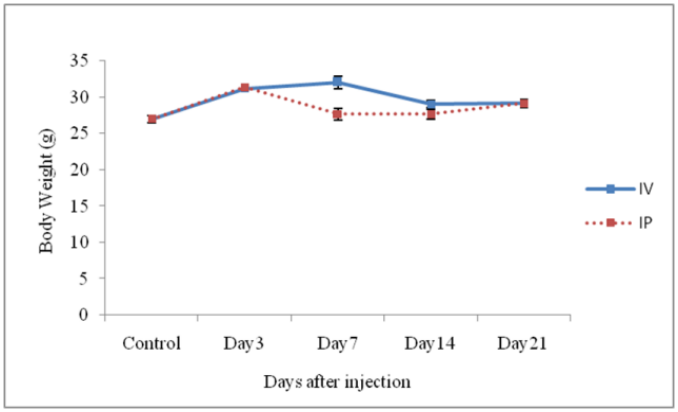

Figure 4.33: Increase in body weight of PrGO treated animals (i.v. and i.p.)

	Groups	Organ indices (mg/g)			
		Liver	Brain	Kidney	Spleen
Intravenous	Control	67.51 ± 2.11	15.97 ± 0.51	12.55 ± 0.71	3.84 ± 0.28
	3 Days	58.93 ± 1.64*	14.24 ± 0.32*	17.03 ± 0.27*	3.75 ± 0.14
	7 Days	66.75 ± 4.79	14.27 ± 0.29*	14.42 ± 0.34*	3.65 ± 0.20
	14 Days	64.47 ± 4.5	13.51 ± 0.92*	11.22 ± 0.24	3.70 ± 0.25
	21 Days	69.27 ± 1.91	15.35 ± 0.30	11.36 ± 0.26	3.51 ± 0.16
Intraperitoneal	Control	67.51 ± 2.11	15.97 ± 0.51	12.55 ± 0.71	3.84 ± 0.28
	3 Days	76.44 ± 1.02*	13.82 ± 0.21*	15.25 ± 0.25*	3.08 ± 0.17*
	7 Days	52.64 ± 1.44*	16.22 ± 0.49	10.05 ± 0.08*	2.78 ± 0.06*
	14 Days	58.19 ± 1.51*	16.00 ± 0.47	10.56 ± 0.42*	5.38 ± 0.22*
	21 Days	57.53 ± 1.23*	15.63 ± 0.58	11.13 ± 0.48*	3.26 ± 0.19*

Table 4.6: Organ indices from PrGO treated animals
All the values were expressed in mean ± SD, n=3
* Statistically significant, $p < 0.05$

4.7.1.4. ABSORPTION, DISTRIBUTION, METABOLISM, EXCRETION AND TOXICITY (ADME & T)

4.7.1.4.1. ABSORPTION

10 mg/kg body weight of PrGO was exposed (single) by intraperitoneal and intravenous injection. The absorption of PrGO was evidenced in the organs of animals. The percentage of PrGO was estimated in organs (liver, kidney, spleen and brain) and was mentioned in the table 4.3.

4.7.1.4.2. DISTRIBUTION

The distribution of PrGO was evaluated with Raman Mapping at 3, 7, 14 and 21 days post exposure. PrGO was distributed in Liver, kidney, spleen and brain (Figure 4.29, Figure 4.30, Figure 4.32, table 4.3).

4.7.1.4.3. METABOLISM

10mg/kg body weight of PrGO exposed to the animals. Blood was collected and subjected to clinical chemistry evaluation. There was a slight alternation in the few of the clinical chemistry values (Table 4.5).

4.7.1.4.4. EXCRETION

Urine sample was collected at 3, 7, 14 and 21 days post exposure (intravenous administration from acute toxicity). Raman mapping indicated the presence of traces of PrGO in urine (Figure 4.31).

4.7.1.4.5. TOXICITY

PrGO was administered (acute toxicity) to Swiss Albino mice by i.v. and i.p. The results suggest that the material was absorbed, distributed, metabolized and excreted as

evident by Raman mapping. It was observed that none of the animals treated with PrGO showed any adverse toxic symptoms. However, there was significant reduction in RBC, HGB, HCT at the end of 7 days. Subsequently these values were normalized to that of control. Increased SGOT and SGPT suggest possible liver damage which is also reflected in histopathological examination.

4.7.2. SUB ACUTE TOXICITY

Swiss Albino mice were given repeated (0, 3 and 5 days) intraperitoneal administration of PrGO (10 mg/ kg body weight). None of the animals showed any clinical symptoms such asrespiratory, motor, convulsion, reflexes, ocular signs, cardiovascular signs, salivation, piloerection, analgesia and gastrointestinal responses during the experimental period. There was no morphological/behavioural changes observed. The body weight of the animals were increased. The feed intake was normal. At the end of 7, 14 and 21 days post exposure, the animals were sacrificed and were examined for gross pathology. Aggregated deposits of PrGO was observed throughout the peritoneal cavity including the major organs (Figure 4.34).

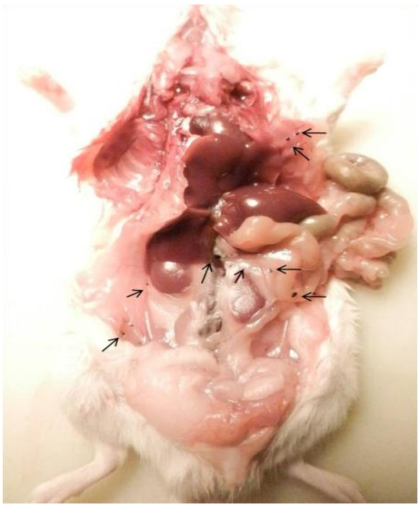

Figure 4.34: Gross necropsy of mice injected (i.p.) with PrGO (repeated exposure). Arrow indicates the deposition of aggregated PrGO inside the body after 21 days of injection.

4.7.2.1. BODY WEIGHT

There was an increase in body weight were noticed in mice after repeated intraperitoneal exposure to PrGO (Figure 4.35).

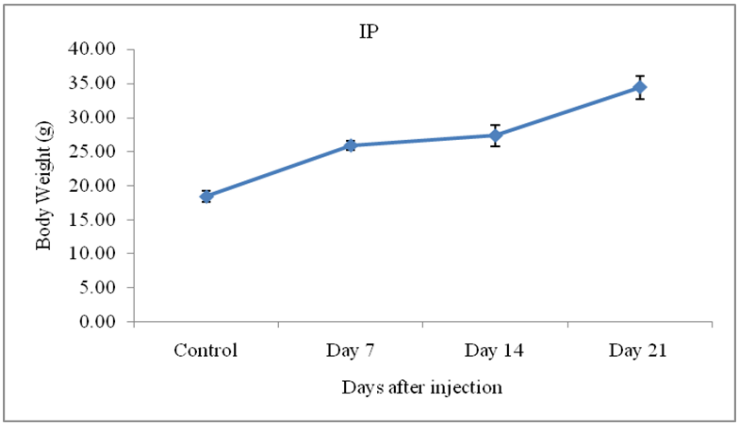

Figure 4.35: Body weight of mice after repeated intraperitoneal injection of PrGO

4.7.2.2. HAEMATOLOGY AND CLINICAL CHEMISTRY

The blood sample collected from animals of subacute toxicity study was analyzed for various haematological (trisodium citrate as anticoagulant) and clinical chemistry

parameters. The result of the study indicated that a similar pattern of changes as observed in acute toxicity. Significant changes were observed in RBC, HGB and HCT values of treated animals. These values were significantly decreased at the end of 7 days (RBC- 4.53 ± 0.73*; HGB-7.25 ± 1.32* and HCT- 22.18 ± 3.48*) and 14 days (RBC- 5.27 ± 0.34*; HGB- 8.83 ± 0.47* and HCT- 26.05 ± 1.27*) post exposure. RBC, HGB and HCT values were comparable to control values at the end of 21 days.

Parameters	Control	7 Days	14 Days	21 Days
WBC	8.83 ± 3.53	6.25 ± 2.14	7.48 ± 2.49	10.5 ± 2.01
RBC	8.21 ± 1.68	4.53 ± 0.73*	5.27 ± 0.34*	7.02 ± 0.50
HGB	13.83 ± 2.70	7.25 ± 1.32*	8.83 ± 0.47*	11.33 ± 0.76
HCT	39.58 ± 8.56	22.18 ± 3.48*	26.05 ± 1.27*	33.3 ± 2.48
MCV	48.1 ± 0.82	49.05 ± 0.87	49.48 ± 1.15	47.48 ± 0.34
MCH	16.88 ± 0.33	15.98 ± 0.59*	16.75 ± 0.53	16.13 ± 0.24*
MCHC	35.13 ± 1.22	32.58 ± 1.50	33.88 ± 0.33	34.03 ± 0.76
PLT	410.5 ± 72.93	269 ± 101.48	401 ± 76.60	514.75 ± 60.51

Table 4.7: Haematological values of PrGO treated animals (sub acute toxicity)
All the values were expressed in mean ± SD, n=4.
*****Statistically significant, $p<0.05$

The result of the study showed that all the clinical chemistry parameters were within the normal range except at the end of 21 days after treatment. It was also observed that an increased SGPT activity found in all animals throughout the experimental period (7 days- 89.00 ±2.65*, 14 days- 164.00 ± 9.17* and 21 days- 155.67 ± 5.51*) which suggest possible hepatic injury.

Parameters	Control	7 day	14 day	21 day
Glucose (mg/dl)	124.48 ± 4.89	154.75 ±17.2	139.75 ± 20.88	180 ± 40.16
Urea (mg/dl)	40.25 ± 42	53.00 ±14.63	42.75 ± 3.59	60.25 ± 6.13*
Creatinine (mg/dl)	0.54 ± 0.13	0.48 ± 0.07	0.57 ± 0.04	0.75 ± 0.03
Cholesterol (mg/dl)	118 ± 7.07	76.75 ±7.46*	135.5 ± 23.10	94.00 ± 8.76*
Albumin (g/dl)	3.62 ± 0.39	3.65 ± 0.26	3.65 ± 0.17	3.80 ± 0.24
SGOT (IU/l)	161.5 ± 22.8	152 ± 41.76	124.40 ± 3.11	230.80 ± 0.01*
SGPT (IU/l)	72 ± 6.48	89.75 ± 2.63*	165.50 ± 8.06*	155.50 ± 4.51*
Total Protein (g/dl)	6.01 ± 0.49	5.97 ± 0.5	5.89 ± 0.47	6.15 ± 0.17

Table 4.8: Clinical chemistry values of PrGO treated animals (sub acute toxicity)
All the values were expressed in mean ± SD, n=4.
*****Statistically significant, $p<0.05$

4.7.2.3. GROSS PATHOLOGY

At the end of 7, 14 and 21 days of post exposure of PrGO, the animals were humanely sacrificed and evaluated for the gross pathology. There was no gross pathological abnormalities were noticed in any of the animals of subacute toxicity studies.

4.7.2.4. HISTOPATHOLOGICAL EXAMINTION

Organs such as brain, liver, kidney and spleen (7, 14 and 21 days post exposure) from the subacute toxicity studies were subjected to histopathological analysis **(Figure 4.36)**. The following lesions were observed in PrGO treated group.

4.7.2.4.1. 7 DAYS PrGO POST EXPOSURE

BRAIN: No changes or abnormalities detected at the cerebral cortex in brain.

LIVER: The central vein appeared normal, the hepatocytes around the central vein showed granular cytoplasm with normal nucleus. In the mid zonal region, vacuolar degeneration and marginalization of cytoplasm was appreciated. Kupffer cells were also observed. Mononuclear cell infiltration was present in the sinusoidal space along with the Kupffer cells in the periportal region.

KIDNEY: In the cortex, the glomerulus was congested and Bowman's capsule appeared normal. Proximal convoluted tubules, distal convoluted tubules and loop of henle were normal in appearance. Interstitial space was congested at multifocal areas. In the medulla, collecting tubules and collecting duct also appeared normal.

SPLEEN: In the white pulp, germinal centre and lymphoid follicles appeared normal. Marginal zone consisted of phagocytic cells (macrophages). Red pulp contained megakaryocytes.

4.7.2.4.2. 14 DAYS PrGO POST EXPOSURE

BRAIN: No abnormalities could be detected at the cerebral cortex.

LIVER: Congestion was noted in the central zone (around central vein). Mononuclear cell infiltration along with a few Kupffer cells was present in the sinusoidal space around the central vein and in the periportal region. Hepatocytes in the mid-zone showed vacuolar changes and granular cytoplasm. Nucleus of these hepatocytes remained intact. Occasional collection of round cells with dark nucleus was noted. Extramedullary heamatopoiesis was observed.

KIDNEY: In the cortex, the glomerulus was slightly congested. Proximal convoluted tubules, distal convoluted tubules and loop of henle were normal in appearance. Interstitial congestion was also noted at multifocal areas.

SPLEEN: In the white pulp, germinal centre and lymphoid follicles appeared normal. Marginal zone consisted of phagocytic cells (macrophages). Megakaryocytes were observed in the red pulp where extramedullary haematopoiesis was well appreciated.

4.7.2.4.3. 21 DAYS PrGO POST EXPOSURE

BRAIN: No abnormalities could be detected at the cerebral cortex.

LIVER: Congestion was noticed in the central zone (around central vein). Mononuclear cell infiltration and proliferation of Kupffer cells was present throughout the hepatic lobule. Hepatocytes showed vacuolar appearance with granular cytoplasm (Moth-eaten appearance). Nucleus of these hepatocytes remained intact.

KIDNEY: In the cortex, the glomerulus was slightly congested. Proximal convoluted tubules, distal convoluted tubules and loop of Henle were normal in appearance. Interstitial congestion was also noted at multifocal areas.

SPLEEN: In the white pulp, germinal centers were small with few cells were observed, moderate amount of lymphoid cells were observed in the follicle region. Marginal zone consisted of phagocytic cells (macrophages) and reticulocytes. In the red pulp region, megakaryocytes (multinucleated large cell) were observed. Extramedullary haematopoiesis was well appreciated.

4.7.2.4.4. CONTROL ANIMALS

BRAIN: No changes or abnormalities could be detected at the cerebral cortex in brain.

LIVER: In control group, the liver showed normal hepatic chord and portal vein. The hepatocytes appeared granular cytoplasm with intact nucleus. Occasional mononuclear cells were seen in the sinusoidal space. Periportal region portal triad remained normal.

KIDNEY: Glomerulus and Bowman's capsule appeared normal. Proximal convoluted tubules, distal convoluted tubules and loop of Henle were normal in appearance. In the medulla, collecting tubules and collecting duct also appeared normal.

SPLEEN: In the white pulp, germinal centre, marginal zone and lymphoid follicles appeared normal. In the red pulp region, splenic trabeculae and megakaryocytes were seen. Multinucleated lymphoblast cells were also observed.

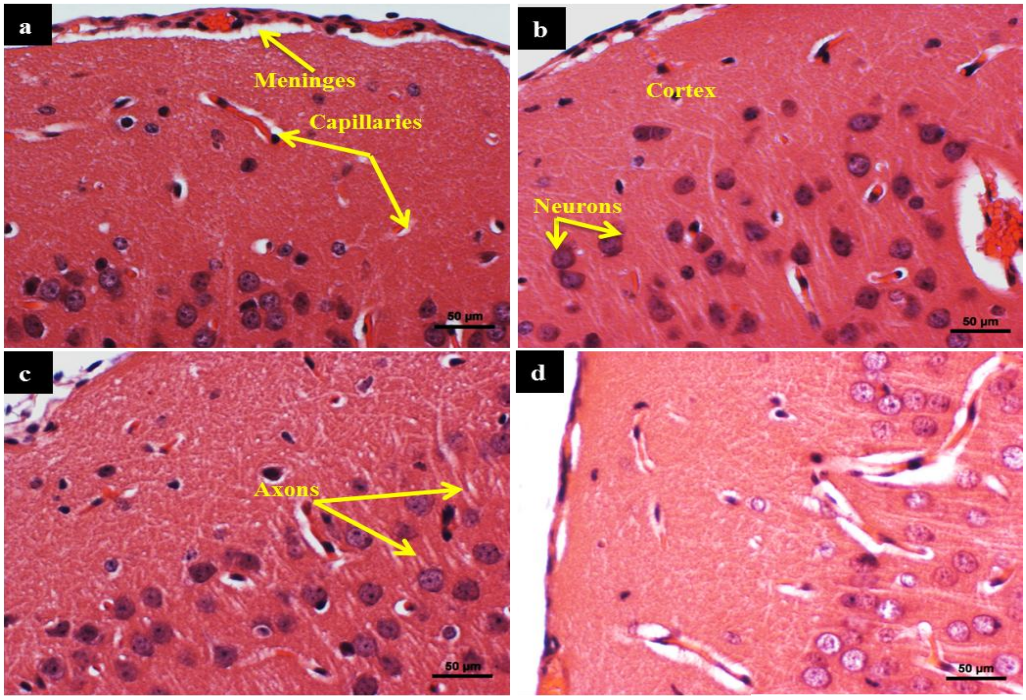

Brain Magnification: 40x

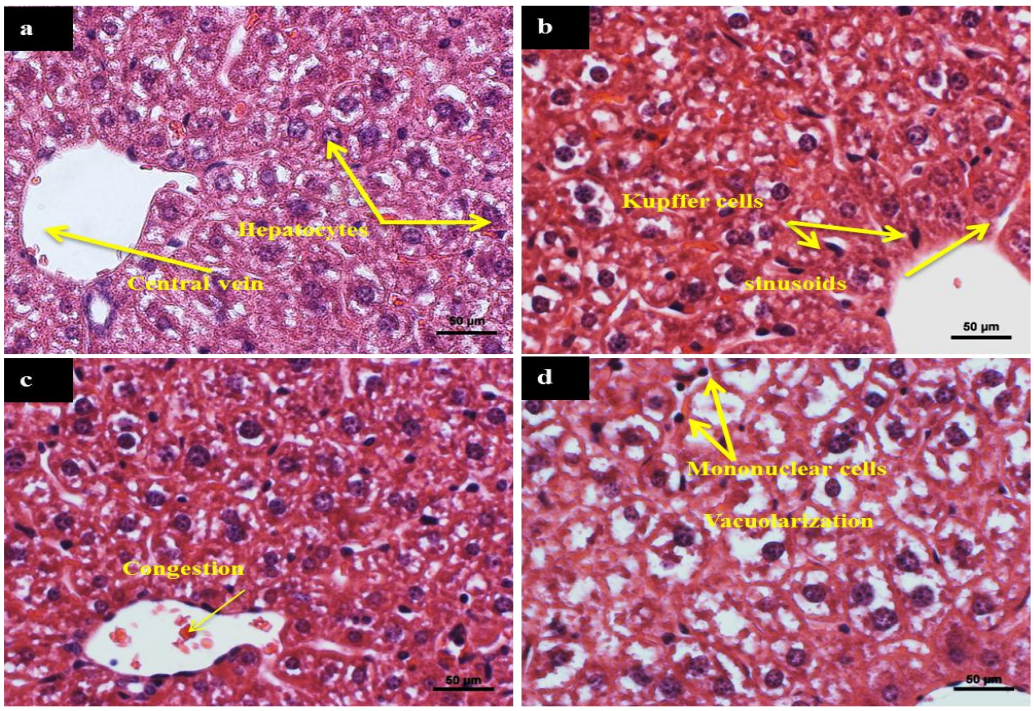

Liver Magnification: 40x

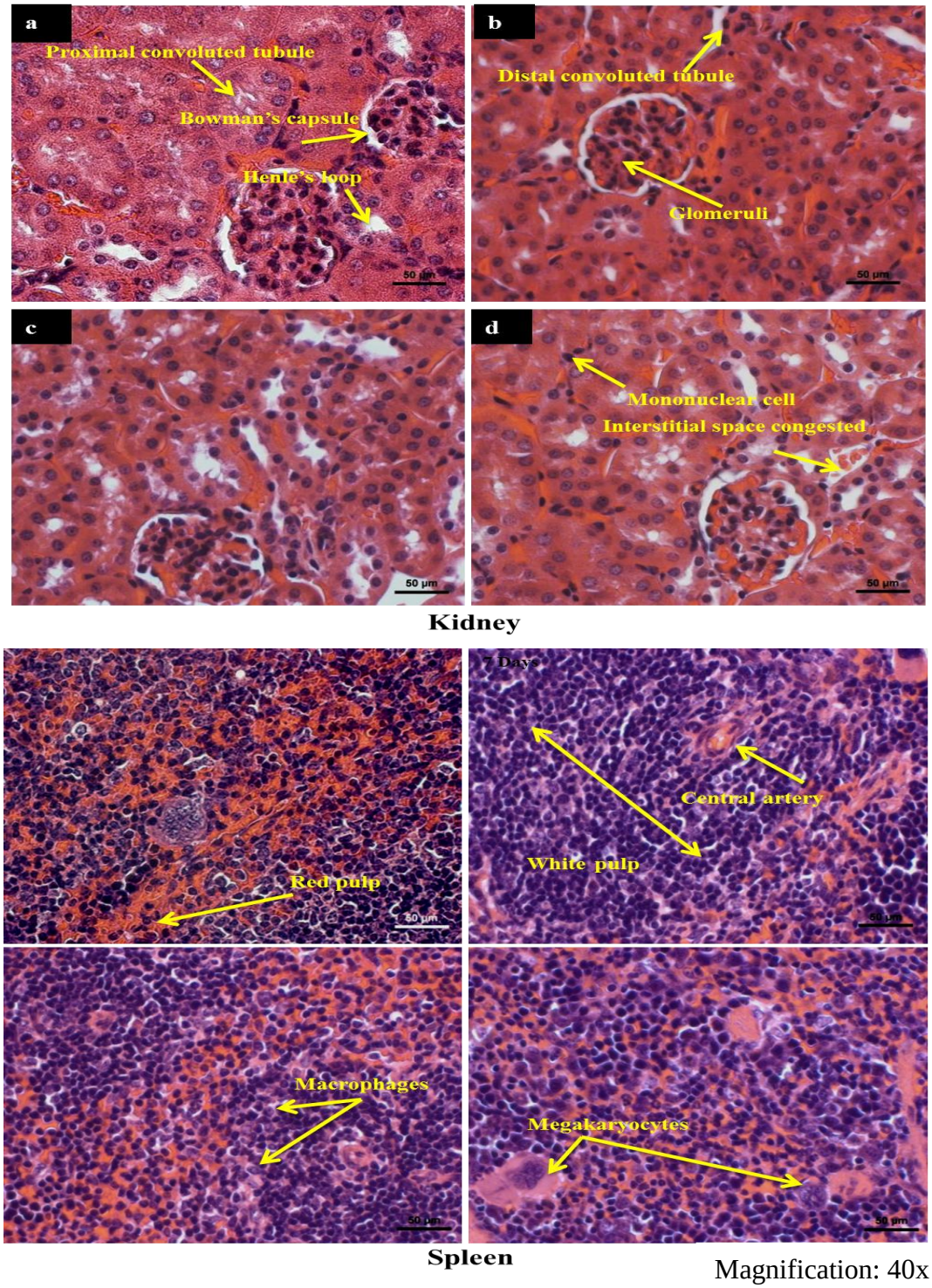

Figure 4.36: Histopathological examination of tissues from PrGO treated mice (sub acute toxicity). (a) Control; (b) 7 days; (c) 14 days; (D) 21 days post exposure.

4.7.2.5. ANTIOXIDANT ASSAYS

Oxidative stress occurs when the cell encounters imbalance between ROS and antioxidant system. There are certain antioxidant enzymes that modulate the redox state of cells either by maintaining cellular antioxidant level or by catalyzing ROS. Measurement of antioxidant enzyme activity and total cellular glutathione (GSH) in mice exposed (repeated) to PrGO showed significant decrease in the activity of SOD and increased GSH at the end of 7 and 14 days of post exposure. It was also observed that SOD activity and GSH level becomes normal and comparable to control at the end of the experimental period (21 days).

4.7.2.5.1. LIPID PEROXIDATION (LPO)

ROS generated inside the body oxidizes lipids resulting in the formation and propagation of lipid radicals. It is a chain reaction initiated by hydrogen abstraction or addition of oxygen radical leads to oxidative damage of polyunsaturated fatty acids. Lipid peroxidation is quantified by the amount of by-product (malondialdehyde) formed. No significant increase in lipid peroxide formation was observed in liver tissue collected from sub acute toxicity studies. The result of the study indicated that the values of the treated animals (7 Days: 5.32 ± 0.29, 14 Days: 5.12 ± 0.34, 21 Days: 5.79 ± 0.54) were comparable to control values(6.64 ± 0.33) (Figure 4.37).

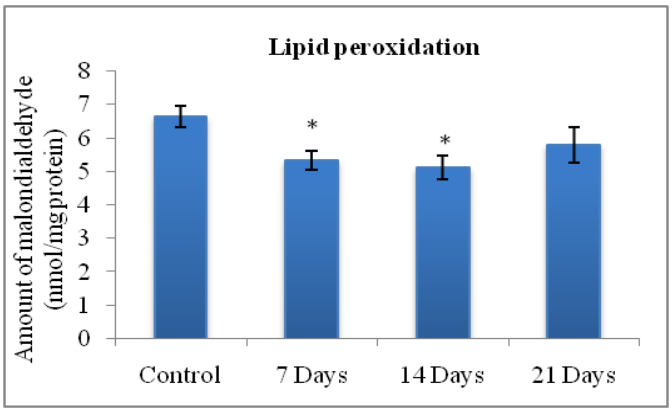

Figure 4.37: Lipid peroxide formation in PrGO treated animals

4.7.2.5.2. TOTAL GLUTATHIONE (GSH)

Glutathione is a natural ubiquitous antioxidant present in tissues. It is a tripeptide that detoxifies both exogenous and endogenous ROS. It was observed that a significant increase in GSH level at the end of 7 Days (0.84 ± 0.11) and 14 Days (0.97 ± 0.14) of PrGO post exposure when compared to control (0.34 ± 0.22) (Figure 4.38).

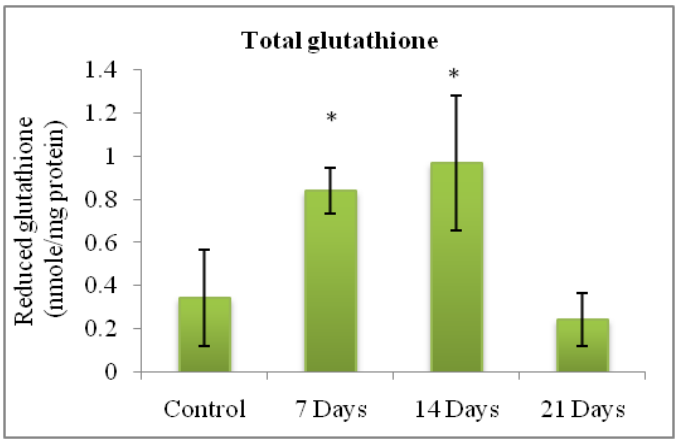

Figure 4.38: GSH level in PrGO treated animals

4.7.2.5.3. GLUTATHIONE PEROXIDASE (GPx)

GPx is an antioxidant enzyme that scavenges ROS formed and protects the cell from oxidative damage. It reduces lipid hydroperoxides, hydrogen peroxide to alcohol

and water. It was observed from the figure 4.39 that the activity of GPx was decreased in all animals treated with PrGO (7 Days: 0.010 ± 0.00, 14 Days: 0.008 ± 0.00, 21 Days: 0.006 ± 0.00). The changes in GPx activity were not significant when compared to control value (0.011 ± 0.00).

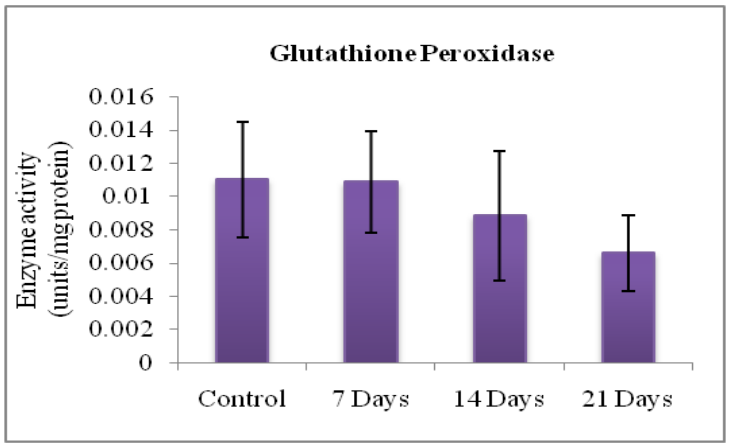

Figure 4.39: GPx activity in PrGO treated animals

4.7.2.5.4. GLUTATHIONE REDUCTASE (GR)

Glutathione reductase catalyzes the reduction of glutathione disulfide (GSSG) to glutathione (GSH). The enzyme activity is determined by measuring the changes in NADPH concentration. GR activity was increased at the end of 7 Days (0.62 ± 0.09), 14 Days (0.63 ± 0.04), 21 Days (0.54 ± 0.07) post exposure. These changes were not significant when compared to control values (0.49 ± 0.15) (Figure 4.40).

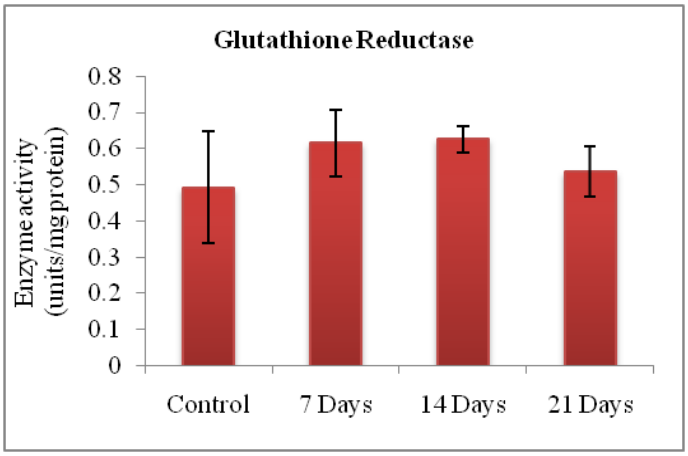

Figure 4.40: GR activity in PrGO treated animals

4.7.2.5.5. SUPEROXIDE DISMUTASE (SOD)

SOD catalyzes the dismutation of superoxide radical into molecular oxygen or hydrogen peroxide. It was observed that SOD activity was significantly reduced in 7 days (0.003 ± 0.00) and 14 days (0.002 ± 0.00) post exposure. The SOD activity was regained at the end of 21 days after exposure (0.009 ± 0.00) (Figure 4.41).

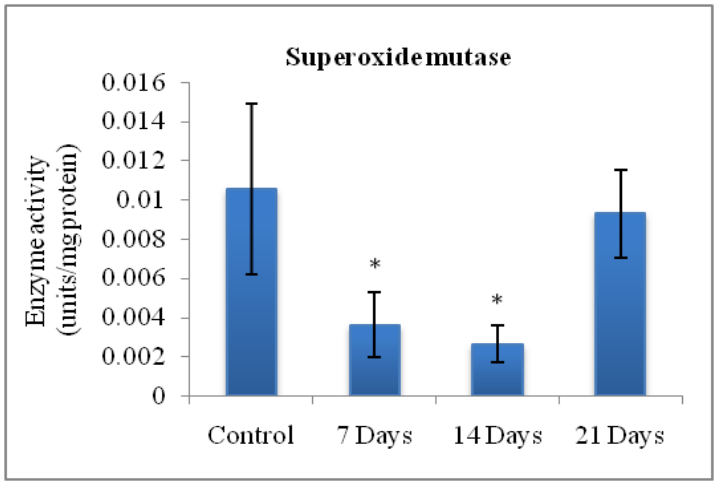

Figure 4.41: SOD activity in PrGO treated animals

4.7.2.6. MORPHOLOGY OF MSCs AFTER PrGO EXPOSURE

Bone marrow was collected from the animals of sub acute toxicity and was subjected to phenotypic evaluation. There was no phenotypic change observed in MSCs isolated from PrGO exposed mice. The cells formed spindle shaped fibroblasts morphology with discrete colonies after 4 days of culture. The cells isolated from the bone marrow at the end of 7 days, 14 days and 21 days attained 80%confluency in two weeks period. In addition to MSCs, fat cells (adipocytes) and osteoblasts were seen after 14 days of culture (Figure 4.42). The lipid granules of adipocytes were stained with Oil Red and the calcium deposits of osteoblasts were stained with Alizarin red to distinguish fat cells and osteoblasts from the underlying MSCs culture (Figure 4.43).

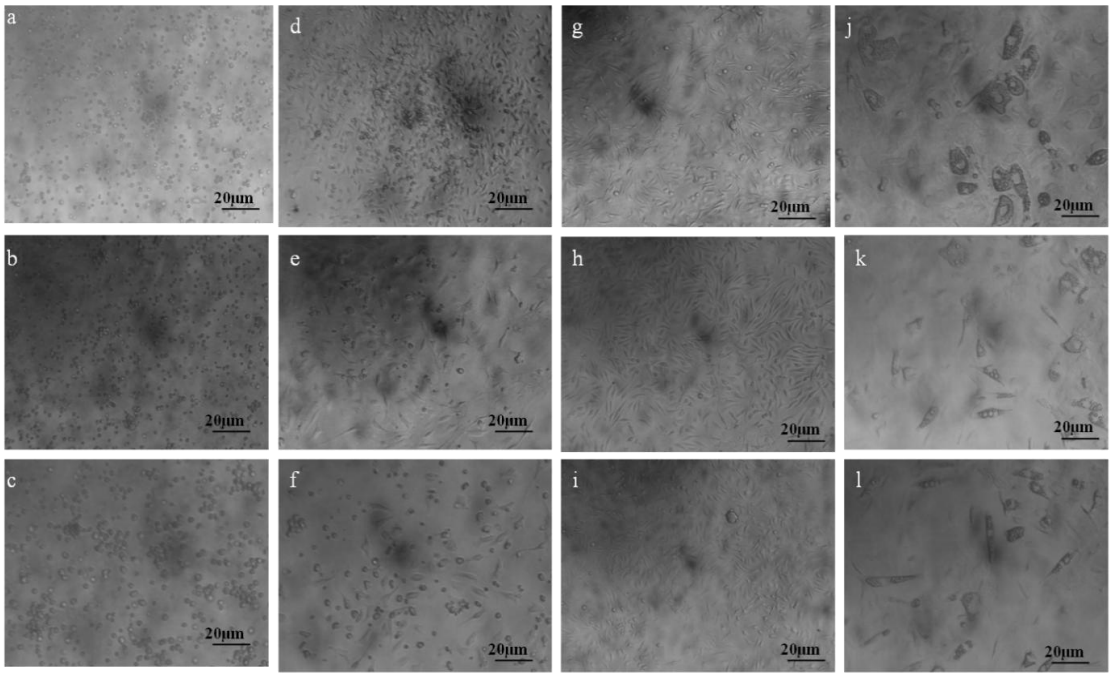

Figure 4.42: Morphology of MSCs isolated from bone marrow of mice exposed to PrGO. (a-j) 7 days group; (b-k) 14 days group; (c-l) 21 days group. (a,b,c- after 1 day of isolation), (d,e,f- after 5 days of isolation), (g,h,i- after 10 days of isolation), (j,k,l- after 14 days of isolation).

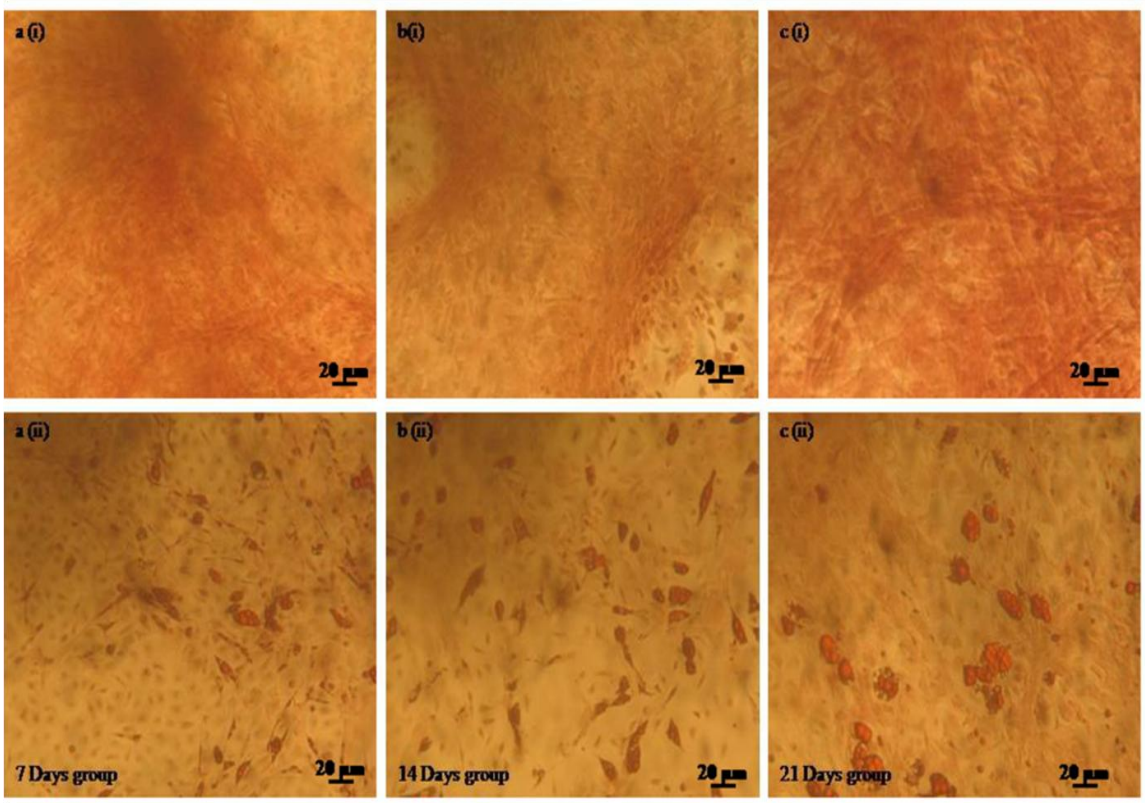

Figure 4.43: Alizarin and Oil red to distinguish the presence of fat cells and osteoblasts

4.7.2.7. IMMUNOTOXICITY

4.7.2.7.1. SPLENOCYTES PROLIFERATION

Spleen is one of the primary lymphoid tissues consisting of B cells, T cells, macrophages and natural killer cells. Spleen were collected from the mice exposed to PrGO (sub acute toxicity) and analyzed for splenocytes proliferation assay using tritiated thymidine incorporation. Proliferation studies were carried out without any stimulant. Figure 4.44 showed significant increase in splenocytes proliferation at the end of 7 days (p<0.001). Subsequently the proliferation was decreased after 14 days and becomes normal at the end of 21 days of exposure.

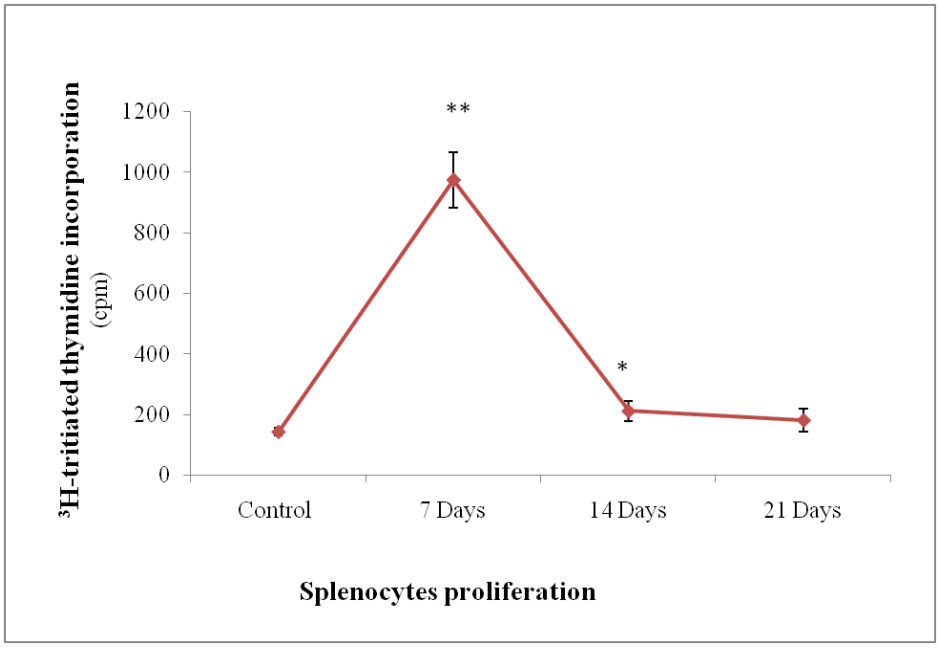

Figure 4.44: Splenocytes proliferation after PrGO exposure

CHAPTER 5: DISCUSSION

5. DISCUSSION

The results of synthesis, characterization of PrGO and their interaction with mouse bone marrow mesenchymal stem cells and its allied molecular toxicity using *in vitro* and *in vivo* methods were discussed in detail in this Chapter.

5.1. SYNTHESIS OF PEGYLATED REDUCED GRAPHENE OXIDE (PrGO)

Graphene oxide (GO) was synthesized from graphite flakes using Hummer's method (Hummer & Offeman, 1958) under extreme acid exfoliation and oxidation. Hummer's method is one of the most commonly used methods for graphite oxidation and is less hazardous, more efficient method for GO synthesis. Graphite flakes has defects on their "$\boldsymbol{\pi}$ "structure that acts as a seeding point for oxidation (Dreyer *et al*., 2010). GO is a non-conductive hydrophilic carbon with enriched oxygen containing groups present on the planar surface as well as the edges. GO form colloidal suspension in water, alcohol and some organic solvents owing to the presence of carboxyl group at the edges. The synthesized GO was covalently coupled with O,O′- Bis(2-aminoethyl) polyethylene glycol to increase their aqueous stability in biological media. In the present study, low molecular weight polyethylene glycol (1900KDa) was used to facilitate cellular uptake and improve biocompatibility because high molecular weight polyethylene glycol (PEG) inhibits cellular uptake (Cruje & Chithrani, 2014). PEGylation also increases the retention time of nanoparticles in circulating blood by preventing opsonization. PEGylation also reduces the nanoparticles retention time in liver, spleen and lungs by promoting their clearance from these organs (Li *et al*., 2014). PrGO was obtained by reducing PEGylated GO with sodium borohydride. The GO-PEG changes its yellow

colour to black (PrGO) during the reduction process and remains stable in water and media. The rational for using sodium borohydride as a reducing agent is that, it slowly hydrolyzed by water and can act as an efficient reductant by reducing carbonyl group than epoxide and carboxylic acid groups (Pei & Cheng, 2012).

5.2. CHARACTERIZATION

The result of the TEM analysis showed that the surface of the synthesized PrGO was clear and smooth with folding and wrinkles appeared throughout the graphene flakes. AFM results indicate that the lateral dimension of PrGO was ~1 µm and average thickness of 8-9 nm with polymer coupling. The FTIR spectra of PrGO showed additional three peaks at 2845, 1442 and 1050 cm^{-1} corresponding to C-H stretching, C-H in plane bending and C-O-C stretching. The peak observed at 2845cm^{-1} corresponds to C-H vibrations on PEG as reported by (Wen *et al*., 2012). Characteristics Raman spectra was clearly observed in PrGO. The D band corresponds to the formation of defects and the G band is assigned to the E_{2g} phonon of C sp^2 atoms. The increase in the intensity of D band indicates the decrease in size of the in-plane sp^2 domains and the presence of defects. The crystal structure of PrGO was studied using XRD and found diffraction peak at 25° (2θ). Generally, graphite shows diffraction peak at 26.5° and GO at 10.4°. The appearance of the broad peak in PrGO indicates the exfoliation of graphite to single or few layered graphene sheets. Similar findings were reported by (Zhou *et al*., 2010). TGA analysis provided further evidence of PEG coating on PrGO, in which the weight loss around 350-400°C was due to the decomposition of PEG. The weight loss at 100°C and above results from the evaporation of water and gasification of labile oxygen containing

functional groups. Presence of prominent peaks at 284.4 eV and 285.2 keV (XPS) indicates sp^2 planar graphitic structure and the sp^3 bonded carbon atoms.

5.3. ENDOTOXIN CONTENT

To avoid false interpretation of toxicity results it is advisable to determine the endotoxin level during the preparation of nanoparticles. The toxicity of the nanoparticles may be due to the biological interaction with the cells or from endotoxin contamination during the production and handling process. The results of the study suggest that the endotoxin content was well below the United States Pharmacopoeia (USP) recommended level (<0.5 EU) (Dobrovolskaia *et al*., 2010).

5.4. ISOLATION AND CHARACTERIZATION OF MSCs

MSCs were cultured in complete DMEM medium containing 20% FBS. Medium was changed frequently to avoid potential contamination by non-adherent haematopoietic stem cells (HSCs). These MSCs are adherent cells and readily attached to the surface of the cell culture dishes. The isolated cells proliferate more rapidly and formed colonies of cells with spindle shaped fibroblast morphology. The cells also readily differentiated into adipocytes and osteoblasts when cultured in adipogenic and osteogenic media. The immuno characterization confirmed that the isolated MSCs expressed positive surface markers (CD 44, CD 90) and negative for CD 45 (HSCs) surface marker.

5.5. PROTEIN CORONA

The results of the protein corona showed that, only BSA firmly attach onto the surface of the PrGO. All other proteins are loosely attached and are washed away during centrifugation forming soft corona. The concentration of BSA present in FBS is much

higher, compared to other proteins. Hence it can effectively bind onto the surface of PrGO and form hard corona. BSA binding may modulate the uptake and intracellular localization of PrGO. It was already cited in the literature that BSA and SWCNT coupled with BSA enters into the cells by endocytosis and are localized in lysosomes (Zhou *et al*., 2010).

5.6. *IN VITRO* EXPERIMENTS

5.6.1. CELLULAR UPTAKE OF PrGO

PrGO was efficiently taken up by MSCs. It was found that the PrGO was distributed throughout the cytoplasm and perinuclear region. The interaction of PrGO does not affect the integrity of the MSCs. None of the PrGO was seen inside the nucleus. This may be due to the size that prevents them from entering the nucleus or because of the surface charge carried by PrGO.

5.6.2. CYTOTOXICITY

5.6.2.1. CELL VIABILITY AND METABOLIC ACTIVITY (MTT ASSAY)

The cytotoxic effect of PrGO on MSCs was assessed by exposing different concentration of PrGO (5, 10, 50 and 100 µg/ml) at different time periods (24, 48 and 72 h). The results from MTT assay showed PrGO does not induce any cytotoxic effects in MSCs. The rate of cell survival was above 80% and was well comparable to control. There were no morphological changes observed in cells treated with PrGO. Similar results were reported by Elkhenany *et al.*, 2014. Ryu & Kim, 2013 stating that graphene enhances the proliferation and growth of MSCs under *in vitro* culture conditions. In addition to MTT assay, cell viability using neutral red assay was carried out, since

graphene is known to interfere with MTT (Jiao *et al*., 2015) by spontaneously reducing them and gives false results.

5.6.2.2. CELL VIABILITY AND LYSOSOMAL ACTIVITY BY NEUTRAL RED ASSAY

The viability of MSCs after exposure to PrGO (10, 25, 50, 100 and 250 µg/ml) was evaluated by neutral red assay. Neutral red is a cationic dye that can penetrate cell membrane and accumulate in lysosomes. Viable cells incorporate neutral red inside their lysosomes whereas dead cells fail to uptake neutral red. The result indicated that the cells exposed to PrGO showed an increased neutral red uptake. The percentage of neutral red uptake increases with increased concentration of PrGO and extended exposure time. This may be due to the increased formation of intracellular acidic vesicle inside the cell because of PrGO uptake. Similar transient increase in neutral red incorporation in endothelial cells with SWCNTs was reported by Albini *et al*., 2010.

5.6.3. REACTIVE OXYGEN SPECIES (ROS) PRODUCTION

ROS are formed inside the cell as a result of normal metabolism or as a result of cellular stress. Oxidative stress damage cellular macromolecules like DNA, protein and lipids when there is imbalance between ROS production and decreased activity of antioxidant enzymes (superoxide dismutase and glutathione peroxidase). Oxidative stress is one of the major paradigms of nanoparticles induced toxicity (Zhang *et al*., 2012). The result of the study showed an increase in ROS production as evident from DCFDA assay, which confirm the potential of PrGO to induce oxidative stress. It was also noticed that there was a concentration and time dependent increase in ROS generation. (Akhavan *et*

al., 2012) reported that average lateral dimension and concentration plays an important role in ROS generation induced by rGO. rGO with lateral dimension ~11 nm was found to induce more ROS formation when compared to ~3.8 µm and could be due to the presence of more defects on the surface of rGO. Physical interaction of rGO with the cell promote oxidative stress whereas GO induces ROS formation by NADPH oxidase. It was also known that graphene induces ROS generation, which leads to disruption of mitochondrial membrane potential and activating apoptosis (Jarosz *et* al., 2016).

5.6.4. MITOCHONDRIAL MEMBRANE POTENTIAL (MMP)

Increased accumulation of ROS inside the cells will leads to mitochondrial membrane depolarization. Mitochondrial membrane depolarization occurs as a result of loss in mitochondrial membrane integrity. Depolarization of MMP in turn increases ROS production, decreases ATP synthesis and induce the release of proapoptotic factors eventually results in apoptosis. The results of MMP showed a slight change in MMP in cells exposed to high concentration of PrGO as evident from increased green fluorescent of JC-1 probe. These findings were supported by the reports of Chatterjee *et al*., 2014 in which rGO decreases the mitochondrial membrane polarization, resulting an increased ROS formation leading to apoptosis.

5.6.5. LYSOSOMAL MEMBRANE DESTABILIZATION (ACRIDINE ORANGE ASSAY)

Lysosomal destabilization was studied in cells using acridine orange (AO) relocation technique. Acridine orange shows red fluorescence when present inside the lysosomes and green when present in cytoplasm. The destabilization of lysosomal

membrane as a result of nanoparticle exposure may disrupt the lysosomal membrane resulting in the release of AO in cytoplasm and thereby increasing the green fluorescence. In the present study, no changes in the percentage of AO relocation was observed in cells exposed to PrGO. However, under fluorescence microscope the cells showed increased red fluorescence with increased PrGO concentration. This might be due to the increased formation of lysosome inside the cells following PrGO uptake. It was already cited in the literature that GO was found to be distributed throughout cytoplasm including lysosomes, mitochondria and endoplasm (Zhang *et al*., 2012). When algal cells were exposed to SWCNT and GO, increased number of lysosomes was observed as a measure of self defense (Hu *et al*., 2015).

5.6.6. CELL ADHESION (ACTIN STAINING)

The results of the actin staining showed that no visible changes were observed in actin morphology of MSCs following PrGO treatment. This confirms that PrGO does not affect the cytoskeletal integrity and cell attachment. The interaction of PrGO with cytoskeletal proteins depends on surface charge and surface oxygen content. Shi *et al.*, 2011 noticed that the moderately reduced GO was shown to enhance cell attachment and proliferation compared to highly reduced GO. Under physiological pH, the actin filaments are usually negative charge and it can bind effectively graphene which possess positive charge (Li *et al*., 2014). Hence in the present study the modification of GO using positively charged O, O′- Bis (2-aminoethyl) polyethylene glycol changes the charge distribution which enhances the binding of PrGO with actin. It was also noticed that the presence of PrGO inside the cells quenches the fluorescence of Cytopainter.

5.6.7. APOPTOSIS

5.6.7.1. ANNEXIN V/PI

Oxidative stress induced in cells as a result of nanoparticles exposure can activate apoptosis (Manke *et al*., 2013). The results of the DCFDA assay showed increased ROS generation in cells after PrGO exposure. Hence the effect of PrGO to induce apoptosis in MSCs was investigated using Annexin V/ PI staining. The cells treated with PrGO showed no cell death except at higher concentration (500 µg/ml), in which few apoptotic cells were observed. The early apoptotic cells were stained positive for Annexin V emitting green fluorescence whereas the late apoptotic cells were stained positive for both Annexin V and PI, emitting both green and red fluorescence under fluorescent microscope. Quantitative analysis by FACS was unable to perform since PrGO (black colour) quenches the fluorescence of PI at higher concentration.

5.6.7.2. CASPASE ASSAY

Apoptosis is a process of programmed cell death and is characterized by release of cytochrome c from the mitochondria, increased caspase activity and release of proapoptotic factors into the cytoplasm (Guo *et al*., 2002). Activity of caspase 3 and caspase 7, the major executioner caspases were studied in MSCs following PrGO treatment for 24 h. The results of the study revealed that no significant increase in caspase activity was monitored in cells exposed to PrGO compared to control cells.

5.6.7.3. APOPTOTIC DNA LADDER ASSAY

Increased ROS formed inside the cells can oxidize the biomolecules such as DNA, protein and lipids (Sharma *et al*., 2012; Cadet & Wagner, 2013) and can also induce DNA fragmentation. DNA fragmentation catalyzed by endogenous endonuclease is a key feature of apoptosis. In the present study, the results of the DNA ladder assay showed absence of any DNA fragments in MSCs exposed to PrGO. The absence of PrGO inside the nucleus and the absence of DNA fragments clearly indicate that PrGO does not affect the integrity of the genetic material. This finding are contradictory to the findings of Chwalibog *et al*., 2014 in which they reported that rGO could penetrate the cellular components and can directly interact with nuclear DNA causing genotoxic effects.

5.6.8. ALKALINE PHOSPHATASE ASSAY (ALP)

Effect of PrGO on the differentiation potential of MSCs was studied using ALP (a marker for osteogenesis) assay. In the present study, MSCs showed an increased ALP activity (evident from increased purple color) when exposed to higher concentration of PrGO (100 µg/ml) and cultured in presence of osteogenic medium. Nayak *et al*., 2011; Qi *et al*., 2014 also reported that graphene promotes the differentiation of MSCs towards osteogenesis with strong ALP activity and promising their potential use as scaffold for tissue engineering.

5.7. *IN VIVO* EXPERIMENTS

5.7.1. ACUTE TOXICITY

Acute toxicity is designed to determine the adverse effects within a short period of time. This determines the dose-response relationship and lethal dose. The result of the acute toxicity clearly emphasize that the PrGO is found to be non-toxic at 10 mg/ kg body weight by i.p. and i.v. (dose commonly used for clinical application).

5.7.1.1. BIODISTRIBUTION AND TOXICOKINETICS

5.7.1.1.1. DETECTION OF PrGO IN TISSUES, BONE MARROW AND URINE BY RAMAN MAPPING

Biodistribution and toxicokinetics were evaluated from the organs of animals used for acute toxicity (intraperitoneal and intravenous administration). At the end of 3, 7, 14 and 21 days exposure, all the animals were sacrificed and organs such as liver, brain, kidney, spleen, bone marrow were collected and subjected to biodistribution and toxicokinetics. Urine was also collected and subjected to evaluate the presence of PrGO. It was evident from Raman confocal microscopy that PrGO was distributed in all the major organs such as liver, spleen, kidney and brain. Presence of PrGO was apparent in all organs throughout the experimental period and the percentage of distribution and kinetics varies with time.

It was reported that the route of administration affects *in vivo* translocation and biodistribution of nanoparticles. Intravenously injected nanoparticles translocate from the circulatory system to organs such as liver, spleen, bone marrow, lymph nodes, small intestine, brain and lungs. Following intraperitoneal administration, the nanoparticles are

first translocated to liver via portal circulation and undergo biotransformation or excrete into bile (Naseem *et al*., 2014). The result of the biodistribution and toxicokinetics study showed an efficient uptake of PrGO by reticulo endothelial system (RES) which are responsible for the clearance of the foreign materials from the body. After intravenous administration, PrGO was rapidly absorbed from systemic circulation and distributed to liver and spleen after 3 days of exposure. Maximum amount of PrGO was seen in liver and spleen (RES) after 3 days of post exposure followed by kidney and brain. The percentage of PrGO decreases in subsequent days. When injected intraperitoneally, PrGO was slowly absorbed from the peritoneal cavity and gradually accumulated in liver. It was observed that maximum uptake of PrGO was in spleen at the end of 3 days. At the end of 21 days, absorption of PrGO was maximum in liver. However, the presence of PrGO was also noticed in kidney. Further, the presence of PrGO was evident in brain (i.p. and i.v.) suggesting that PrGO has the potential to cross blood brain integrity and accumulates in brain.

Significant distribution of PrGO in bone marrow was noticed in Raman mapping following intraperitoneal injection. This clearly indicates that PrGO crosses blood-bone marrow barrier and interacts with the bone marrow haematopoietic and mesenchymal stem cells.

The presence of trace amount of PrGO in urine sample indicates that a small portion of the PrGO was excreted via urine. The traces of PrGO may be due to the excretion of small sized PrGO in urine, whereas large sized PrGO aggregates and

accumulates in body. This result was supported by the findings of Yang *et al*., 2013 where nanoparticles retained in body tissues over a long period of time.

5.7.1.1.2. DETECTION OF PrGO IN BLOOD

10 mg/ kg body weight of PrGO was administered intravenously and intraperitoneally to Swiss Albino mice. At the end of 1, 3, 6, 24, 48, 72 h and 7 days of post exposure, blood was collected and subjected to Raman confocal microscopy. The result of the toxicokinetics and biodistribution was clearly shown in Raman mapping. Raman mapping showed maximum release of PrGO occurs at the end of 3 h of exposure. The intensity of PrGO decreases with time and the lowest intensity of PrGO were observed at the end of 7 days (i.p. and i.v.). This confirms the distribution of PrGO to various organs from the systemic circulation.

5.7.1.2. BODY WEIGHT AND ORGAN INDICES

There was no change in body weight observed in animals treated with PrGO. However, there is a significant changes noticed in organ indices. It was well known that decreased organ index is a measure of atrophy or degenerative changes whereas increased organ index is a result of hypertrophy or edema.

5.7.1.3. HAEMATOLOGY AND CLINICAL CHEMISTRY

Blood was collected from the animals of acute toxicity. The anticoagulated blood was used for haematology and serum was used for clinical chemistry evaluation. It was observed that PrGO caused significant decrease in RBC, HGB count and HCT value at the end of 7 days. At the end of 21 days all the values were similar to that of control values. The decreased RBC and HGB content leads to less amount of oxygen for

metabolism. The decreased RBC count may be due to the effect of PrGO on haematopoietic system or the free radicals produced by PrGO. Liao *et al*., 2011 reported that graphene oxide and graphene sheets induce hemolysis by disrupting RBC membrane. The negatively charged oxygen containing groups on GO and the positively charged phosphotidylcholine on RBC membrane promote strong electrostatic interaction resulting in membrane damage.

The result of the clinical chemistry values indicates that there is a significant increase in the values of SGOT and SGPT. This suggests a possible liver injury. Albumin and total protein was found normal and comparable to control except at the end of 21 days. The level of urea was significantly increased at the end of 21 days post exposure which may leads to kidney damage.

5.7.1.4. ABSORPTION, DISTRIBUTION, METABOLISM, EXCRETION AND TOXICTY (ADME & T)

Dose/concentration, duration of exposure and their persistence in body determines the toxicity of a compound. Systemic analysis of absorption, distribution, metabolism and excretion (ADME & T) is important to understand its interaction within the body.

Absorption is the process of transfer of chemicals from the site of exposure to the systemic circulation. Absorption involves the passage of compound across the cell membrane from the site of exposure. In the present study, absorption of PrGO following intravenous and intraperitoneal administration was evident from Confocal Raman mapping. PrGO was effectively absorbed from systemic circulation to liver, brain, kidney, spleen and bone marrow.

During the distribution process, compounds were transferred from the circulatory system to various organs. The compound will be distributed throughout the body and diluted by the blood. Size, charge and surface functional coating determines the distribution profile of any nanoparticles (Duan *et al*., 2013). Here, Raman mapping indicated that PrGO was distributed in organs such as liver, kidney, brain, spleen and bone marrow. The distribution profile and the percentage of distribution vary at different time period.

The process of biotransformation of compounds from highly toxic to less toxic or becomes more water soluble compound is known as metabolism. It was reported that inert nanoparticles are unlikely to be metabolized. However, nanoparticles modified with functional groups may be metabolized by liver. The effect of PrGO on metabolism was evidenced in the clinical chemistry parameters. The changes observed in SGOT and SGPT enzyme activity clearly states that the metabolic profile in animals were altered upon PrGO exposure.

Nanoparticles which are absorbed in the systemic circulation can excrete by various routes, mostly by renal clearance. Various blood transport and binding proteins advocate the unidirectional flow of nanoparticles that are finally expelled out of the body (An *et al*., 2014). In some cases, nanoparticles are accumulated at various sites inside the body and fail to undergo complete excretion. In the present study, traces of PrGO were evident in urine sample at 3, 7, 14 and 21 days of post exposure. This suggests that only a small portion of injected PrGO excreted via urine.

PrGO was administered to Swiss Albino mice by i.v. and i.p. The results suggest that the material was absorbed, distributed, metabolized and excreted as evident by Raman mapping. It was observed that none of the animals treated with PrGO showed any adverse toxic symptoms except fluctuation in SGOT and SGPT activity. However, there was significant reduction in RBC, HGB, HCT at the end of 7 days. Subsequently these values were normalized to that of control. Increased SGOT and SGPT suggest possible liver damage.

5.7.2. SUBACUTE TOXICITY

Sub acute toxicity involves repeated exposure of a compound to the animals, over a prolonged period. Sub acute toxicity provides information on the target organs affected by the compound. The animals treated with PrGO showed no clinical signs such as respiratory, motor, convulsion, reflexes, ocular signs, cardiovascular signs, salivation, piloerection, analgesia and gastrointestinal responses. All the animals were normal during the experimental period. There was no abnormality seen during the gross necropsy. However aggregation of PrGO observed throughout the intraperitoneal cavity. Body weight of all the animals was normal when compared with control animals.

5.7.2.1. HAEMATOLOGY AND CLINICAL CHEMISTRY

Blood was collected from the animals (sub acute toxicity) treated with PrGO, for haematological (anticoagulated blood) and clinical chemistry (serum) parameters. The results of the study showed significant decrease in RBC count, HGB content and HCT value at the end of 7 days and 14 days post exposure of PrGO. The RBC, HGB and HCT values were similar to that of control values at the end of 21 days. Similar observations in

RBC, HGB and HCT were noticed in acute toxicity of PrGO. In addition, significant changes were noticed in MCH value following PrGO exposure. The decreased RBC in turn results in decreased HGB content and decreased availability of oxygen for metabolism and this leads to hypoxia or transient anemic conditions.

The results of the clinical chemistry of the PrGO exposed animals indicated that, there is a significant change in SGPT and SGOT activity throughout the experimental period. Increase in SGPT was monitored throughout the experimental period whereas increase in SGPT activity was found at 21 days post exposure. A similar response in SGPT activity (increased) was observed in acute toxicity. It was well known that SGPT is a major constituent enzyme present in liver, which is released upon liver injury (Bheeman *et al*., 2014). This increased SGPT and SGOT activity is a direct indication of hepatic injury. It was also noted that the value of total protein and cholesterol were significantly decreased in mice exposed repeatedly with PrGO.

5.7.2.2. HISTOPATHOLOGICAL EXAMINATION

Organs such as liver, brain, kidney and spleen were collected from the animals of sub acute toxicity (repeated exposure of PrGO) and subjected to histopathological examinations. It was evident from the histopathological findings, that the PrGO induces hepatic damage such as congestion, granulation, vacuolar degeneration and macrophage infiltration. This observation complement with the increased SGOT and SGPT activity observed in both acute and sub acute toxicity studies. Extramedullary haematopoiesis and presence of megakaryocytes were well manifested in spleen. There is a congestion observed in glomerulus of kidneys, and no other changes were noticed in distal and

proximal convoluted tubules. The histopathological findings indicated that the brain showed normal architecture even after repeated administration of PrGO. However the PrGO disrupt BBB and translocate in brain after single exposure (acute toxicity) of PrGO as evidenced in the Raman Mapping.

5.7.2.3. ANTIOXIDANT ASSAYS

Oxidative stress occurs when the cell encounters imbalance between ROS and antioxidant system. There are certain antioxidant enzymes that modulate the redox state of cells either by maintaining cellular antioxidant level or by catalyzing ROS. Nanoparticles induced ROS can also modulate the activity of antioxidant enzymes like glutathione peroxidase, superoxide dismutase and catalase (Manke *et al*., 2013).The results of the antioxidant enzyme activity and total cellular glutathione (GSH) (sub acute toxicity) showed significant decrease in the activity of SOD and increased GSH at the end of 7 and 14 days of PrGO exposure. It was also observed that SOD activity and GSH level becomes normal and comparable to control at the end of the experimental period (21 days). The details of each parameter are discussed in the subsequent paragraph.

5.7.2.3.1. LIPID PEROXIDATION (LPO)

Increased ROS production inside the cells leads to the formation of lipid peroxidation and causes irreversible oxidative damage to the cells. Unsaturated lipid molecules in liver tissues are more susceptible to oxidation resulting in the formation of malondialdehyde (MDA). (Krishnamoorthy *et al*., 2012) reported that graphene can induce ROS formation and lipid peroxidation in bacteria leading to disintegration of cell membrane. However, the results of the present study showed no increase in MDA

formation in liver tissue, when mice were exposed to PrGO repeatedly. This may be due to the PEG coating of the nanomaterial.

5.7.2.3.2. TOTAL GLUTATHIONE (GSH)

GSH is an endogenous antioxidant present in almost all the cells and protects them from oxidative stress. Glutathione occurs in reduced form and regenerated from oxidized glutathione (Mylonas & Kouretas, 1999; Owen & Butterfield, 2010). (Sies & Akerboom, 1984) reported that cellular defense against ROS becomes impaired when GSH level goes down ensuing peroxide injury. The result of the present study indicates an increase in GSH level in 7 and 14 days following PrGO exposure. This advocate that the cells tries to combat the oxidative stress by maintaining the intracellular GSH content and prevent oxidation of major cellular components. At the end of 21 days post exposure, the level of GSH was comparable to control.

5.7.2.3.3. GLUTATHIONE REDUCTASE (GR)

Oxidized glutathione (GSSG) is converted to GSH by the action of GR, a homodimeric flavoprotein. The ratio of GSSG/GSH is maintained by GR and also takes part in the detoxification of ROS, synthesis of DNA and proteins (Brown *et al*., 2004). The increase in GR activity observed in the present study at the end of 7 and 14 days correlates with the increased GSH production following PrGO exposure.

5.7.2.3.4. GLUTATHIONE PEROXIDASE (GPx)

GPx reduces lipid hydroperoxides and free hydrogen peroxide to alcohol and water (Omotayo *et al*., 2010). GPx and GR are the two major enzymes involved in the GSSG/GSH cycle. Formation of ROS inside the cells is scavenged by GSH, which is

converted to oxidized GSSG catalyzed by GPx. The low activity of GPx in the present study indicates that, exposure of PrGO causes mere oxidative stress during the initial period (7 and 14 days) and normalized at the end of the experimental period (21 days).

5.7.2.3.5. SUPEROXIDE DISMUTASE (SOD)

Superoxide radicals ($O_2^{\cdot-}$) are produced by mitochondria as a result of normal cellular metabolism. Free radicals formed inside the cells are scavenged by SOD that acts as a first line of defense against ROS. SOD catalyzes the dismutation of superoxide to H_2O_2 (Okado Matsumoto & Fridovich, 2001) and hydroxyl radical ($^{\cdot}OH$) is the most reactive ROS formed from H_2O_2 .The main role of SOD is to catalyze the dismutation of superoxide radical to form oxygen and H_2O_2 and protect the cellular components from oxidative damage. The results of the study pointed that decrease in SOD activity observed at the end of 7 and 14 days relates to the increased ROS formation inside the cells and noticeable oxidative stress resulting from PrGO exposure. The activity of SOD was regained to normal at the end of 21 days.

The *in vivo* antioxidant assays correlates with the increased ROS formation in *in vitro* assays stating that the exposure to PrGO induces transient increases in ROS formation and slight oxidative stress during the initial period. In *in vivo* conditions the cells overcome the oxidative stress by promoting the cellular antioxidant defense system at the end of 21 days post exposure.

5.7.2.4. MORPHOLOGY OF MSCs AFTER PrGO EXPOSURE

MSCs were isolated from bone marrow of mice (sub acute toxicity) exposed to PrGO. The isolated cells rapidly adhered onto the tissue culture plates. MSCs showed

characteristics spindle shaped fibroblasts like morphology and proliferated efficiently in DMEM medium.

It was observed that MSCs formed discrete colonies with spindle shaped morphology after 4 days of culture. Whereas in *in vitro* culture conditions, the characteristics spindle shaped was observed within 7-10 days of culture. No phenotypic or morphological changes were noticed in MSCs. In addition to MSCs, fat cells and osteoblasts appeared in culture after 10 days. The results validate that sub acute exposure of PrGO does not affect the bone marrow integrity or niche in animals.

5.7.2.5. IMMUNOTOXICITY

Immunotoxicity of graphene is one of the less explored areas. Systemic immune response induced upon repeated exposure to PrGO was studied using splenocytes proliferation assay. The results showed an increased proliferation of splenocytes at 7 and 14 days of post exposure. The proliferation becomes normal at the end of 21 days. Changes in splenic index were evident in the spleen of acute toxicity study. The histology examination revealed extramedullary hematopoiesis which is associated with pathological lesions. The increased splenocytes observed in 7 and 14 days suggest that the immune response was activated in mice as a consequence of PrGO exposure which was found normal at the end of 21 days.

CHAPTER 6: SUMMARY AND CONCLUSION

6. SUMMARY AND CONCLUSION

6.1. SUMMARY

Graphene, a 2D carbon material is going to revolutionize the modern scientific era with potential applications in energy technology, material sciences and biomedical field. Graphene has raised the global importance and created intense interest in the scientific community because of its versatile application. Despite the increased worldwide production, the research on toxicity and harmful effects imposed by graphene towards the ecosystem remains obscure and the outcomes of the studies were conflicting. Hence the present study emphasizes on the bio-nano interaction of nanographene (PrGO: PEGylated Reduced Graphene Oxide) using mesenchymal stem cells (MSCs) as *in vitro* model. Further its allied toxicity at molecular level was evaluated in Swiss Albino mice. The biological interaction of PrGO with MSCs was studied because MSCs are the most widely used cells for tissue regeneration and graphene has a scope to be used as a scaffold material for tissue engineering.

In the present study, PrGO was successfully synthesized from graphene oxide (GO). GO was synthesized from graphite flakes using Hummer's method. Nano sized GO was obtained by conjugating O,O′- Bis(2-aminoethyl) polyethylene glycol and the larger sheets were separated by centrifugation and filtration. PrGO was synthesized by the reduction of GO-PEG with sodium borohydride. The synthesized PrGO was characterized by TEM, AFM, XRD, XPS, FTIR, Raman and TGA. The lateral dimension of PrGO was found to be ~1µm with the thickness of 8-9 nm.

The synthesized PrGO was screened for endotoxin contamination and found that the endotoxin level was well below the recommended range (<0.5 EU). The formation of protein corona plays a significant role in modulating the physico-chemical properties of the nanoparticles and their interaction with the biological system. Hence, the isolation of hard corona proteins around PrGO was carried out to determine the type of protein adhered onto the surface of PrGO. SDS-PAGE showed that BSA as the only protein firmly adhered to the surface of PrGO and form hard corona. Presence of BSA on the surface of PrGO may alter its cellular uptake and distribution

The cell viability or cytotoxic effects of PrGO on MSCs were studied by MTT and Neutral red uptake assays and found non toxic. The study also showed PrGO greatly supports the growth and proliferation of MSCs. The cells effectively metabolized MTT and uptake neutral red, which indicates that the cells are active and viable. Further, the presence of PrGO was observed throughout the cytoplasm as evident in cellular uptake study.

Oxidative stress occurs when there is an excess production of ROS inside the cells as a result of nanoparticle exposure. ROS formed inside the cells can disrupt the cellular homeostasis when antioxidant defense system fails to protect the cells from damage. ROS can oxidize cellular biomolecules such as DNA, protein, lipid and also affects the cellular metabolism and signaling. Excess of ROS formed inside the cells also induce mitochondrial membrane depolarization and lysosomal destabilization which eventually promote apoptosis. The result of the study indicated that PrGO induces ROS production in a concentration and time dependent manner. Mitochondrial membrane potential

(MMP) analysis by JC-1 probe showed decreased MMP at higher concentration (500 µg/ml) as evident from increased green fluorescence. There were no changes observed in lysosomes following PrGO exposure. Acridine orange staining of lysosomes in cells exposed to 500 µg/ml showed increased red fluorescence, which may be due to the increased formation of lysosomes inside the cells.

It was found that PrGO does not affect the cell integrity and cell attachment onto the culture plates as evident in actin staining using Cytopainter. The presence of PrGO inside the cells masked the fluorescence emitted by Cytopainter.

Increased ROS can act as an initiating factor for inducing intrinsic apoptosis. ROS induced mitochondrial membrane damage can release cytochrome c into the cytoplasm, activates cascade of caspase enzymes and release proapoptotic factors inside the cells. On exposure to PrGO (500 µg/ml), the presence of few early and late apoptotic cells were noticed in Annexin V/ PI staining. MSCs treated with different concentration of PrGO showed no significant increase in caspase activity, when compared to control. DNA ladder assay in cells was carried out as a measure of apoptosis. This confirmed that PrGO does not affect the integrity of DNA and fails to induce DNA fragmentation. Absence of PrGO inside the cell nucleus further confirms that PrGO does not cause damage to genetic material.

Differentiation potential of MSCs after PrGO exposure was studied by alkaline phosphatase assay. It was found that the cells exposed to PrGO in presence of osteogenic medium showed an increased ALP activity when compared to control. The results of the *in vitro* studies clearly confirm that the PrGO fails to induce any toxic effects in MSCs.

The present study suggests that PrGO can be used as a scaffold for stem cell culture in tissue engineering for bone regeneration. Further, this study promises the use of stem cells as an *in vitro* model for predictive toxicity screening or as an alternative to animal experimentation.

Acute and sub acute toxicity of PrGO (10 mg/kg body weight) was studied in mice following intravenous and intraperitoneal administration. The result of the study indicated that none of the animals showed any clinical symptoms or death during the acute or sub acute toxicity studies. The biodistribution and toxicokinetics study showed that PrGO was distributed in major organs such as liver, brain, kidney and spleen after acute exposure as evidenced in Confocal Raman mapping. Maximum absorption of PrGO was observed in liver and spleen after three days of intravenous injection. The maximum percentage of PrGO was observed in liver at the end of 21 days of intraperitoneal administration. The presence of PrGO in brain suggests that PrGO crossed the blood brain barrier system. Excretion of PrGO was confirmed in urine by Raman mapping. The weak intensity of PrGO peaks state that only a small portion of the injected PrGO excreted via urine. Presence of PrGO was also evident in bone marrow throughout the experimental period and there is a possibility of interaction between PrGO and stem cells resides in bone marrow niche. Analysis of blood collected from mice (PrGO exposed) at different time period showed the maximum release of PrGO occurs after 3 h of administration and decreased in subsequent hours. A weak PrGO signal was monitored in blood sample stating that most of the injected PrGO was absorbed and distributed in various organs at the end of 7 days of exposure.

There was a significant decrease in RBC, HGB and HCT values observed at the end 7 days of exposure and becomes normal at the end of 21 days. Similarly, there was a significant changes observed in the activity of liver enzymes such as SGOT, SGPT throughout the experimental period and suggests possible liver injury. Although no changes were observed in body weight, significant differences were noticed in organ index suggesting either atrophy or hypertrophy.

Absorption, distribution, metabolism, excretion and toxicity (ADME & T) study revealed that PrGO was effectively absorbed from the site of injection into the blood circulation. It was also found to distribute from the systemic circulation into various major organs such as liver, brain, kidney and spleen. Also trace amount of PrGO was observed in urine. There were few changes observed in the metabolic profile of mice following PrGO exposure as evident from changes in clinical chemistry values. Increased liver enzyme activity manifested after PrGO administration suggests hepatotoxicity.

Sub acute toxicity of PrGO was studied in mice after intraperitoneal administration (10 mg/ kg body weight). All the animals were normal during the experimental period and the body weights of the animals were normal. Gross pathology of the animals showed no abnormalities in major organs. The presence of PrGO was observed in the peritoneal cavity even after 21 days of injection, stating that smaller sized PrGO excreted via urine whereas the larger sheets aggregates and accumulates at various sites inside the body. Further, bone marrow of the animals was collected and MSCs were isolated and cultured in media. It was observed that there was no phenotypic change in MSCs. In addition to MSCs, fat cells and osteoblasts were also observed.

Blood was collected from the sub acute toxicity and the result showed significant decrease in RBC, HGB and HCT values at the end of 7 and 14 days post exposure. These values were normalized at the end of 21 days. Significant increases in SGOT and SGPT activity was noticed. Histopathological findings showed that there was congestion, cytoplasmic granulation and vacuolar degeneration in liver tissue which confirms hepatic injury. Congestion of glomerulus was noticed in kidney. Megakaryocytes and extramedullary haematopoiesis were seen in spleen tissue. Thymidine incorporation study revealed increased splenocytes proliferation at the end of 7 days of exposure which decreases subsequently at the end of 21 days post exposure.

Liver tissues from the sub acute activity were examined for oxidative stress. Oxidative stress occurs when the cellular antioxidant defense system fails to protect the cells from increased ROS. There was no lipid peroxidation occurs as a result of PrGO treatment. There were no significant changes observed in GPx and GR activity. Significant decrease in SOD activity observed at the end of 7 and 14 days implies initial oxidative stress encountered by the cells following PrGO treatment. The cell tries to overcome the acute oxidative stress by increasing the amount of reduced glutathione, an ubiquitous antioxidant present in almost all the cells. All the oxidative stress related antioxidant was comparable to control at the end of 21 days.

6.2. METHODOLOGY ADAPTED

- Synthesis of GO from graphite flakes.
- Covalent coupling of GO with O,O′- Bis(2-aminoethyl) polyethylene glycol under EDC chemistry.
- Reduction of GO-PEG to form PrGO.
- Physico-chemical characterization of PrGO and RGO.
    - Characterization of surface morphology of PrGO and RGO by TEM.
    - Measurement of size and lateral dimension of both PrGO and RGO by AFM.
    - Analysis of elemental composition of PrGO and RGO by XPS.
    - TGA and FTIR to confirm O,O′- Bis(2-aminoethyl) polyethylene glycol coating.
    - Analyze the presence of characteristics graphene peaks by Raman Spectroscopy.
    - Examine the crystal diffraction pattern by XRD.
- Evaluation of endotoxin content in PrGO.
- Isolate and characterize mesenchymal stem cells from mouse bone marrow.
    - Characterize the expression of surface markers by immunostaining and FACs.
    - Evaluate the differentiation of MSCs towards adipogenesis and osteogenesis.
- Isolation of hard corona proteins that bind to the surface of PrGO.

- Evaluate the cellular uptake of PrGO by phase contrast microscope and TEM.
- Evaluate the cytotoxicity and cell viability of MSCs exposed to PrGO by MTT and Neutral red assay.
- Measurement of ROS formation in MSCs after exposure to PrGO by DCFHDA assay.
- Examine the changes in mitochondrial membrane potential as a result of PrGO treatment.
- Study the effect of PrGO on lysosomal destabilization by quantitative and qualitative analysis of AO relocation.
- Examine the effect of PrGO on cytoskeletal arrangement and cell adhesion by Actin staining.
- Measurement of apoptosis induced after exposure to PrGO by Annexin V/ PI staining live dead assay.
- Estimation of caspase activation in MSCs after PrGO by Caspase 3/7 assay.
- Study the potential of PrGO to induce DNA fragmentation by Apoptotic DNA ladder assay.
- Examine the effect of PrGO on osteogenic differentiation of MSCs by alkaline phosphatase assay.
- Examine the biodistribution, toxicokinetics of PrGO in mice after single acute exposure by Confocal Raman mapping.

- Determine the effect of PrGO on changes in body weight, organ indices, hematological and clinical chemistry parameters.
- Investigate the absorption, distribution, metabolism, excretion and toxicity of PrGO after acute exposure by Confocal Raman mapping.
- Evaluate the effect of PrGO on hematological and clinical chemistry parameters in mice after repeated exposure by Sub acute toxicity study.
- Examine the pathological changes in major organs after PrGO by histopathology.
- Find out the effect of PrGO on cellular antioxidant defense system by estimation of LPO, GSH, GPx, GR and SOD activity.
- Examine the effect of PrGO on mouse bone marrow stem cells phenotype.
- Evaluate the effect of repeated exposure of PrGO on immune system by splenocytes proliferation assay.

6.3. MAJOR FINDINGS OF THE STUDY

- PrGO with the thickness of 8-9 nm was successfully synthesized and characterized by TEM, AFM, XRD, FTIR, Raman, TGA and XPS.
- Endotoxin level of PrGO was measured and the results confirmed that the endotoxin level was < 0.1 EU/ml
- MSCs were successfully isolated from mouse bone marrow. The isolated MSCs expressed positive CD markers and are readily differentiated into adipocytes and osteoblasts.

- Hard corona proteins that bind to the surface of PrGO were isolated and separated. BSA was the only protein attached on the surface of PrGO.
- PrGO was effectively internalized by MSCs and was found to distribute throughout the cytoplasm. No PrGO were seen in nucleus. Despite the entry, the cells remain intact without any morphological distortion.
- Cytotoxicity and cell viability of MSCs after PrGO exposure showed no loss of cell viability and no changes in metabolic activity of the cells.
- PrGO was found to induce increased ROS production in cells in concentration and time dependent manner leading to oxidative stress.
- The evaluation of MMP and lysosomal destabilization showed PrGO did not cause mitochondrial membrane depolarization or lysosomal destabilization except at higher concentration (500 µg/ml). Increased uptake of PrGO might increase the number of lysosomes inside the cells.
- The cell adhesion and cytoskeletal orientation was not affected by PrGO treatment. Apoptosis study showed PrGO did not induce cell death. Also the cells did not exhibit significant caspase activation or DNA fragmentation.
- No changes in differentiation potential of MSCs were noticed after PrGO treatment as evident in ALP activity.
- Acute toxicity (10 mg/kg body weight) of PrGO was studied in Swiss Albino mice with single exposure via both intraperitoneal and intravenous injection.

- Biodistribution and toxicokinetics showed PrGO was distributed in liver, brain, kidney, spleen and bone marrow throughout the experimental period. Excretion of a small portion of PrGO was observed in urine as evident from Raman mapping.
- Organ indices of the animals exposed to PrGO changed significantly. Changes in hematological and clinical chemistry parameters were noted after acute exposure.
- ADME & T investigation showed PrGO was effectively absorbed from systemic circulation, distributed in major organs and excretes via urine. Acute liver injury may result after PrGO treatment.
- Sub acute toxicity: Repeated exposure of PrGO (10 mg/kg body weight) in Swiss Albino mice via intraperitoneal injection.
- Changes in hematological and clinical chemistry parameters were noticed
- Degranulation, vacuolarization and marginalization of cytoplasm in liver cells, congestion of glomerulus and interstitial spaces in kidney, presence of megakaryocytes and extra medullary hematopoiesis in spleen were observed in histopathology.
- Significant increase in GSH content and decrease in SOD activity was monitored in liver tissue of PrGO treated animals which become normal at the end of 21 days post exposure.
- No phenotypic changes were observed in MSCs isolated from bone marrow of PrGO administered animals. In addition, adipocytes and osteoblasts were also seen in culture.

- Exposure to PrGO initiates immune response by increasing the splenocytes proliferation at 7 and 14 days of post exposure which becomes normal at the end of 21 days.

6.4. Conclusion

Nano sized PEGylated reduced graphene oxide (PrGO) of size 8-9 nm was successfully synthesized and characterized using TEM, AFM, SAED, XRD, Raman, FTIR, XPS and TGA. *In vitro* toxicity assays confirmed that the synthesized PrGO was non toxic and does not affect the growth, proliferation and functional aspects of MSCs. There were no changes observed in the phenotype of MSCs after exposure to PrGO. The preliminary toxicity screening using MSCs as an *in vitro* model suggest that PrGO can be used as a scaffold for culturing MSCs in tissue engineering or can be used for the development of biomedical implants for delivering stem cells. The present study also supports the use of stem cells as an *in* vitro model for predictive toxicity screening or as an alternative to animal experimentation. In *vivo* toxicity studies in mice showed that PrGO slightly affects the integrity of the organs. There were no systemic effects observed during biodistribution or toxicokinetics evaluation. The molecular toxicity, immunotoxicity and biochemical evaluation showed slight alteration and the same was recovered to the normal range. Histopathological analysis showed few lesions in liver, kidney and spleen. Further long term toxicity studies will be required to declare PrGO is a validated to be safe nanomaterial for clinical application.

6.5. Future Prospects

- Mechanism of cellular uptake.
- Role of Protein corona in modulating the interaction of PrGO inside the biological system.
- *In vivo* Bio-distribution with repeated dose of PrGO.
- Evaluation of Tumorogenicity and genotoxicity.
- Detailed Target organ studies after repeated exposure of PrGO.

REFERENCES

Akhavan O, Ghaderi E (2010) Toxicity of graphene and graphene oxide nanowalls against bacteria. *ACS Nano* 4(10):5731-5736.

Akhavan O, Ghaderi E, Akhavan A (2012) Size-dependent genotoxicity of graphene nanoplatelets in human stem cells. *Biomaterials* 33: 8017-8025.

Alarifi S, Ali D, Y AO, Ahamed M, Siddiqui MA, Al-Khedhairy AA (2013). Oxidative stress contributes to cobalt oxide nanoparticles-induced cytotoxicity and DNA damage in human hepatocarcinoma cells. *Int J Nanomedicine* 8:189-199.

Albini A, Mussi V, Parodi A, Ventura A, Principi E, Tegami S, Rocchia M, Francheschi E, Sogno I, Cammarota R (2010) Interactions of single-wall carbon nanotubes with endothelial cells. *Nanomed-Nanotechnol* 6(2): 277-288.

Apopa PL, Qian Y, Shao R, Guo NL, Schwegler-Berry D, Pacurari M, Porter D, Shi X, Vallyathan V, Castranova V, Flynn DC (2009) Iron oxide nanoparticles induce human microvascular endothelial cell permeability through reactive oxygen species production and microtubule remodeling. *Part Fibre Toxicol* 6:1. DOI: 10.1186/1743-8977-6-1.

An S, Shim K, Hulme J, Meang E, Kim M (2014) Analysis of zinc oxide nanoparticles binding proteins in rat blood and brain homogenate. *Int J Nanomedicine* 9:217-224.

Baksh D, Song L, Tuan RS (2004) Adult mesenchymal stem cells: characterization, differentiation, and application in cell and gene therapy. *J Cell Mol Med* 8:301-316.

Ball BR, Smith KM, Veranth JE, Aust A (2000) Bioavailability of iron from coal fly ash: Mechanisms of Mobilization and of Biological Effects. *Inhal Toxicol* 12:209-225.

Bheeman D, Sugumaran S, Mathan R, Sivanesan D, Bellan C (2014) Oxidative Stress Induced Biochemical Alterations Due to Novel In TiO Nanoparticles Exposure. *Nanosci Nanotechnol Lett* 6:457-463.

Bressan E, Ferroni L, Gardin C, Sbricoli L, Gobbato L, Ludovichetti F, Tocco I, Carraro A, Piattelli A, Zavan B (2014) Graphene based scaffolds effects on stem cells commitment. *J Transl Med* 12:296. DOI: 10.1186/s12967-014-0296-9.

Brodie B (1859) On the Atomic Weight of Graphite. *P R Soc London* 10:11-12.

Brown D, Kinloch, I, Bangert U, Windle A, Walter D, Walker G, Scotchford C, Donaldson K, Stone V (2007) An *in vitro* study of the potential of carbon nanotubes and

nanofibres to induce inflammatory mediators and frustrated phagocytosis. *Carbon* 45:1743-1756.

Brown LA, Harris FL, Ping XD, Gauthier TW (2004) Chronic ethanol ingestion and the risk of acute lung injury: a role for glutathione availability? *Alcohol* 33:191-197.

Buchsteiner A, Lerf A, Pieper J (2006) Water Dynamics in Graphite Oxide Investigated with Neutron Scattering. *J Phys Chem B* 110:22328-22338.

Buffle J (2006) The Key Role of Environmental Colloids/Nanoparticles for the Sustainability of Life. *Environ Chem* 3:155-158.

Cadet J, Wagner J (2013) DNA Base Damage by Reactive Oxygen Species, Oxidizing Agents, and UV Radiation. *Cold Spring Harb Perspect Biol* 5:a012559-a012559.

Cao X, Deng W, Wei Y, Yang Y, Su W, Wei Y, Xu X, Yu J (2012) Incorporating pTGF-b1/ calcium phosphate nanoparticles with fibronectin into 3-dimensional collagen/chitosan scaffolds: efficient, sustained gene delivery to stem cells for chondrogenic differentiation. *Eur Cell Mater* 23:81-93.

Chatterjee N, Eom H, Choi J (2014) A systems toxicology approach to the surface functionality control of graphene–cell interactions. *Biomaterials* 35:1109-1127.

Chellat F, Merhi Y, Moreau A, Yahia L (2005) Therapeutic potential of nanoparticulate systems for macrophage targeting. *Biomaterials* 26:7260-7275.

Chen G, Yang H, Lu C, Chao Y, Hwang S, Chen C, Lo K, Sung L, Luo W, Tuan H, Hu Y (2012) Simultaneous induction of autophagy and toll-like receptor signaling pathways by graphene oxide. *Biomaterials* 33:6559-6569.

Chung C, Kim Y, Shin D, Ryoo S, Hong B, Min D (2013). Biomedical Applications of Graphene and Graphene Oxide. *Acc Chem Res* 46:2211-2224.

Chwalibog A, Hinzmann M, Kutwin M, Jagiello J, Kozinski R, Wierzbicki M, Grodzik M, Lipinska L, Sawosz E, Jaworski S (2014) Nanoparticles containing allotropes of carbon have genotoxic effects on glioblastoma multiforme cells. *Int J Nanomedicine* 9: 2409–2417.

Corsi K, Chellat F, Yahia L, Fernandes J (2003) Mesenchymal stem cells, MG63 and HEK293 transfection using chitosan-DNA nanoparticles. *Biomaterials* 24:1255-1264.

Cruje C, Chithrani DB (2014) Polyethylene Glycol Density and Length Affects Nanoparticle Uptake by Cancer Cells. *J Nanomed Res* 1: DOI: 10.15406/jnmr.2014.01.00006.

De M, Ghosh P, Rotello V (2008) Applications of Nanoparticles in Biology. *Adv Mater* 20: 4225-4241.

Dobrovolskaia M, Neun B, Clogston J, Ding H, Ljubimova J, McNeil S (2010) Ambiguities in applying traditional Limulus Amebocyte Lysate tests to quantify endotoxin in nanoparticle formulations. *Nanomedicine* 5:555-562.

Dreyer D, Park S, Bielawski C, Ruoff R (2010) The chemistry of graphene oxide. *Chem Soc Rev* 39:228-240.

Duan X, Li Y (2013) Physicochemical characteristics of nanoparticles affect circulation, biodistribution, cellular internalization, and trafficking. *Small* 9:1521-1532.

Ekstrand-Hammarström B, Akfur C, Andersson P, Lejon C, Österlund L, Bucht A (2011) Human primary bronchial epithelial cells respond differently to titanium dioxide nanoparticles than the lung epithelial cell lines A549 and BEAS-2B. *Nanotoxicology* 6:623-634.

Elkhenany H, Amelse L, Lafont A, Bourdo S, Caldwell M, Neilsen N, Dervishi E, Derek O, Biris A, Anderson D and Dhar M (2014) Graphene supports in vitro proliferation and osteogenic differentiation of goat adult mesenchymal stem cells: potential for bone tissue engineering. *J Appl Toxicol* 35:.367-374.

Elsaesser A, Howard CV (2012) Toxicity of nanoparticles. *Adv Drug Deliv Rev* 64:129-137

Fan HL, Wang LL, Zhao KK, Li N, Shi ZJ, Ge ZG, Jin ZX (2010) Fabrication, mechanical properties, and biocompatibility of graphene reinforced chitosan composites. *Biomacromolecules* 11:2345-2351.

Fan X, Peng W, Li Y, Li X, Wang S, Zhang G, Zhang F (2008) Deoxygenation of Exfoliated Graphite Oxide under Alkaline Conditions: A Green Route to Graphene Preparation. *Adv Mater* 20: 4490–4493.

Feng LZ, Zhang S, Liu Z (2011) Graphene based gene transfection. *Nanoscale* 3:1252-1257.

Feynman R (1959) There's Plenty of Room at the Bottom, Annual meeting of American Physical Society, California Institute of Technology.

Friedenstein AJ, Gorskaja JF, Kulagina NN (1976) Fibroblast precursors in normal and irradiated mouse hematopoietic organs. *Exp Hematol* 4:267-274.

Fu P, Xia Q, Hwang H, Ray P, Yu H (2014) Mechanisms of nanotoxicity: generation of recative oxygen species. *J Food Drug Anal* 22: 64-75

GAO or GAO report number GAO-10-549 entitled 'Nanotechnology: Nanomaterials Are Widely Used in Commerce, but EPA Faces Challenges in Regulating Risk' June 25, 2010.

Gharibshahi E, Saion E (2012) Influence of Dose on Particle Size and Optical Properties of Colloidal Platinum Nanoparticles. *Int J Mol Sci* 13:14723-14741.

Gonçalves G, Vila M, Bdikin I, de Andrés A, Emami N, Ferreira RA, Carlos LD, Grácio J, Marques PA (2014) Breakdown into nanoscale of graphene oxide: confined hot spot atomic reduction and fragmentation. *Sci Rep* 4:6735. DOI: 10.1038/srep06735.

Guo C, Zheng X, Lu Z, Lou X, Li C (2010) Biointerface by Cell Growth on Layered Graphene-Artificial Peroxidase-Protein Nanostructure for In Situ Quantitative Molecular Detection. *Adv Mater* 22:5164-5167.

Guo X, Mei N (2014) Assessment of the toxic potential of graphene family nanomaterials. *J Food Drug Anal* 22:105-115.

Guo Y, Srinivasula SM, Druilhe A, Fernandes-Alnemri T, Alnemri ES (2002) Caspase-2 induces apoptosis by releasing proapoptotic proteins from mitochondria. *J Biol Chem* 277: 13430-13437.

Holzinger M, Goff AL, Cosnier S (2014) Nanomaterials for biosensing applications: a review. *Front Chem* 2: 63. DOI: 10.3389/fchem.2014.00063

Hwang S, Nam J, Jung S, Song J, Doh H, Kim S (2014) Gold nanoparticle-mediated photothermal therapy: current status and future perspective. *Nanomedicine (Lond)* 9:2003-2022.

Huang Y, Dong X, Liu Y, Li LJ, Chen P (2011) Graphene-based biosensors for detection of bacteria and their metabolic activities. *J Mater Chem* 21:12358–12362.

Huang Z, Xu HP, Meyers AD, et al Photodynamic therapy for treatment of solid tumors-Potential and technical challenges. *Technol Cancer Res T*. 2008; 7(4): 309-20.

Hu X, Ouyang S, Mu L, An J, Zhou Q (2015) Effects of Graphene Oxide and Oxidized Carbon Nanotubes on the Cellular Division, Microstructure, Uptake, Oxidative Stress, and Metabolic Profiles. *Environ Sci Technol* 49:10825-10833.

Hummers W, Offeman R (1958) Preparation of Graphitic Oxide. *J Am Chem Soc* 80:1339-1339.

ISO 10993-1:2009, Biological evaluation of medical devices. 1-21

Jakkaraju S, Zhe X, Pan D, Choudhury R, Schuger L (2005) TIPs are tension-responsive proteins involved in myogenic versus adipogenic differentiation. *Dev Cell* 9:39-49.

Jarosz A, Skoda M, Dudek I, Szukiewicz D (2016) Oxidative Stress and Mitochondrial Activation as the Main Mechanisms Underlying Graphene Toxicity against Human Cancer Cells. Oxidative Medicine and Cellular Longevity. *Oxid Med Cell Longev* DOI: 10.1155/2016/5851035

Jeon EJ, Lee KY, Choi NS, Lee MH, Kim HN, Jin YH, Ryoo HM, Choi JY, Yoshida M, Nishino N, Oh BC, Lee KS, Lee YH, Bae SC (2006) Bone morphogenetic protein-2 stimulates Runx2 acetylation. *J Biol Chem* 281:16502-16511.

Jiao G, He X, Li X, Qiu J, Xu H, Zhang N, Liu S (2015) Limitations of MTT and CCK-8 assay for evaluation of graphene cytotoxicity. *RSC Adv* 5(66): 53240-53244.

Jin S, Kim D, Jun G, Hong S, Jeon S (2013) Tuning the Photoluminescence of Graphene Quantum Dots through the Charge Transfer Effect of Functional Groups. *ACS Nano* 7:1239-1245.

Kalbacova M, Broz A, Kong J, Kalbac M (2010) Graphene substrates promote adherence of human osteoblasts and mesenchymal stromal cells. *Carbon* 48:4323-4329.

Karlsson H, Cronholm P, Gustafsson J,Möller L (2008) Copper Oxide Nanoparticles Are Highly Toxic: A Comparison between Metal Oxide Nanoparticles and Carbon Nanotubes. *Chem Res Toxicol* 21:1726-1732.

Kaushik A, Khan R, Solanki PR, Pandey P, Alam J, Ahmad S, Malhotra BD (2008) Iron oxide nanoparticles-chitosan composite based glucose biosensor. *Biosens Bioelectron* 24: 676-683.

Khan MS, Shakoor A, Khan GT, Sultana S, Zia A (2015) A Study of Stable Graphene Oxide Dispersions in Various Solvents. *J Chem Soc Pak* 37: 62-67.

Knetsch M, Koole L (2011) New Strategies in the Development of Antimicrobial Coatings: The Example of Increasing Usage of Silver and Silver Nanoparticles. *Polymers* 3:340-366.

Koch K (1982) Oxidation by Mn207: An impressive demonstration of the powerful oxidizing property of dimanganese heptoxide. *J Chem Educ* 59:973. DOI: 10.1021/ed059p973.3

Kolf CM, Cho E, Tuan RS (2007) Biology of adult mesenchymal stem cells: regulation of niche, self-renewal and differentiation. *Arthritis Res Ther* 9:204 DOI:10.1186/ar2116

Konios D, Stylianakis MM, Stratakis E, Kymakis E (2014) Dispersion behaviour of graphene oxide and reduced graphene oxide. *J Colloid Interface Sci* 430:108–112.

Krishnamoorthy K, Veerapandian M, Zhang LH, Yun K, Kim SJ (2012) Antibacterial Efficiency of Graphene Nanosheets against Pathogenic Bacteria via Lipid Peroxidation. *J Phys Chem C* 116:17280−17287.

Kumar A, Lee CH , Synthesis and Biomedical Applications of Graphene: Present and Future Trends, http://dx.doi.org/10.5772/55728

Kundrotas G (2012) Surface markers distinguishing mesenchymal stem cells from fibroblasts. *Acta medica Lituanica* 19:75-79.

Kunzmann A, Andersson B, Thurnherr T, Krug H, Scheynius, A, Fadeel B (2011) Toxicology of engineered nanomaterials: Focus on biocompatibility, biodistribution and biodegradation. *Biochim Biophys Acta* 1810:361-373.

Lee W, Lim C, Shi H, Tang L, Wang Y, Lim C, Loh K (2011) Origin of Enhanced Stem Cell Growth and Differentiation on Graphene and Graphene Oxide. *ACS Nano* 5:7334-7341.

Lerf A, Buchsteiner A, Pieper J, Schöttl S, Dekany I, Szabo T, Boehm H (2006) Hydration behavior and dynamics of water molecules in graphite oxide. *J Phys Chem Solids* 67:1106-1110.

Liao K, Lin Y, Macosko C, Haynes C (2011) Cytotoxicity of Graphene Oxide and Graphene in Human Erythrocytes and Skin Fibroblasts. *ACS Appl Mater Interfaces* 3:2607-2615.

Li B, Zhang X, Yang J, Zhang Y, Li W, Fan C, Huang Q (2014) Influence of polyethylene glycol coating on biodistribution and toxicity of nanoscale graphene oxide in mice after intravenous injection. *Int J Nanomedicine* 9: 4697–4707.

Li N, Zhang X, Song Q, Su R, Zhang Q, Kong T, Liu L, Jin G, Tang M, Cheng G (2011) The promotion of neurite sprouting and outgrowth of mouse hippocampal cells in culture by graphene substrates. *Biomaterials* 32:9374-9382.

Li T, Oloyede A, Gu Y (2014) Adhesive characteristics of low dimensional carbon nanomaterial on actin. *Appl Phys Lett* 104. DOI: 10.1063/1.4862200.

Li Y, Liu Y, Fu Y, Wei T, Le Guyader L, Gao G, Liu R, Chang Y, Chen C (2012) The triggering of apoptosis in macrophages by pristine graphene through the MAPK and TGF-beta signaling pathways. *Biomaterials* 33:402-411.

Li Y, Schluesener H, Xu S (2010) Gold nanoparticle-based biosensors. *Gold Bull* 43:29–41.

Lim HN, Huang NM, Lim SS, Harrison I, Chia CH (2011) Fabrication and characterization of graphene hydrogel via hydrothermal approach as a scaffold for preliminary study of cell growth. *Int J Nanomed* 6:1817- 1823.

Liu S, Zeng T, Hofmann M, Burcombe E, Wei J, Jiang R, Kong J, Chen Y (2011) Antibacterial activity of graphite, graphite oxide, graphene oxide, andreduced graphene oxide: membrane and oxidative stress. *ACS Nano* 5:6971–6980.

Liu Z, Robinson JT, Sun XM, Dai H (2008) PEGylated nanographene oxide for delivery of water-insoluble cancer drugs. *J Am Chem Soc* 130: 10876-10877.

Loh KP, Bao Q, Eda G, Chhowalla, M (2010) Graphene oxide as a chemically tunable platform for optical applications. *Nat Chem* 2:1015-1024.

Lowry OH, Rosebrough NJ, Farr AL, Randall RJ (1951) "Protein Measurement with the Folin Phenol Reagent." *J Biol Chem* 193: 265–275.

Lu CH, Yang HH, Zhu CL, Chen X, Chen GN (2009) A graphene platform for sensing biomolecules. *Angew Chem Int Ed* 48:4785–4787.

McAllister M, Li J, Adamson D, Schniepp H, Abdala A, Liu J, Herrera-Alonso M, Milius D, Car R, Prud'homme R, Aksay I (2007) Single Sheet Functionalized Graphene by Oxidation and Thermal Expansion of Graphite. *Chem Mater* 19:4396-4404.

Magaye R, Zhao J, Bowman L, Ding M (2012) Genotoxicity and carcinogenicity of cobalt-, nickel- and copper-based nanoparticles. *Exp Ther Med* 4:551-561.

Manke A, Wang L, Rojanasakul Y (2013) Mechanisms of Nanoparticle-Induced Oxidative Stress and Toxicity. *BioMed Research International* 1-15. http://dx.doi.org/10.1155/2013/942916

Marcano DC (2010) Improved Synthesis of Graphene Oxide. *ACS Nano* 4; 4806-4814.

Marklund S, Marklund G (1974) "Involvement of the Superoxide Anion Radical in the Autoxidation of Pyrogallol and a Convenient Assay for Superoxide Dismutase." *Eur J Biochem* 47: 469–474.

Mitra S, Gaur U, Ghosh PC, Maitra AN (2001) Tumour targeted delivery of encapsulated dextran–doxorubicin conjugate using chitosan nanoparticles as carrier. *J Control Release* 74:317-323.

Mize CE, Langdon RG (1962) "Hepatic Glutathione Reductase. I. Purification and General Kinetic Properties." *J Biol Chem* 237: 1589–1595.

Mohamed B, Verma N, Prina-Mello A, Williams Y, Davies A, Bakos G, Tormey L, Edwards C, Hanrahan J, Salvati A, Lynch I, Dawson K, Kelleher D, Volkov Y (2011) Activation of stress-related signaling pathway in human cells upon SiO2 nanoparticles exposure as an early indicator of cytotoxicity. *J Nanobiotechnology* 9:29. DOI: 10.1186/1477-3155-9-29.

Mohanan PV, Syama S, Sabareeswaran A, Sreekanth PJ, Varma HK (2014) Molecular toxicity of dextran coated ferrite nanoparticles after dermal exposure to Wistar rats. *J of Toxicology and Health* 104:406-422.

Moron MS, Depierre JW, Mannervik B (1979) "Levels of Glutathione, Glutathione Reductase and Glutathione S-Transferase Activities in Rat Lung and Liver." *Biochim Biophys Acta* 582: 67–78.

Murphy JM, Fink DJ, Hunziker EB, Barry FP (2003) Stem cell therapy in a caprine model of osteoarthritis. *Arthritis Rheum* 48:3464-3474.

Mylonas C, Kouretas D (1999) Lipid peroxidation and tissue damage. *In Vivo* 13:295-309.

Naseem S, Gatoo MA, Dar AM, Qasim K (2014) In vivo toxicity of nanoparticles: Modalities and treatment. *Eur Chem Bull* 3: 992-1000.

Nayak TR, Andersen H, Makam VS, Khaw C, Bae S, Xu X, Ee PR, Ahn JH, Hong BH, Pastorin G, Ozyilmaz B (2011) Graphene for con-trolled and accelerated osteogenic differentiation of human mesenchymal stem cells. *ACS Nano* 5: 4670-4678.

Novoselov KS, Geim AK, Morozov SV, Jiang D, Zhang Y, Dubonos SV, Grigorieva IV, Firsov AA (2004) Electric field effect in atomically thin carbon films. *Science* 306: 666-669

Nowack B, Bucheli T (2007) Occurrence, behavior and effects of nanoparticles in the environment. *Environ Pollut* 150:5-22.

Nuttall ME, Gimble JM (2004) Controlling the balance between osteoblastogenesis and adipogenesis and the consequent therapeutic implications. *Curr Opin Pharmacol* 4:290-294.

Ohkawa H, Ohishi N, Yagi K (1979) "Assay for Lipid Peroxides in Animal Tissues by Thiobarbituric Acid Reaction." *Anal Biochem* 95: 351–358.

Ohno T, Sarukawa K, Tokieda K, Matsumura, M (2001) Morphology of a TiO2 Photocatalyst (Degussa, P-25) Consisting of Anatase and Rutile Crystalline Phases. *J Catal* 203:82-86.

Okado Matsumoto A, Fridovich I (2001) Subcellular distribution of superoxide dismutases (SOD) in rat liver: Cu, Zn-SOD in mitochondria. *J Biol Chem* 276:38388-38393.

Omotayo OE, Siti AS, Wahab MSA, Sirajudeen KNS, Salleh MS, Sunil G (2010) Antioxidant protective effect of glibenclamide and metformin in combination with honey in pancreas of streptozotocin-induced diabetic rats. *Int J Mol Sci* 11:2056-2066.

Owen JB, Butterfield DA (2010) Measurement of oxidized/reduced glutathione ratio. *Methods Mol Biol* 648:269-277.

Park S, Mohanty N, Suk J, Nagaraja A, An J, Piner R, Cai W, Dreyer D, Berry V, Ruoff R (2010) Biocompatible, Robust Free-Standing Paper Composed of a TWEEN/Graphene Composite. *Adv Mater* 22:1736-1740.

Park S, Park J, Sim S, Sung M, Kim K, Hong B, Hong S (2011) Enhanced Differentiation of Human Neural Stem Cells into Neurons on Graphene. *Adv Mater* 23:263-267.

Pei S, Cheng H (2012) The reduction of graphene oxide. *Carbon* 50(9): 3210-3228.

Pietruska J, Liu X, Smith A, McNeil K, Weston P, Zhitkovich A, Hurt R, Kane A (2011) Bioavailability, Intracellular Mobilization of Nickel, and HIF-1 Activation in Human Lung Epithelial Cells Exposed to Metallic Nickel and Nickel Oxide Nanoparticles. *Toxicol Sci* 124: 138-148.

Porter A, Muller K, Skepper J, Midgley P, Welland M (2006) Uptake of C60 by human monocyte macrophages, its localization and implications for toxicity: Studied by high resolution electron microscopy and electron tomography. *Acta Biomater* 2:409-419.

Qi W, Yuan W, Yan J, Wang H (2014) Growth and accelerated differentiation of mesenchymal stem cells on graphene oxide/poly- l -lysine composite films. *J Mater Chem B* 2: 5461-5467.

Reinhold MI, Kapadia RM, Liao Z, Naski MC (2006) The Wnt-inducible transcription factor Twist1 inhibits chondrogenesis. *J Biol Chem* 281:1381-1388.

Remya NS, Syama S, Gayathri V, Varma HK, Mohanan PV (2014) An in vitro study on the interaction of hydroxyapatite nanoparticles and bone marrow mesenchymal stem cells for assessing the toxicological behaviour. *Colloids Surf B Biointerfaces* 117:389-397.

Robinson JT, Tabakman SM, Liang Y, Wang H, Casalongue HS, Vinh D, Dai H (2011) Ultrasmall Reduced Graphene Oxide with High Near- Infrared Absorbance for Photothermal Therapy. *J Am Chem Soc* 133:6825–6831.

Rotruck JT, Pope AL, Ganther HE, Swanson AB, Hafeman DG, Hoekstra WG (1973) Selenium: Biochemical Role as a Component of Glutathione Peroxidase. *Science* 179: 588–590.

Ryoo SR, Kim YK, Kim MH, Min DH (2010) Behaviors of NIH-3T3 fibroblasts on graphene/carbon nanotubes: proliferation, focal adhesion, and gene transfection studies. *ACS Nano* 4: 6587-6598.

Ryu S, Kim B (2013) Culture of neural cells and stem cells on graphene. *Tissue Eng Regen Med* 10:39-46.

Salata OV (2004) Applications of nanoparticles in biology and medicine. *J Nanobiotechnology* 2:3. DOI: 10.1186/1477-3155-2-3

Sasidharan A, Panchakarla L, Chandran P, Menon D, Nair S, Rao C, Koyakutty M (2011) Differential nano-bio interactions and toxicity effects of pristine versus functionalized graphene. *Nanoscale* 3: 2461-2464.

Sayyar S, Murray E, Thompson B, Gambhir S, Officer D, Wallace G (2013) Covalently linked biocompatible graphene/polycaprolactone composites for tissue engineering. *Carbon* 52:296-304.

Scholz G, Genschow E, Pohl I, Bremer S, Paparella M, Raabe H, Southee J, Spielmann H (1999) Prevalidation of the Embryonic Stem Cell Test (EST)—A New In Vitro Embryotoxicity Test. *Toxicol In Vitro* 13:675-681.

Sekiguchi A, Kinjo R, Ichinohe M (2004) A stable compound containing a silicon – silicon tripple bond. *Science* 305: 1755-1757

Sharma P, Jha A, Dubey R, Pessarakli M (2012) Reactive Oxygen Species, Oxidative Damage, and Antioxidative Defense Mechanism in Plants under Stressful Conditions. *Journal of Botany* 2012:1-26. http://dx.doi.org/10.1155/2012/217037.

Shen H, Zhang L, Liu M, Zhang Z (2012) Biomedical Applications of Graphene, *Theranostics*. 2(3):283-294.

Shen J, Zhu Y, Chen C, Yang X, Li C (2011). Facile preparation and upconversion luminescence of graphene quantum dots. *Chem Commun* 47:2580-2582.

Shi X, Chang H, Chen S, Lai C, Khademhosseini A, Wu H (2011) Regulating Cellular Behavior on Few-Layer Reduced Graphene Oxide Films with Well-Controlled Reduction States. *Adv Funct Mater* 22:751-759.

Shin HJ, Sim KK, Benayad A, Yoon SM, Park HK, Jung IS, Jin MH, Jeong HK, Kim JM, Choi JY, Lee YH (2009) Efficient reduction of graphite oxide by sodium borohydride and its effect on electrical conductance. *Adv Funct Mater* 19:1987-1992.

Shin SW, Song IH, Um SH (2015) Role of Physicochemical Properties in Nanoparticle Toxicity. *Nanomaterials* 5:1351-1365.

Sies H, Akerboom TP (1984) Glutathione disulfide (GSSG) efflux from cells and tissues. *Methods Enzymol* 105:445-451.

Slee EA, Harte MT, Kluck RM, Wolf BB, Casiano CA, Newmeyer DD, Wang HG, Reed JC, Nicholson DW, Alnemri ES, Green DR, Martin SJ (1999) Ordering the cytochrome c-initiated caspase cascade: hierarchical activation of caspases-2, -3, -6, -7, -8, and -10 in a caspase-9-dependent manner. *J Cell Biol* 144: 281–292.

Sohaebuddin S, Thevenot P, Baker D, Eaton J, Tang L (2010) Nanomaterial cytotoxicity is composition, size, and cell type dependent. *Part Fibre Toxicol* 7:22. DOI: 10.1186/1743-8977-7-22.

Sohni A, Verfaillie C (2013) Mesenchymal Stem Cells Migration Homing and Tracking. *Stem Cells Int* 2013:1-8. http://dx.doi.org/10.1155/2013/130763

Son BR, Marquez-Curtis LA, Kucia M, Wysoczynski M, Turner AR, Ratajczak J, Ratajczak MZ, Janowska-Wieczorek A (2006) Migration of bone marrow and cord blood mesenchymal stem cells in vitro is regulated by stromal-derived factor-1-CXCR4 and hepatocyte growth factor-c-met axes and involves matrix metalloproteinases. *Stem Cells* 24:1254-1264.

Srivastava S, Jain K, Singh V, Singh S, Vijayan N, Dilawar N, Gupta G, Senguttuvan T (2012) Faster response of NO_2 sensing in graphene–WO_3 nanocomposites. *Nanotechnology* 23:205501. DOI: 10.1088/0957-4484/23/20/205501

Stern ST, McNeil SE (2008) Nanotechnology safety concerns revisited, *Toxicol Sci* 101:4–21.

Sun X, Liu Z, Welsher K, Robinson J, Goodwin A, Zaric S, Dai H (2008) Nano-graphene oxide for cellular imaging and drug delivery. *Nano Res* 1:203-212.

Syama S, Reshma SC, Sreekanth PJ, Varma HK, Mohanan PV (2013) Effect of Zinc Oxide nanoparticles on cellular oxidative stress and antioxidant defense mechanisms in mouse liver. *Toxicol Environ Chem* 95: 495-503.

Syama S, Reshma SC, Gayathri V, Varma HK, Mohanan PV (2014a) Assessment of hydroxyapatite nanoparticles induced oxidative stress- An in vitro study. *J Free Rad Antioxidants* 140: 286-293.

Syama S, Sreekanth PJ, Varma HK, Mohanan PV (2014b) Zinc oxide nanoparticles induced oxidative stress in mouse bone marrow mesenchymal stem cells. *Toxicol Mech Methods* 24:644-53.

Syama S, Gayathri V,Mohanan PV (2015) Assessment of Immunotoxicity of Dextran Coated Ferrite Nanoparticles in Albino Mice. *Mol Biol Intl* http://dx.doi.org/ 10.1155/ 2015/518527

Syama S, Mohanan PV (2016) Safety and biocompatibility of graphene: A new generation nanomaterial for biomedical application. *Int J Biol Macromolec* 86:546-555.

Talukdar Y, Rashkow J, Lalwani G, Kanakia S, Sitharaman B (2014) The effects of graphene nanostructures on mesenchymal stem cells. *Biomaterials* 35:4863-4877.

Tripathi S, Gupta K, Kumar P (2013) Polyethyleneglycol cross linked N-(2-hydroxyethyl)-polyethylenimine nanoparticles as efficient non-viral vectors for DNA and siRNA delivery *in vitro* and *in vivo*. *Mol BioSyst* 9: 2322-2330.

USP 30 NF 25. 85 (2007) Bacterial Endotoxins Test.

Vance M, Kuiken T, Vejerano E, McGinnis S, Hochella M, Rejeski D, Hull, M (2015) Nanotechnology in the real world: Redeveloping the nanomaterial consumer products inventory. *Beilstein J Nanotechnol* 6:1769-1780.

Wang G, Yang J, Park J, Gou X, Wang B, Liu H, Yao J (2008) Facile Synthesis and Characterization of Graphene Nanosheets. *J Phys Chem C* 112:8192–8195.

Wang A, Pu K, Dong B, Liu Y, Zhang L, Zhang Z, Duan W, Zhu Y (2013) Role of surface charge and oxidative stress in cytotoxicity and genotoxicity of graphene oxide towards human lung fibroblast cells. *J Appl Toxicol* 33:1156–1164.

Wen H, Dong C, Dong H, Shen A, Xia W, Cai X, Song Y, Li X, Li Y, Shi D (2012) Engineered Redox-Responsive PEG Detachment Mechanism in PEGylated Nano-Graphene Oxide for Intracellular Drug Delivery. *Small* 8:760-769.

Wu ZS, Ren W, Ago L, Liu B, Jiang C, Cheng HM (2009) Synthesis of high-quality graphene with a pre-determined number of layers. *Carbon* 47:493-499.

Yang F, Cho SW, Son SM, Bogatyrev SR, Singh D, Green JJ, Mei Y, Park S, Bhang SH, Kim BS, Langer R, Anderson DG (2010) Genetic engineering of human stem cells for enhanced angiogenesis using biodegradable polymeric nanoparticles. *Proc Natl Acad Sci U S A* 107:3317-3322.

Yang G, Su J, Gao J, Hu X, Geng C, Fu Q (2013) Fabrication of well-controlled porous foams of graphene oxide modified poly (propylenecarbonate) using supercritical carbon dioxide and its potential tissue engineering applications. *J Supercrit Fluids* 73: DOI: 10.1016/j.supflu.2012.11.004.

Yang K, Feng L, Shi X, Liu Z (2013) Nano-graphene in biomedicine: theranostic applications. *Chem Soc Rev* 42:530–547.

Yang K, Gong H, Shi X, Wan J, Zhang Y, Liu Z (2013) *In vivo* biodistribution and toxicology of functionalized nano-graphene oxide in mice after oral and intraperitoneal administration. *Biomaterials* 34:2787-2795.

Yang K, Zhang S, Zhang GX, Sun XM, Lee ST, Liu Z (2010) Graphene in mice: ultrahigh in vivo tumor uptake and efficient photothermal therapy. *Nano Lett* 10:3318-3323.

Zhang LM, Lu Z, Zhao Q, Huang J, Shen H, Zhang Z (2011) Enhanced chemotherapy efficacy by sequential delivery of siRNA and anticancer drugs using PEI-grafted graphene oxide. *Small* 7:460–464.

Zhang LM, Xia J, Zhao Q, Liu L, Zhang Z (2010) Functional graphene oxide as a nanocarrier for controlled loading and targeted delivery of mixed anticancer drugs. *Small* 6:537–544.

Zhang TY, Zhang D (2011) Aqueous colloids of graphene oxide nanosheets by exfoliation of graphite oxide without ultrasonication. *Bull Mater Sci* 34:25-28.

Zhang X, Hu W, Li J, Tao L, Wei Y (2012) A comparative study of cellular uptake and cytotoxicity of multi-walled carbon nanotubes, graphene oxide, and nanodiamond *Toxicol Res* 1:62-68.

Zhang Y, Ali SF, Dervishi E, Xu Y, Li Z, Casciano D, Biris AS (2010) Cytotoxicity effects of graphene and single-wall carbon nanotubes in neural phaeochromocytoma-derived PC12 cells. *ACS Nano* 4:3181–3186.

Zhou F, Xing D, Wu B, Wu S, Ou Z, Chen W (2010) New Insights of Transmembranal Mechanism and Subcellular Localization of Noncovalently Modified Single-Walled Carbon Nanotubes. *Nano Letters* 10:1677-1681.

Zhou M, Wang Y, Zhai Y, Zhai J, Ren W, Wang F, Dong S (2009) Controlled Synthesis of Large-Area and Patterned Electrochemically Reduced Graphene Oxide Films. *Chemistry* 15:6116-6120.

Zhou T, Chen F, Liu K, Deng H, Zhang Q, Feng J, Fu Q (2010) A simple and efficient method to prepare graphene by reduction of graphite oxide with sodium hydrosulfite. *Nanotechnology* 22:045704. DOI: 10.1088/0957-4484/22/4/045704.

Zhu X, Hondroulis E, Liu W, Li C (2013) Biosensing Approaches for Rapid Genotoxicity and Cytotoxicity Assays upon Nanomaterial Exposure. *Small* 9:1821-1830.

LIST OF PUBLICATIONS

1. **Syama S**, Mohanan PV (2016). Safety and biocompatibility of graphene: A new generation nanomaterial for biomedical application. Int J Biol Macromol. 86:546-555.

2. Reshma SC, **Syama S**, Mohanan PV (2016) Nano-biointeractions of PEGylated and bare reduced graphene oxideon lung alveolar epithelial cells: A comparative *in vitro* study. Colloids and Surfaces B: Biointerfaces 140, 104–116

3. **Syama S**, Reshma SC, Aby CP, Toru Maekawa, Sakthikumar D, Mohanan PV (2015). Synthesis and characterization of pegylated reduced graphene oxide: Determination of toxicity using bone marrow mesenchymal stem cells. Journal of Applied Chemical Science International 5(1):1-11.

4. **Syama S**, Sreekanth PJ, Varma HK, Mohanan PV (2014) Zinc Oxide nanoparticles induced oxidative stress in mouse bone marrow mesenchymal stem cells. Toxicol Mech Methods. 2014 Sep 3:1-10. PMID: 25138636.

5. Remya NS*, **Syama S***, Gayathri V, Varma HK, Mohanan PV (2014). An *in vitro* study on the interaction of hydroxyapatite nanoparticles and bone marrow mesenchymal stem cells for assessing the toxicological behavior. Colloids Surf B Biointerfaces, 28(117C), 389-397. (*equal authorship).

6. Cherian RS, Sreejith R, **Syama S**, Sruthi S, Gayathri V, Toru Maekawa, Sakthikumar D and Mohanan PV (2014). Evaluation of Toxicity of Maura Reduced Graphene Oxide using *In vitro* Systems. J Nanomed Nanotechnol 5: 200. doi:10.4172/2157-7439.1000200.

7. **Syama S**, Willi Paul, Sabareeswaran A and Mohanan PV, Raman spectroscopy for the detection of organ distribution and clearance of PEGylated reduced graphene oxide and biological consequences (under review).

8. **Syama S**, Aby CP, Toru Maekawa, Sakthikumar D, Mohanan PV, Nano biocompatibility of PEGylated reduced graphene oxide on mesenchymal stem cells (under review).

CONFERENCE PRESENTATIONS

1. **Syama S**, Mohanan PV (2016) Toxicity of PEGylated reduced graphene oxide in Swiss Albino mice. 36th Annual Session of the Academy of Environmental Biology and National Symposium on Impact of Emerging Toxic Chemicals on Humans, Plants, Diseases and Sustainable Development (IET 2016), 25-27 November 2016, Jamia Hamdard University, New Delhi.

2. Reshma SC, **Syama S**, Mohanan PV (2015) Determination of toxicity of in-housed synthesized PEGylated Nano Graphene using bone marrow mesenchymal stem cells. INRS 2015 Occupational Health Research Conference, Nancy, France

3. **Syama S**, Reshma SC, Gayathri V, Mohanan PV (2013). Assessment of nanohydroxyapatite toxicity on mouse bone marrow mesenchymal stem cells. J.Clin. Toxicol 2013, 3:5, 97 (Presented at the 2nd International Summit on Toxicology, 7-9 October, 2013, Las Vegas, USA)

4. Reshmitha TR, **Syama S**, Reshma SC, Gayathri V, Mohanan PV (2013). Toxicity evaluation using mouse bone marrow mesenchymal stem cells: A predictive model for in vitro studies. J.Clin. Toxicol 2013, 3:5